Geophysical Studies in the Delson St. Consultant Area

GEOPHYSICAL FIELD STUDIES IN THE DELSON-St.CONSTANT AREA (St.LAWRENCE LOWLAND MONTREAL)

© by

Abuaysha, M. A.

THESIS

PRESENTED TO FACULTY OF GRADUATE STUDIES AND RESEARCH

DEPARTMENT OF GEOLOGICAL SCIENCES

McGill University

In partial fulfillment of the requirment for the degree of Master Of Science In Geophysics

McGill University

December, 1988

Resume

Nous avons réalisé une étude géophysique combinée des structures géologiques d'une portion de la région des plaines littorales du St-Laurent au sud-est de Montreal. La région à l'étude repose sur des roches sédimentaires du cambrien et de l'ordovicien qui sont traversées d'est en ouest par des failles et des filons intrusifs du montérégien.

Parmi les études géophysiques réalisées, mentionnons des études électromagnétiques à trés basse fréquence, des études magnétiques, des études radiométriques et des études de résistivité en courant continu.

L'étude a été réalisee pour localiser la faille Delson ainsi qu'un filon de contact stratigraphique et l'existence éventuelle de filons instrusifs du montérégien. En combinant toutes les mesures géophysiques, il a été possible de localiser comme prevu la faille Delson à fort pendage et un filon intrusif du montérégien dans une région, sans pouvoir localiser la faille dans une autre région. Seule une combinaison d'études de résistivité à trés basse fréquence et en courant continu a permis de localiser un filon de contact stratigraphique à faible pendage entre les mêmes formations qui étaient séparées par la faille Delson.

Dans cette étude, toutes les réponses géophysiques, les intérpretations et la modélisation ont été comparées de

très près aux données géologiques pour obtenir des renseignements plus détaillés sur la région à l'étude.

ABSTRACT

A combined geophysical study of geological structures in a portion of the St. Lawrence Lowland area southeast of Montreal was carried out. The area under investigation is underlain by Cambrian and Ordovician sedimentary rocks which are cut by east-west fault systems and by Monteregian intrusives .

The geophysical studies included very low frequency electromagnetics (VLF), magnetics, radioactivity and DC resistivities. The study was carried out to locate the Delson fault, a stratigraphic contact and the possible existance of Monteregian intrusives. An integration of all the geophysical measurements located the projected steeply-dipping Delson fault and a Monteregian intrusive in one area, but failed to locate the fault ln another. Only a combination of VLF and DC resistivity located a shallowly-dipping stratigraphic contact between the same formations as were separated by the Delson fault .

In this study, all geophysical responses, interpretations and modelling have been correlated as closely as possible to geological data to provide more detailed information on the area under investigation.

TABLE OF CONTENTS

LIST OF FIGURES

LIST OF TABLES

ACKNOWLEDGEMENTS

I thank my thesis adviser Prof. V.A. Saull who suggested the subject of this thesis and acted as director until mid-November 1987. During his supervision Professor Saull provided instruction in field procedures, prepared equipment, and helped occasionally to take field measurements. He also critically read a manuscript of the thesis. Many thanks to Professor W.M. Telford for discussions and constructive comments that improved the thesis. I would also like to thank Professor W.H. Maclean for his assistance with the final manuscript. Professor O.J.Jensen and Crossley, D.J. both call for special thanks for their valuable suggestions. Thanks are also due to Dr. A. Abdel-Rahman for his helpful discussions. Mr. Marc Deschenes of Canada Cement Lafarage is thanked for his cooperation in supplying geophysical information and permission to work on their properties. Many thanks to Ms. P. King-Edwards for editing the manuscript. The use of McGill's facilities are gratefully acknowledged.

Finally, not only did my wife spend hours drafting, but she has also been a constant source of encouragement and understanding.

Chapter 1 : Introduction

Chapter 1: Introduction

1.1 General Introduction

From April - August 1987, a geophysical field study was carried out in a portion of the St Lawrence Lowland south-east of Montreal. The area investigated extends from 3 Km southeast of Delson and about 2 Km north-west of St Constant (see Fig 1.1). The geology of the general region has been described by Clark (1952), (1972) and by Globensky (1986), (1987). However, except for the gravity survey conducted by D.G.McDonald (1965), comparatively little of the area has been explored by geophysical methods as far as we know. The variety and the complexity of the geology of the Montreal region requires that any further investigation should employ multiple geological mapping-geophysical methods, which should be closely correlated to the geology of the area.

In this study, very low frequency (VLF) electromagnetics were used to try to reveal contacts, faults, and conductive bodies. Magnetic surveys were employed to try to detect both the structure (faults, shears, etc.) and to detect the possible existence of intrusions or other bodies with high magnetic susceptibility. Resistivity surveys were also employed to obtain information on the lateral resistivity contrasts and on the depth of the overburden. Radon emanation and gamma-ray scintillometer profiles were also

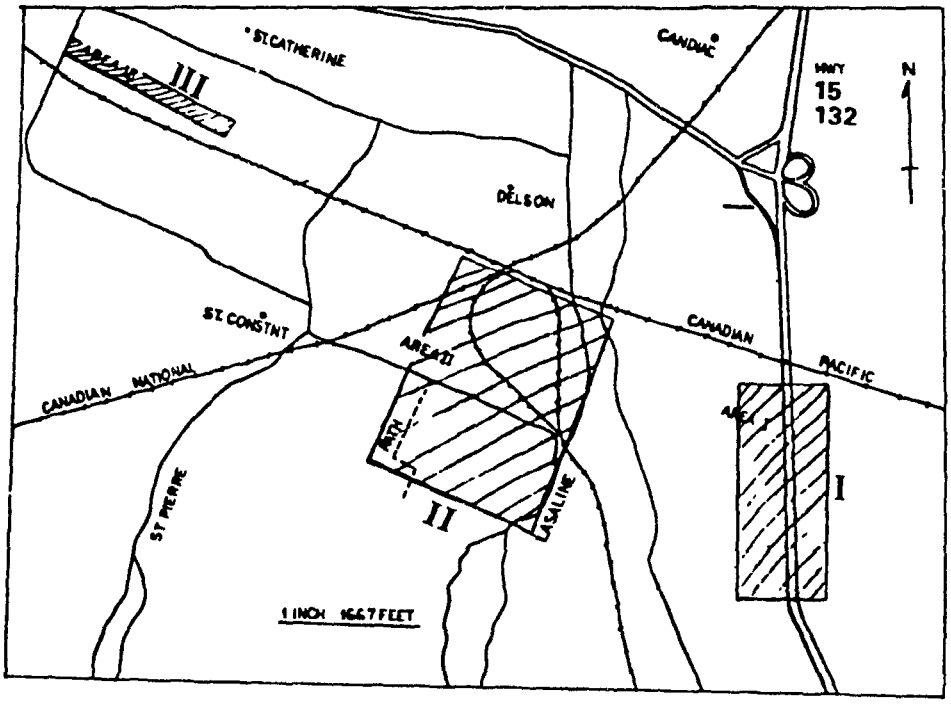

1.1 Index Map Showing the Field Sites.

obtained as rocks in the Montreal region have only slight variations in physical properties such as conductivity.

In this geophysical study :

1- Approximately 840 VLF-EM16 measurements on 22 traverses and over 80 VLF-EM16R measurements on 5 traverses were conducted to delineate the Delson fault and the stratigraphic contact between the Trenton limestone-shale and the Utica formation shale.

2- A total of 25 DC resistivity measurements on two traverses were taken to substantiate the VLF results over the Delson fault and the geologic contact.

3- Depth sounding Wenner resistivity measurements were made at two stations to determine approximatley the resistivity and the depth of the overburden.

4- Over 380 magnetic measurements on 11 traverses outlined a well defined magnetic anomaly . The body which is modelled as a vertical thin-sheet is assumed to belong to the basaltic Monteregian intrusives.

5- A total of 280 radioactive measurements by the emanometer and the scintillometer on 10 traverses were used to substantiate the geophysical measurements over the Delson fault.

1.2 Previous Work

There have been no previous multiple ground geophysical surveys of this area. A previous gravity survey was conducted by D.G.McDonald during the autumn of 1963 and the summer of 1964 to investigate the gravity effect of the Delson and Tracy Brook faults. The work was done by exploring the area with a gravimeter and from the value of Bouguer anomaly a gravity anomaly map was constructed. A total of four gravity profiles were constructed across the Delson fault. Profile 1 at Delson confirmed the existence of the fault as shown by the geology. Profiles 2,3 and 4, east of profile 1, indicated the fault extended to the east for at least 8 miles from profile 1.

The results of the survey indicated that both faults are complex and nearly vertical (see McDonald MSc thesis McGill University Montreal 1965).

1.3 Purpose of the Project

The surveyed area lies in a seismically active and heavily farmed and urban developed farmland as well as an industrial sector. Therefore, the elucidation of the structures (faults and intrusions etc.) has economic as well as geological importance.

The main object of this thesis is to interpret the various geological mapping - geophysical methods together with the geological information in order to obtain more detailed information on the area under investigation.

In this study, specific attention also was given to the different (VLF) responses between a stratigraphic contact and a fault contact. The VLF interpretations are based on research in the use of this method in geological mapping developed by King and Telford (1971) at the Department of Mining and Metallurgical Eng., McGill University, Montreal.

Chapter 2: Geology of The Area and Field Procedure

Chapter 2: Geology of the Area

2.1 General Geology

The St. Lawrence Lowlands are generally divided into three parts: first, an area extending from the Frontenac axis to the Oka anticline, called the Ottawa-St Lawrence Lowland; a second area straddling the St Lawrence from Montreal to Quebec called the Quebec Lowland; and a third area comprised of Anticosti Island and Mingan Islands in the Gulf of St. Lawrence.

The St. Lawrence Lowlands have been designated as being entirely underlain by unfolded sedimentary rocks of the Cambrian and Ordovician period except for the restricted occurrences of Precambrian rocks and intrusive Cretaceous rocks (McDonald, 1965). The area under study is underlain entirely by Paleozoic sedimentary rocks of Cambrian and Ordovician period.

The surveyed area lies within the Quebec Lowland and is circumscribed by 73°30 W and 73°36 W longitude and 45°20 N and 45°23 N latitude, south of the St Lawrence River (see fig. 2.1). In this thesis the area under investigation is divided into three: area I, area II, and area III (fig.1.1).

Clark (1952,1972) and Globensky (1986,1987) give a comprehensive description of the geology of the Montreal area. Fig. 2.2 is a geological sketch map of the area and the surrounding parts of the St Lawrence lowlands. A

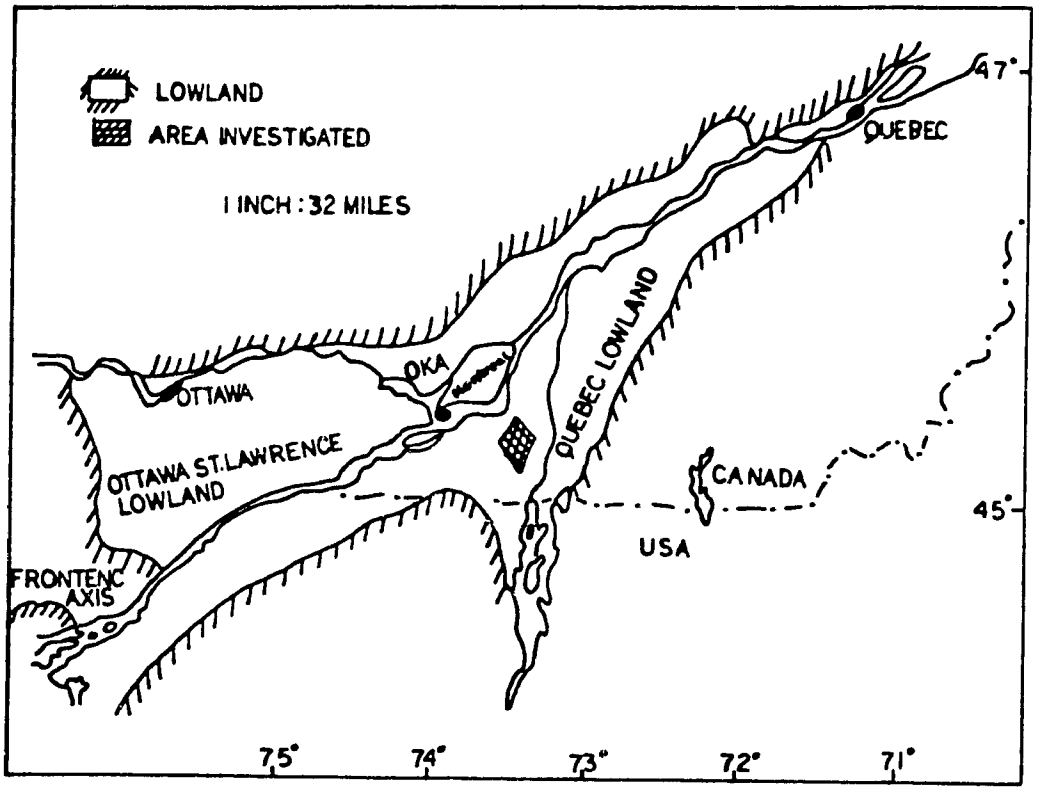

2.1 St.-Lawrence Lowland .

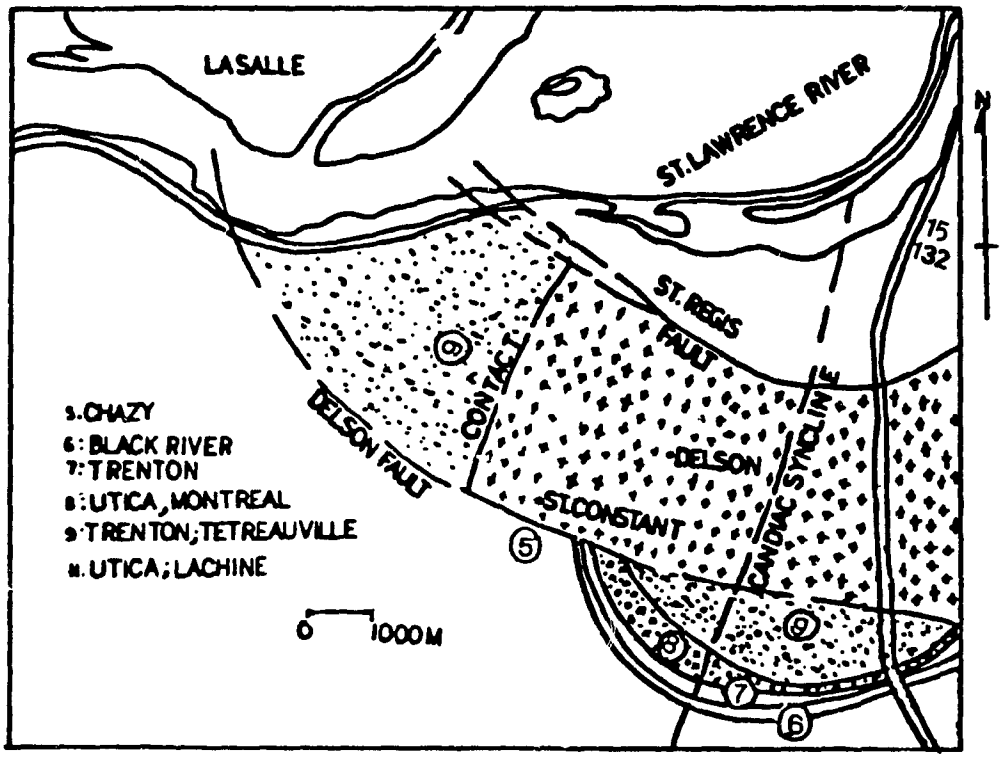

2.2 Geology of the Area (Clark,1972) .

detailed description of the stratigraphy and petrography of these formations can be found in the reports of Clark (1952,1972) and Globensky (1986,1987).

Overburden covers virtually the entire area. Fig. 2.3, constructed from the McDonald's thesis (1965), shows a geologic section across the Delson fault at the Mercier Bridge. The schematic diagram assumes the beds to be perfectly horizontal and the fault vertical.

The dominant structural features in this area are the Delson fault, the St. Regis fault, the Candiac syncline, and the contact between the Utica and Trenton formations northwest of St-Constant .

2.1.1 Delson Fault

The Delson fault strikes approximately south-east in the Montreal area. It separates Chazy from Upper Trenton, rocks immediately east of Caughnawaga, trends south-eastward, gradually bends around so as to leave the area, trending nearly east and west (fig. 2.2).

According to Clark (1972) the mapped position and direction of this fault have been fixed by St. Lawrence Seaway drilling and by drilling for limestone in the Delson-St. Constant area.

Geophysical (gravity) research (McDonald, 1965) indicates that this is a double fault.

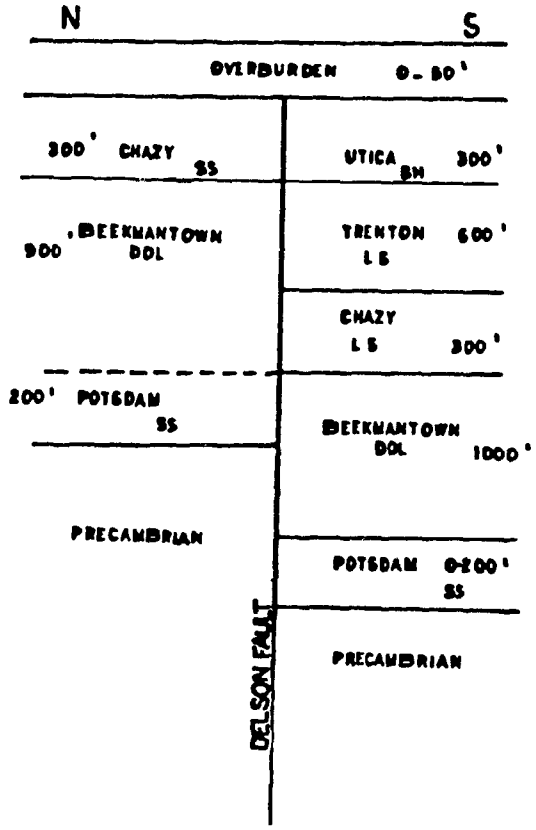

2.3 Geological Section Across the Delson Fault near the Mercier Bridge (McDonald, 1965) .

2.1.2 St-Regis Fault

This fault has almost the same strike as the Delson fault. Evidence for it comes solely from Seaway drill cores, from which the distribution of Tetraultville, Utica, and Lorraine rocks necessitates a fault, or a double fault (see fig. 2.2) (Clark, 1972). The St-Regis fault may be assumed as a branch of the Delson fault. However, the data taken in the field did not show a continuation of the Delson fault near St-Constant area. This will be discussed later.

2.1.3 Utica-Trenton Contact

This contact lies north-west of St-Constant , (see fig. 2.2). Clark (1972) reported that this is a contact between the Tetraultville formation (Trenton) and the Lachine formation (Utica). While Globensky (1982) reported it as a contact between the Montreal formation (limestone-shale) and Utica (shale).

2.2 Description of Geologic Formations

Trenton limestone is one of the best-known Ordovician rocks in the St-Lawrence Lowlands.

Clark (1972) described it as well-bedded black or dark bluish-grey limestone, abundantly fossiliferous, and characterized by shale partings between the successive beds (from a fraction of an inch to a foot thick). As the top of

the group is approached, the shale content of the beds becomes more apparent and important.

The Black River Group and the Trenton limestone are very similar to one another. According to Clark (1972), it is sometimes difficult to point to the dividing line between the Trenton Group and Black River Formations. Globensky (1986, pp. 122-127) gives a comprehensive description of the Black River Group. Utica shale is a black shale formation that outcrops at Delson and contacts Trenton rocks near St-Constant in area III (see fig. 2.2). Field borings near St-Constant confirmed this contact between the two formations. Clark (1972,p.109) describes the Utica shale as " a fine disintegration shale". It contains thin beds of quartz sandstone, and flattened concretions, and has a high proportion of clay.

The Chazy formations is mostly a grey crystalline limestone. Scarcely one-half of it, though, is limestone, the remainder being shale. Clark (1972) gives a comprehensive description of the Chazy group (pp. 50-68).

Table 2.1 summarizes the formations in the Quebec Lowlands (from McDonald, 1965). Monteregian intrusives occur in the areas under investigation. The magnetic survey showed a dyke-like body striking E-W which is presumed to belong to the Monteregian intrusives. The Monteregian hills are notable common topographic features of the St-Lawrence Lowlands region, formed by igneous intrusions into the Sedimentary basin rocks. These hills are magnetic as well as topographic anomalies because of their pronounced

Table 2.1 Formations in the Quebec Lowland

Period	Sub-Epoch	Formations and Members
Quaternary	Recent	Fluvial sands and gravels Saxicava sand - Leda clay
	Pleistocene	Glacial till
Unconformity		
Cretaceaus	Monteregian intrusives; alkaline gabbro nepheline-syenite and many other types of dykes and sills.	
Devonian	Helderberg-Oriskany ls	
Ordovician	Richmond Group	Becancour River; red ss and sh
		Pontgrave River; calcerious sh
	Lorraine Group	Nicolet River; mainly shales
	Utica Group	Lachine; sh
Disconformity		

Table 2.1 Formations in the Quebec Lowland

Period	Sub-Epoch	Formations and Members	
Ordovician	Trenton Group	Terrebonne; ls	
		Tetraultville; ls	
		Montreal	Rosemount; ls Lacolle; conglomerate St-Michet; ls
		Mile End; ls	
	Black River Group	Leray; ls	
		Lowville; ls	
		Pamelia; ls	
	Disconformity		
	Chazy Group	Laval	St-Martin; ls
			Ste-Therese; ls
		Beldens; dolomitic ls	
	Disconformity		
Cambrian	Beekmantown Group	Beauharnois; dol	
		Theresa; dolomitic ss	
	Upper Cambrian	Potsdam; ss	
	Great Unconformity		
Precambrian		Crystalline ls, quartz-paragneiss, granite, anorthosite, granite gneiss, etc.	

susceptibility contrast with the sediments, (Telford et al., 1976, p.195).

2.3 Description of the Area and Field Procedure

The area under study lies south of the St-Lawrence River between Delson and St-Constant .

This area is very flat, but it is heavily populated farmland dotted with farm buildings. The area also has an extensive road and railway network. Artificial objects such as power lines, telephone cables, and barbed wire restricted the continuation of profiles and the setting up of a grid system, and also caused a great distortion in the VLF and magnetometer readings. In order to avoid these objects which created noise in the profiles the profiles themselves had to be shortened

Laying out grids and obtaining exact measurements was also complicated by, tree lines, and farmed areas. In these places one had to follow the road which created a constant "noise" in the geophysical measurements, especially with the electromagnetic instruments and with the magnetometer. However, most roads and paths ran almost perpendicular to the strike of the geological formations.

During the investigations long reconnaissance profiles were made and then shorter ones depending on the anomalies found. The distance between shorter profiles in area I and area III was 100-200 feet (30-60m). In area II it was impossible to do a uniform grid due to heavily cropped land and scattered houses. When approaching an

anomaly or if a big difference in readings occurred, an "in-between" measurement was taken. Profiles were made as perpendicular as possible to the strike of the formations.

Six different geophysical measurements were applied in area I: electromagnetics at VLF frequencies (EM16-EM16R) , magnetic, radiometries, (emanometer, gamma-ray scintillometer), and DC resistivity. Pace-and compass, air photos, and sometimes tape measuring techniques were used throughout the survey. The results were plotted in profile form.

In area II, the VLF reconnaissance work found no significant anomaly. The great amount of cropland in this area forced one to follow the road or walk along a narrow path. All of the above measurements were also applied, in area II. Time constraints and the slowness of the radon emanation method as well the results obtained in area I (and the preliminary survey with scintillation method) discouraged further use of radon in area II.

In area III only VLF and resistivity measurements were carried out to locate the geological contact.

During the VLF electromagnetic surveys, the transmitting station (Cutler, Maine) occasionally shut down (Monday and Thursday mornings).

Chapter 3: VLF-EM16

VLF-EM16R

DC Resistivities & VLF-EM16R

Chapter 3: Electromagnetic VLF Survey

3.1 Basic Equations:

The equations describing the behaviour of the natural electromagnetic fields have been described by many authors. (Cagniard (1953), Keller, Frischknecht (1966), and Swift (1969)). Comprehensive description of the following discussion can be found in Geophysical Applications of Surface Wave Impedance Measurements edited by Collett and Jensen (1982).

In the following discussion all media are assumed to be homogeneous and isotropic, to have permeability (μ), conductivity (σ) and permittivity (ϵ). The SI system of units and Cartesian coordinates were used.

The electric field $\underline{E}$ and magnetic field $\underline{H}$ must satisfy Maxwell's equations.

$$\nabla \times \underline{E} = - \frac{\partial}{\partial t} \underline{B} \qquad (3.1.1\ (a))$$

$$\nabla \times \underline{H} = \underline{J} + \frac{\partial}{\partial t} \underline{D} \qquad (3.1.1\ (b))$$

These quantities can be related to the electrical properties of the medium by:

$$\underline{D} = \epsilon \underline{E} \qquad [\text{coulomb/m}^2]$$

$$\underline{B} = \mu \underline{H} \qquad [\text{Weber/m}^2]$$

$$\underline{J} = \sigma \underline{E} \qquad [\text{Amp/m}^2]$$

and $$\epsilon = \epsilon_o \epsilon_r$$

$$\mu = \mu_o \mu_r$$

where ϵ_o = permittivity of free space
$= 8.85 \times 10^{-12}$ Farad/m

μ_o = permeability of free space
$= 12.56 \times 10^{-7}$ Henry/m

ϵ_r = relative permittivity

μ_r = relative permeability

substituting for $\underline{B}$, $\underline{J}$, and $\underline{D}$ in 3.1.1:

$$\nabla \times \underline{E} = - \mu \frac{\partial}{\partial t} \underline{H} \qquad (3.1.1\ (c))$$

$$\nabla \times \underline{H} = \sigma \underline{E} + \epsilon \frac{\partial}{\partial t} \underline{E} \qquad (3.1.1\ (d))$$

By taking the curl of the above and assuming a time dependant signal e^{iwt}, the equations become:

$$\nabla^2 \underline{E} = i \mu w \sigma \underline{E} - w^2 \mu \epsilon \underline{E}$$

$$\nabla^2 \underline{H} = i \mu w \sigma \underline{H} - w^2 \mu \epsilon \underline{H}$$

These can be combined into the Vector, Helmholtz or diffusion equations:

$$\nabla^2 \begin{bmatrix} \underline{E} \\ \underline{H} \end{bmatrix} + K^2 \begin{bmatrix} \underline{E} \\ \underline{H} \end{bmatrix} = 0 \qquad (3.1.2)$$

where $K^2 = i\mu w\sigma - w^2\mu\epsilon$; K is commonly called the wave number or the propagation constant of the medium. At magnetotelluric frequencies ($\leq$ 5KHz) K is dominated by the conduction term, thus $K^2 \approx iw\mu\sigma$. The effective wave penetration, commonly known as the skin depth, is the distance in which the signal is reduced by 1/e, that is, to 37%. This is expressed by:

$$Z_s = 500 \sqrt{(\rho / f)}$$

where Z_s = skin depth [meters]
ρ = resistivity [ohm-meters]
f = frequency [Hz]

Table 3.1 shows skin depth variations with frequency and resistivity (Telford et al, 1976, p. 474).

The solution of the Helmholtz equations for either a homogeneous or horizontally layered earth is straightforward. The one-dimensional nature of the problem makes all fields laterally invariant:

$$\frac{\partial}{\partial x} = \frac{\partial}{\partial y} = 0$$

Considering any two orthogonal components E_x and H_y. In this case, for homogeneous ground, the vector equation (3.1.2) becomes a scalar equation.

$$\frac{\partial 2}{\partial z^2} E_x = - i K^2 E_x$$

$$\frac{\partial 2}{\partial z^2} H_y = - i K^2 H_y$$

After some manipulations and unit conversions the resulting equation is:

$$\rho = \frac{1}{w\mu} \left| \frac{E_x}{H_y} \right|^2 \qquad (3.1.3)$$

which may be written as

$$\rho = 0.2 \, T \, |E_x/H_y|^2$$

where

$\rho = 1/\sigma$ = resistivity (ohm m)

$T = 1/f$ = period (seconds)

E_x = electric field at surface (mv/Km)

H_y = magnetic field at surface (gamma)

The ratio E_x/H_y is known as the electromagnetic impedance of the ground.

Magnetotelluric signals can be either H-polarized, where the electric field component is normal to the strike

Table 3.1: Skin depth variation with frequency and resistivity

ρ=	10^{-4} Ωm	10^{-2} Ωm	10 Ωm	10^{2} Ωm	10^{4} Ωm
f (Hz)	z_s(m)	z_s(m)	z_s(m)	z_s(m)	z_s(m)
10^{-3}	160	1600	1.6×10^{4}	1.6×10^{5}	1.6×10^{6}
10^{-2}	50	500	5000	5×10^{4}	5×10^{5}
10^{-1}	16	160	1600	1.6×10^{4}	1.6×10^{5}
1	5	50	500	5000	5×10^{4}
10	1.6	16	160	1600	1.6×10^{4}
10^{2}	0.5	5	50	500	5000
10^{3}	0.16	1.6	16	160	1600
10^{4}	0.05	0.5	5	50	500
10^{6}	0.005	0.05	0.5	5	50
10^{8}	----	0.005	0.05	0.5	5

direction, or E-polarized, when the electric field component is parallel to the strike (see fig. 3.1). The "E parallel" polarization has an associated vertical magnetic field, which is more convenient to use with regards to VLF electromagnetic measurements.

3.2 VLF EM-16

The basic principle on which the VLF-EM system works is that the receiver unit detects the secondary field, generated by any conductive discontinuity in the ground when subjected to a primary field. The primary field, which for distant stations is horizontal, is generated from VLF transmitting stations with a frequency range of about 15 to 25 KHz. These transmitters use vertical dipole antennae which produce a concentric horizontal magnetic field round them.

Since H_Z and H_X differ in phase in the vicinity of a conductive discontinuity, the resultant EM value is elliptically polarized (for a more complete treatment see Paterson and Ronka, 1971). The total normalized vertical field can be directly calculated from:

$$R = \surd (\tan^2\theta + r^2)$$

where r and $\tan\theta$ are in fact two quantities which are measured by the Geonics EM-16.

The receiver unit detects VLF signals and measures a tilt angle (in phase) and a quadrature component by means of two mutually perpendicular coils wound on ferrite. The

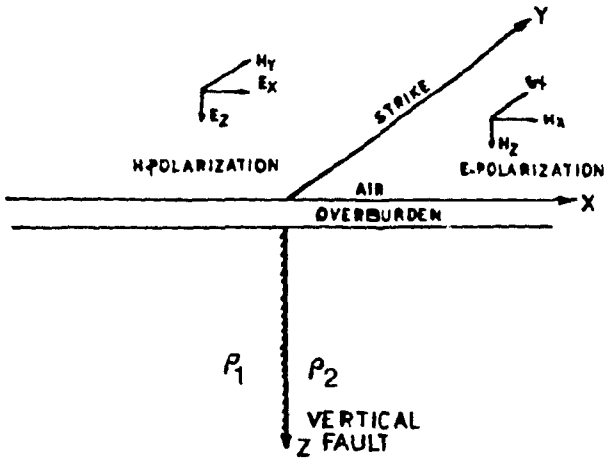

3.1 Field Components for E-Polarization and H-Polarization

core with a usually vertical axis is first held horizontal and then rotated in azimuth to find a minimum. This direction is then in line with the transmitter station. The same coil is then held vertical and tilted about a horizontal axis parallel to the minimum azimuth. The tilt angle is read from a clinometer on the instrument (calibrated both in degrees and percent). The quadrature signal, which has roughly the same azimuth as the primary field, is then balanced by the other coil after a phase shift of 90°. The amplitude of this signal is adjustable on the quadrature dial, which reads percent plus-or-minus. By tilt and quadrature adjustments, a good minimum (null detection) in the earphone is obtained.

For areas I and II the selected transmitting station was Cutler, Maine (NAA) with a frequency of 24 KHz. That is to say the strike of the fault is slightly greater than 45° to the transmitting station. The horizontal magnetic field lines from the transmitter are not exactly perpendicular to areas I and II. All readings were taken facing approximately south-east.

The selected station for area III was Annapolis, Md. (NSS) with a frequency of 21.4 KHz. The traverses were approximately east-west and the dip angles were measured facing east.

The receiver unit used was an EM-16 VLF (designed by Vaino Ronca and manufactured by Geonics Limited) with an accuracy of ±1%.

The distance between stations was 50 feet (16m), whereas the distance between traverses was 200 feet (65m) for area I.

3.3 VLF EM-16R (Radiohm)

In section 3.1, the relation for resistivity ρ, equation (3.1.3) was derived from a plane wave simplification of the diffusion equation, in which the displacement currents were considered insignificant. However, this assumption may not be valid for frequencies >5 KHz. (Crossley, 1981-I gives a complete treatment of this subject.)

According to D.Jones (1980) if a negligible displacement current is assumed, the layer resistivity must be restricted to values below about $10^4 \Omega M$, as in the case of conductive overburden. However, our field data is much below the higher limit.

In the radiohm technique, the apparent resistivity of the earth is determined by a magnetotelluric measurement of the field radiated from a remote radio transmitter.

The EM-16R instrument measures apparent resistivity and phase angle in the form

$$\rho_a = \frac{1}{2\pi f \mu_o} \left| \frac{E}{H} \right|^2 = \frac{1}{2\pi f \mu_o} |Z_o|^2$$

where f = frequency
$\Phi = \tan^{-1}$ (Im Zo / Re Zo)

where $\underline{E}$ and $\underline{H}$ are orthogonal, horizontal, electric and magnetic fields respectively with units of mv/km and gammas (nT) respectively while Z_o is a complex surface impedance, in ohms, in the site vicinity.

If the ground is homogeneous and isotropic the measured value will be the true resistivity and the phase angle 45°. Over stratified ground of several layers of different resistivity and thickness, $\int_a$ is a function of these parameters and the phase will not be 45°, This depends particularly on the nature of the top bed which controls the depth of the wave penetration.

The instrument used in this survey was a Geonics EM-16R which obtains H_y by means of an integral coil and E_x by means of two ground probes spaced 10 m apart. The measurement is made by orienting the instrument so that the coil is maximally coupled to H_y (determined from an audio signal) and inserting the two ground probes along the direction indicated by the instrument orientation. After the audio signal has been nulled by means of two controls, the phase angle and the apparent resistivity values can be read directly from the instrument. The apparent transmitter azimuth may be determined from the orientation of the instrument.

In the present study the signal used was from NSS, Annapolis, Md. with a frequency of 21.4 KHz for areas I and area II, whereas NAA, Cutler, Maine with frequency 24 KHz was used for area III. Also station NSS was tested in area

III and compared to the results obtained by station NAA. This will be shown in the next section.

3.4 Filtering of VLF-EM16:

First derivative technique, introduced by Whittles (1969), removes the effects of elevation changes on EM16 readings.

This filter computes readings by subtracting the tilt angle of one station from the one adjacent to it, dividing by the distance between these two stations, (i.e. the slope), and plotting the resulting at the mid-point.

This technique was not applied because there was no overall topographic relief or large elevation changes in any of the survey lines.

3.5 Results : EM-16

Figure 3.2A shows the theoretical response of in-phase and out-of-phase components over a vertical fault. The amplitude of the response depends on the depth and resistivity of overburden and on the resistivity contrast between the two sides of the contact, (a detailed description of the response can be found in Telford et al., 1977).

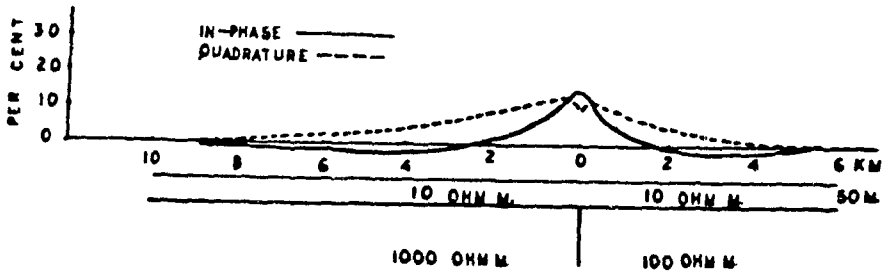

3.2A Theoretical response of the In-Phase and the Quadrature Components Over a Vertical Fault (Telford et al.,1977).

3.5.1 Area I

Almost all the traverses exhibited an anomaly where the Delson fault is expected to occur. These anomalies consists of positive in-phase and quadrature peak, with the latter being generally displaced from the peak of the in-phase response. They are comparable in shapes to the theoretical ones (see Telford et al.,1977).

Several lines (6+00E, 1+00W, 8+00W, and 8+00E) exhibit a double peak on the profiles.

Two sharp crossovers on the line (1+00E) and one sharp crossover on line (0+00) are caused by a thin buried drainage pipe. As these two traverses follow the highway (15), the latter profile is between the roads.

The profiles especially those of the west side traverses had to be shortened because of the heavy farmland and dense bush in the south. Barbed wire in the tree lines on the west side of the higway distorted the profiles somewhat, especially the profile 10+00W.

At the beginning of the survey three very long profiles (line 0+00, line 1+00E, and line 1+00W) were conducted along the highway as a reconnaissance, to determine the presence of the fault. Where an anomaly was found, parallel profiles were set up on both sides of the highway. The profiles were 200 feet (65m) apart, and the station interval was 50 feet (16m). All results were plotted in profile form; in-phase is a solid line , while the quadrature component is a broken line.

Line 0+00: (fig. 3.3)

This traverse is situated in the middle of the highway 15. The sharp cross-over at 14+50N is caused by a shallowly buried drainage pipe. There is a fault type response at 2+00N. The in-phase and quadrature both displayed positive peaks, with the quadrature response being somewhat broader and the in-phase component being quite noisy in this vicinity. The pronounced in-phase offset of about 7% is probably due to decrease in the depth of overburden as the profile parallel the highway.

Line 1+00E: (fig. 3.4)

This traverse is situated on the east side of the highway. The large EM-16 cross-over at 33+00N at the beginning of the profile (about 75 feet north of the beginning) is caused by a railway tracks. Two other large crossovers at the 13+00N and 21+25N are caused by a drainage pipe.

A weak response at 8+00N may have been caused by a large cement drainage pipe crossing under the highway at this station.

The profile crosses the fault at 2+00N and a response occurs similar to that observed previously. The in-phase and out-phase (quadrature) both display positive peaks, and the quadrature component displays a local minimum at 1+50N. A false cross-over in the in-phase and out-of-phase components occurs at 1+98S and 2+50S respectively where both of the components change their signs.

It was impossible to get a reading in the vicinity

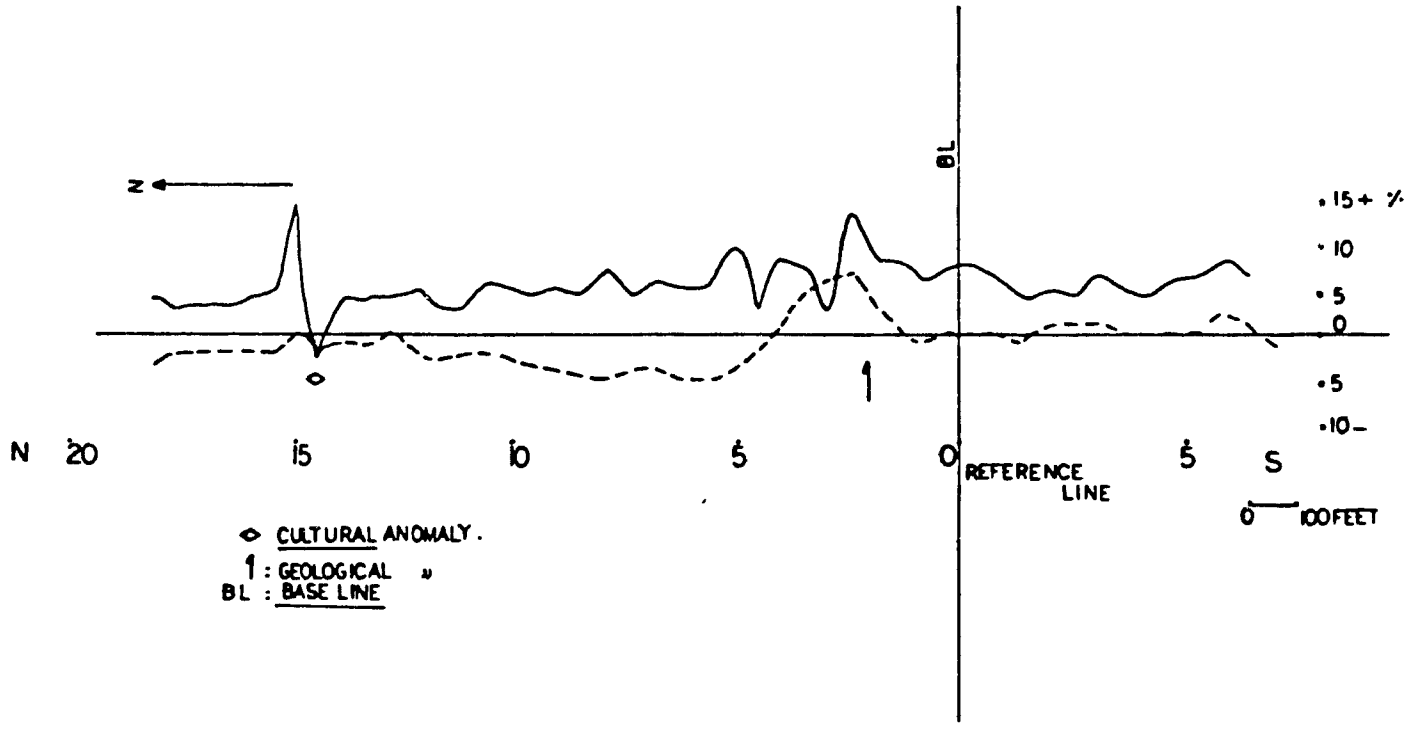

3.3 EM-16 Profile on Line 0+00 (Area I) .

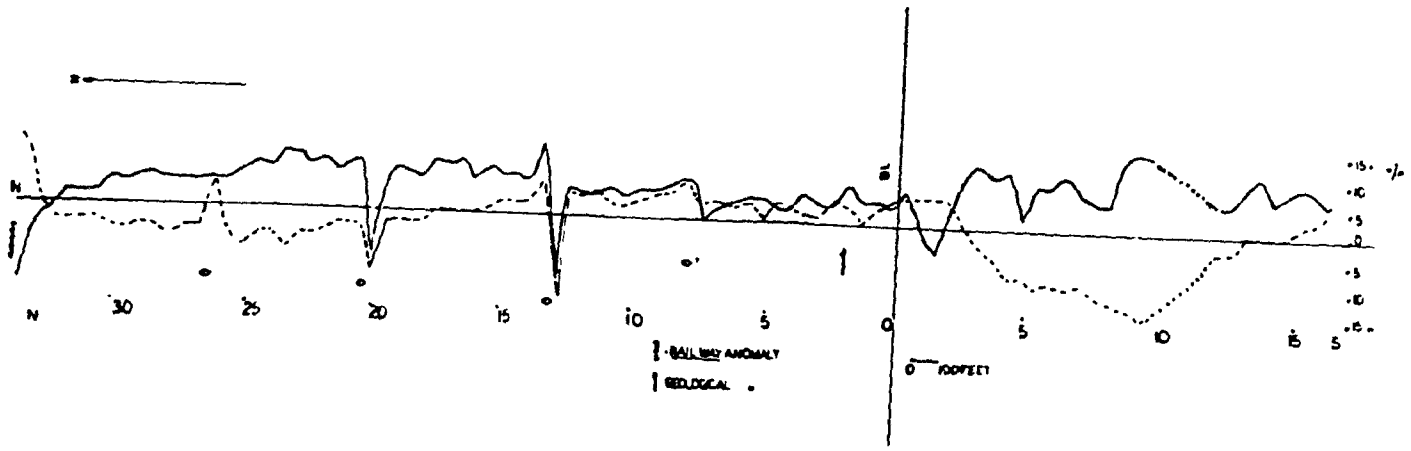

3.4 EM-16 Profile on Line 1+00 E (Area I) .

of 10+00S because of street lamps and a truck weigh-station at the side of the road.

Line 2+00E: (fig. 3.5)

A definite fault type response occurs in the vicinity of station 7+00N. Both components display a positive, nearly symmetrical peak at this station, while the quadrature seems displaced slightly north, where it peaks at 8+00N. The reason for a cross-over occurring in the in-phase at 9+25N is not clear. It could be from old buried barbed wire in the tree line in the vicinity of station 9+00N.

Line 4+00E: (fig. 3.6)

There is a broad, positive quadrature peak and a small positive in-phase peak at 5+00N and 3+00N respectively. The in-phase component is somewhat distorted where there is a cross-over at 6+00N. Again, this cross over may be due to a buried barbed wire in the tree line in the vicinity of that station.

Line 6+00E: (fig. 3.7)

There are possibly two distinct anomalies in this profile; one at station 0+50S and the other at station 5+00S. Both components in-phase and quadrature display positive peaks (the latter being displaced somewhat north). A false cross-over occurred at 2+25S, where the in-phase component changed from negative to positive.

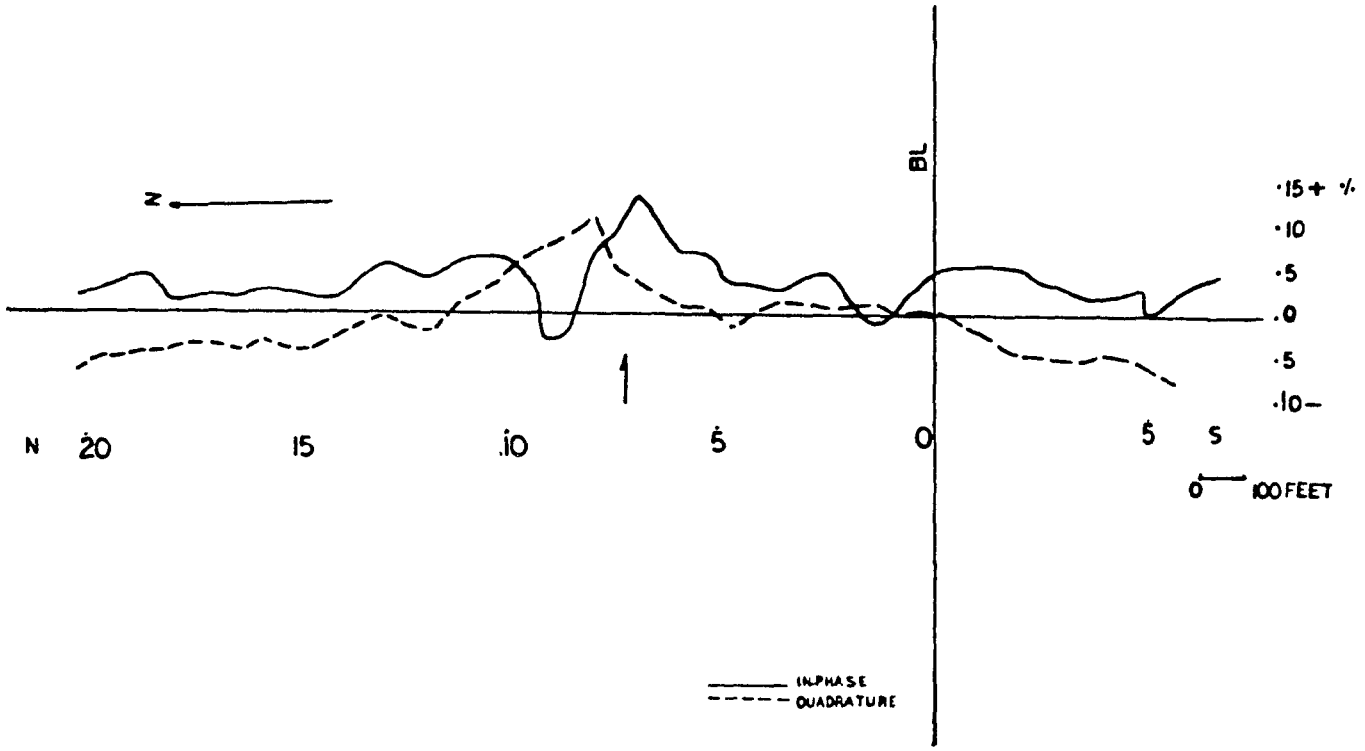

3.5 EM-16 Profile on Line 2+00E (Area I) .

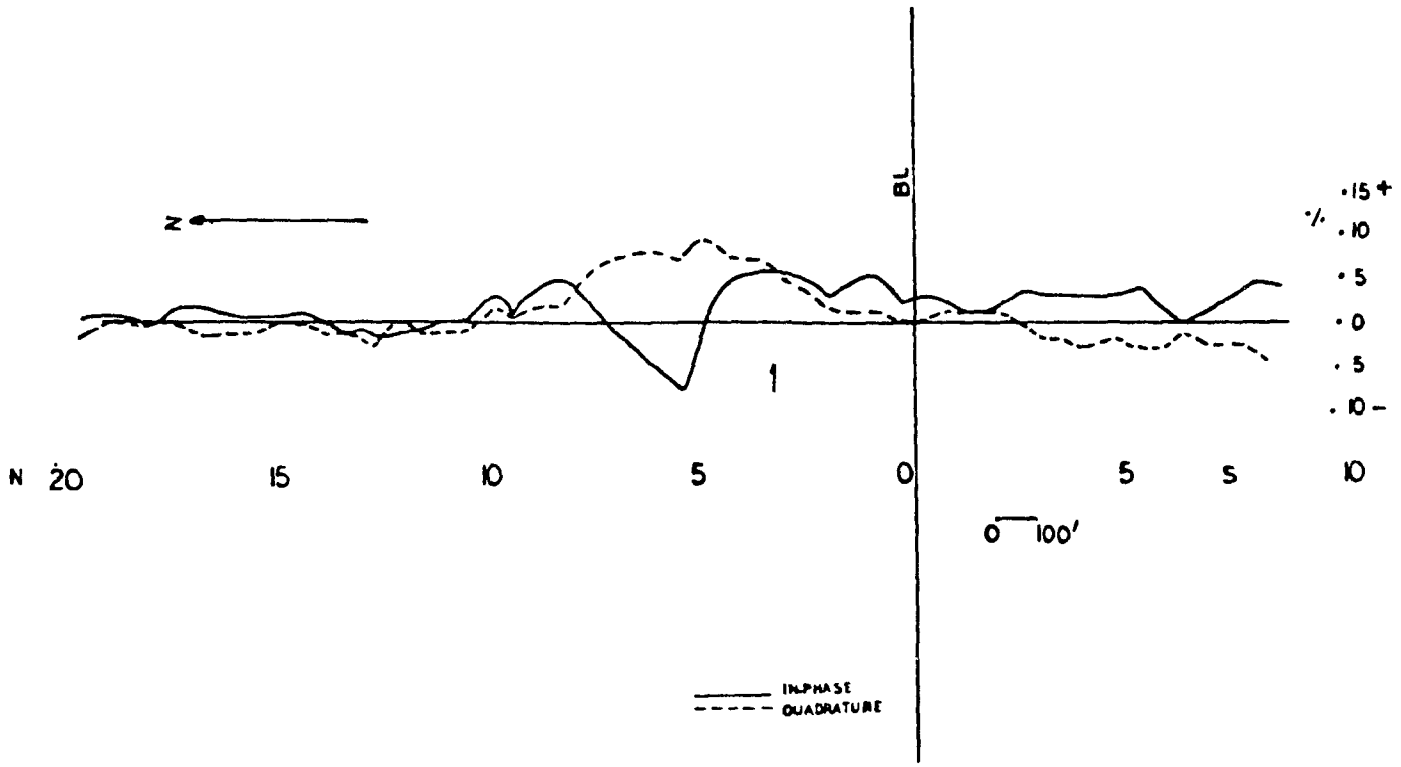

3.6 EM-16 Profile on Line 4+00E (Area I) .

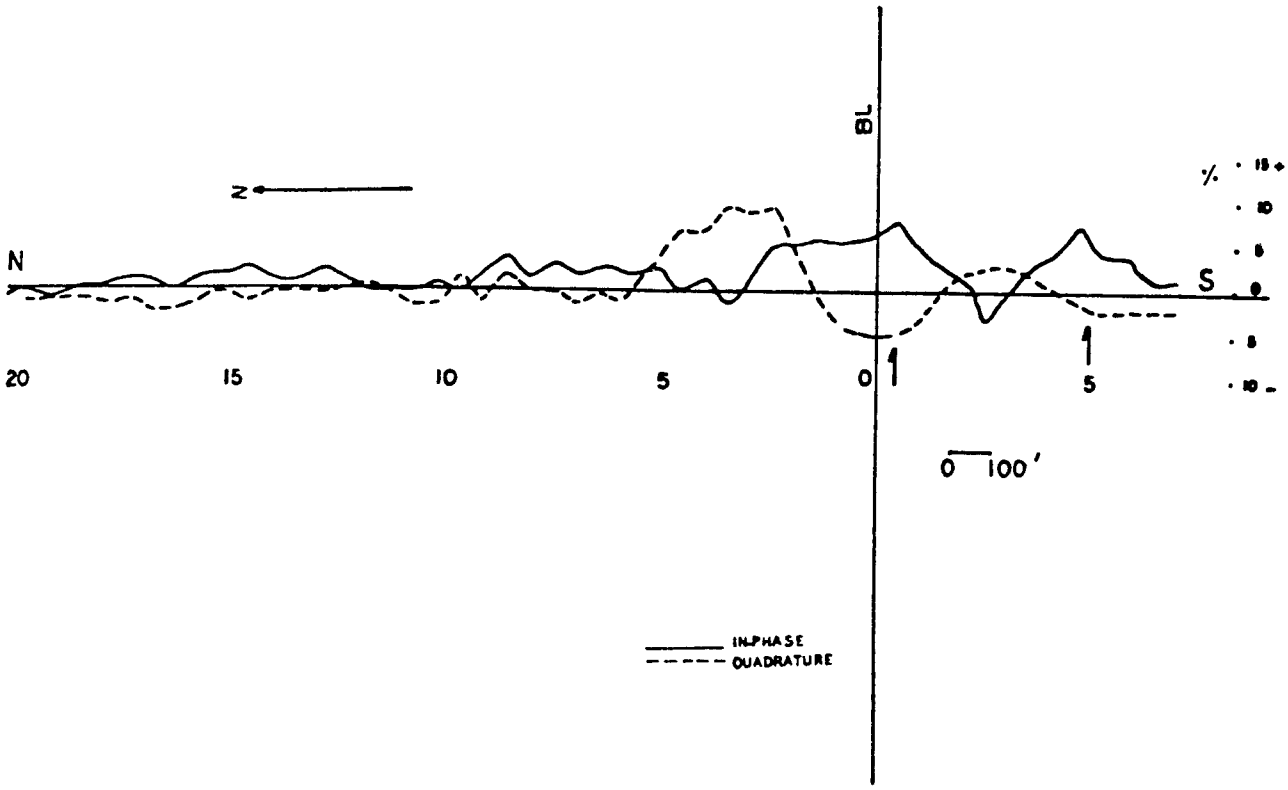

3.7 EM-16 Profile on Line 6+00E (Area I) .

Line 8+00E: (fig. 3.8)

A contact type response occurs in the vicinity of station 10+00N. This is a small in-phase peak, with a smaller quadrature peak which may indicate a contact at this station. There is a double positive in-phase peak at 4+50N and 1+00S, but there is only one quadrature peak between the in-phase ones. The quadrature response is quite large compared to the in-phase ones.

A small in-phase cross-over occurs, at 2+50S where the in-phase component changed to negative after crossing the fault.

Line 1+00W: (fig. 3.9)

This profile is situated just west of the highway. This line is characterized by two in-phase highs, these are situated at stations 3+00N and 1+50S with a maximum value of 17%. The quadrature response coincides, however, with that of the in-phase, where it peaks at 3+00N and is displaced further south at station 1+50S.

The in-phase component is generally noisy, but it has two distinct high peaks, which may be due to the decrease in the depth of overburden during the construction of the highway, as the profiles parallel the road.

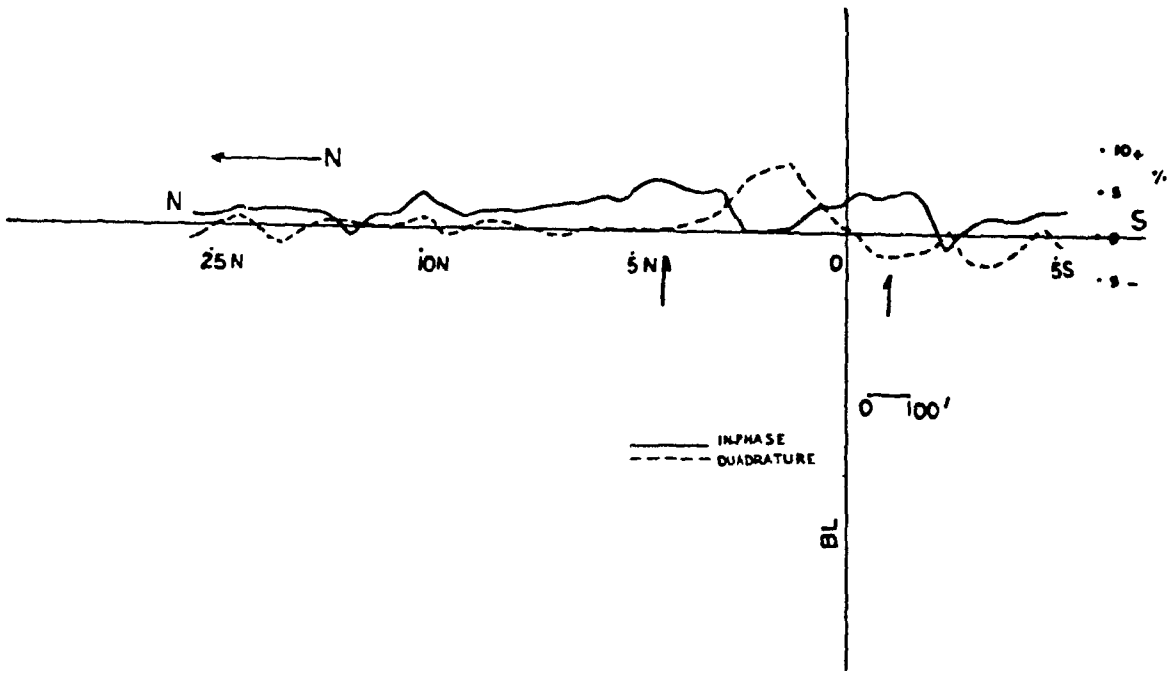

3.8 EM-16 Profile on Line 8+00E (Area I) .

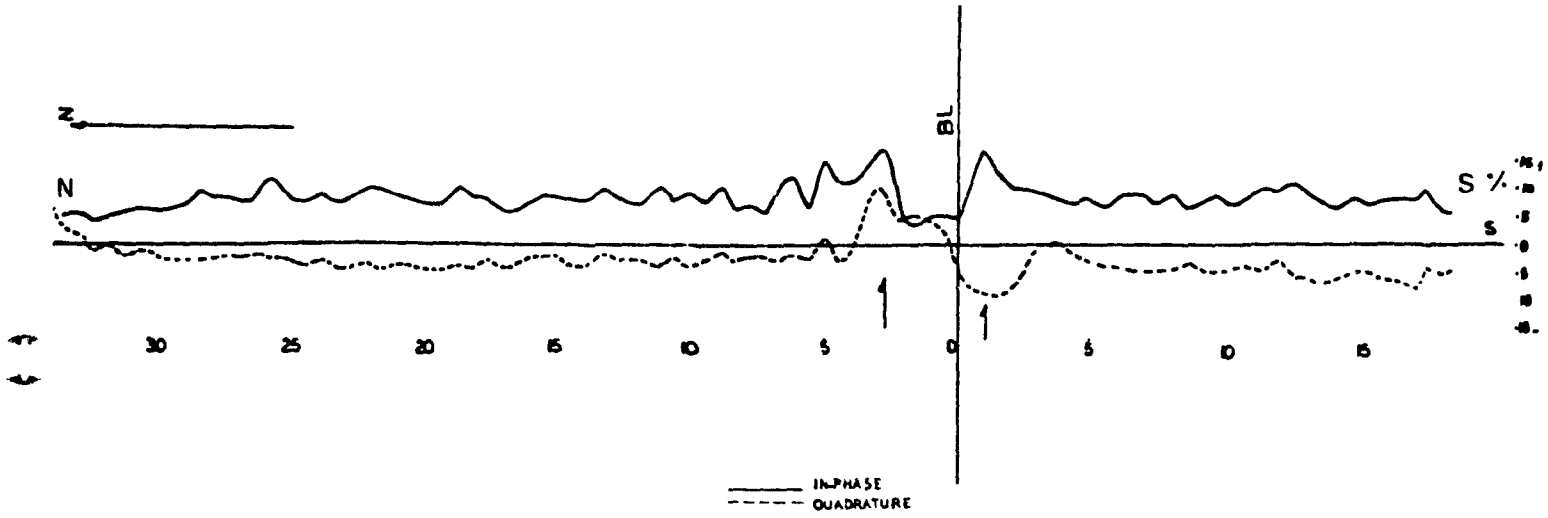

3.9 EM-16 Profile on Line 1+00W (Area I) .

Line 2+00W: (fig. 3.10)

This traverse is characterized by a high in-phase component occuring at station 1+50N. This is probably due to the thinner overburden. A false cross-over occurred again at station 0+00 and may have been due to an electric pole to the east of this station. The quadrature component on the other hand is displaced further north and displays two distinct peaks at 4+00N and 0+50S respectively.

Line 4+00W: (Fig. 3.11)

A response similar to the previous one was obtained on this line except the in-phase peak shifted a little north at station 4+00N. A fault type response occurred in the vicinity of station 10+00N. This may have been due to the presence of a tree line and barbed wire close to the station.

Line 6+00W: (fig. 3.12)

A response similar to line 4+00W occurred, where the in-phase component peaked in the vicinity of station 5+00N. An anomaly-like response also occurred in the vicinity of station 10+00N. The anomalies here are less pronounced though than in the previous case.

Line 8+00W: (fig. 3.13)

There are possibly two distinct anomalies in this profile - one at 6+75N and the other at 0+75S. Both components in-phase and quadrature displayed positive

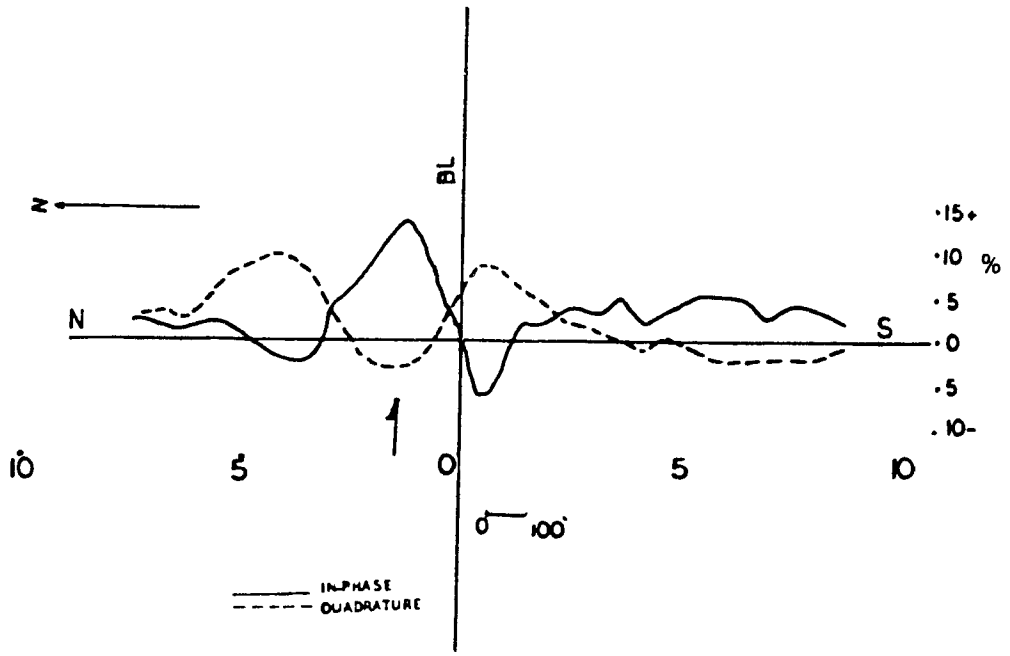

3.10 EM-16 Profile on Line 2+00W (Area I) .

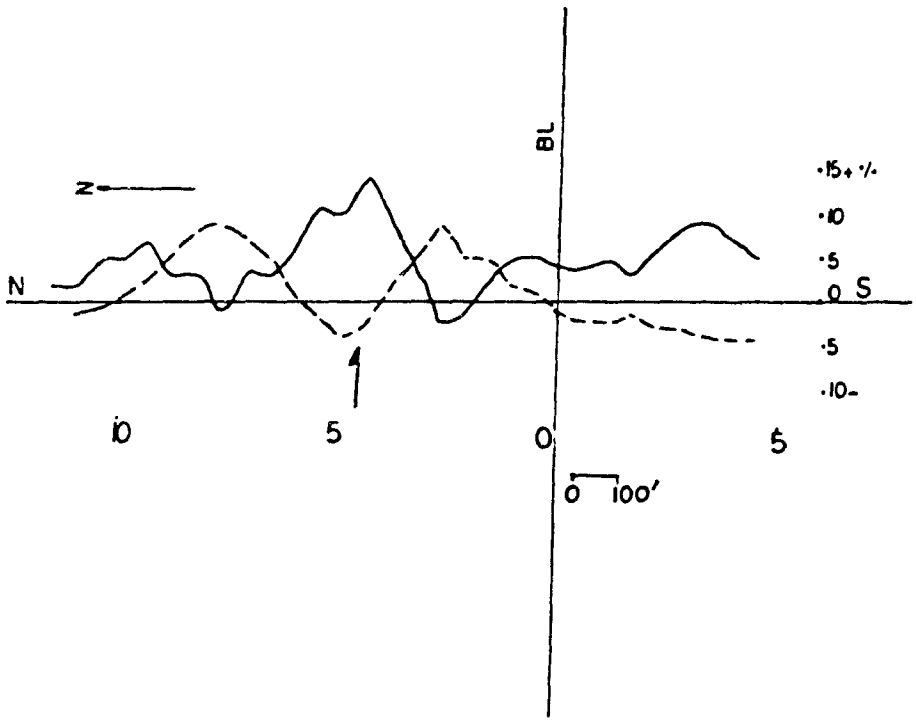

3.11 EM-16 Profile on Line 4+00W (Area I) .

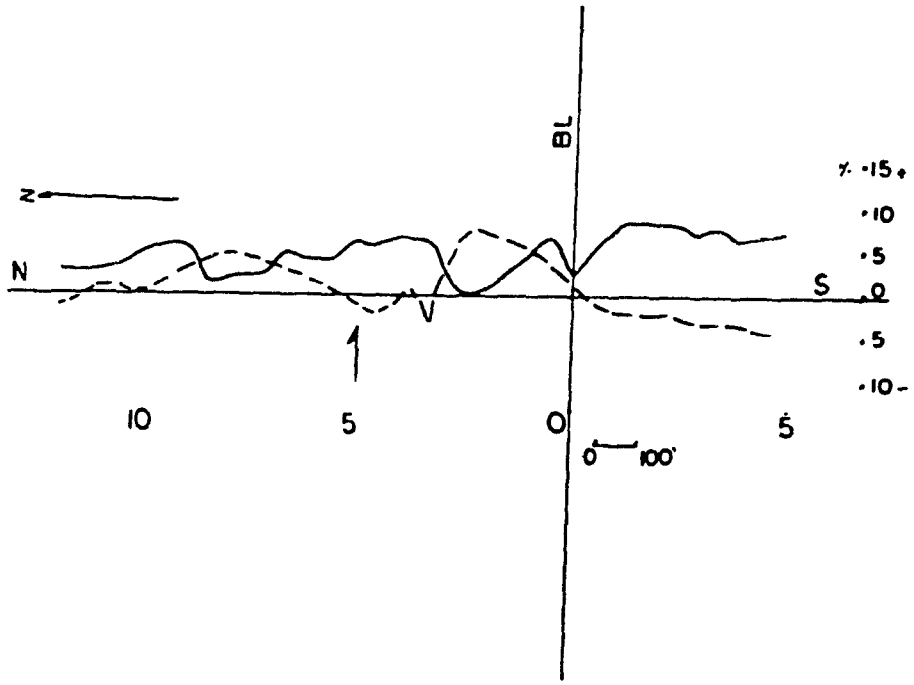

3.12 EM-16 Profile on Line 6+00W (Area I) .

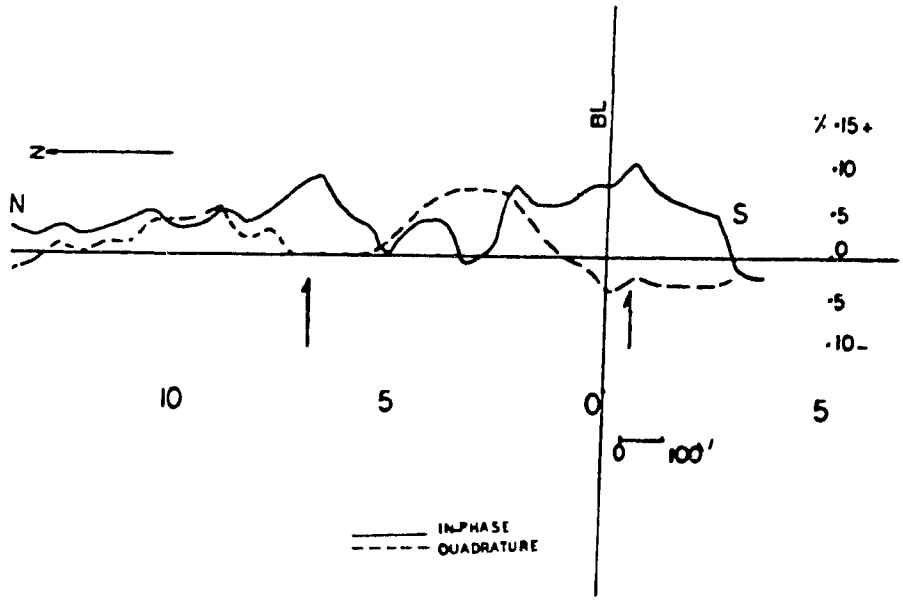

3.13 EM-16 Profile on Line 8+00W (Area I) .

peaks. The peak of the quadrature was again displaced a little north. The response at station 0+75S was more pronounced than that at station 6+75N, probably due to a thinner overburden. The traverse was not extended beyond station 3+00S because the crops were just coming up.

Line 10+00W: (fig.3.14)

There is a distinct peak at station 8+50N. The in-phase component is bigger but the quadrature component is broader. Unfortunately, before station 8+00N, both the in-phase and quadrature components became very noisy and somewhat distorted. The reason for this is unknown but there was a tree line about 100 m ahead with old pieces of barbed wire amongst it. It was not possible to extend the profile further because of farmland to the south.

Line 12+00W: (fig.3.15)

This line was similar to the previous one, where the in-phase component peaked in the vicinity of 8+00N and the quadrature component was smaller and broader. The same distortion, unfortunately occurred again before 8+00N probably for the same reasons. Again farmland in the south disallowed for an extension of the profile.

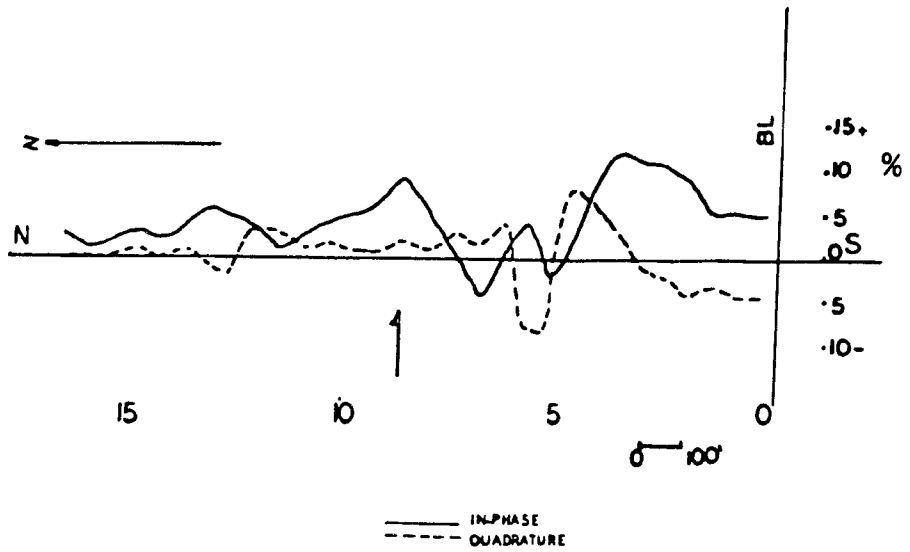

3.14 EM-16 Profile on Line 10+00W (Area I) .

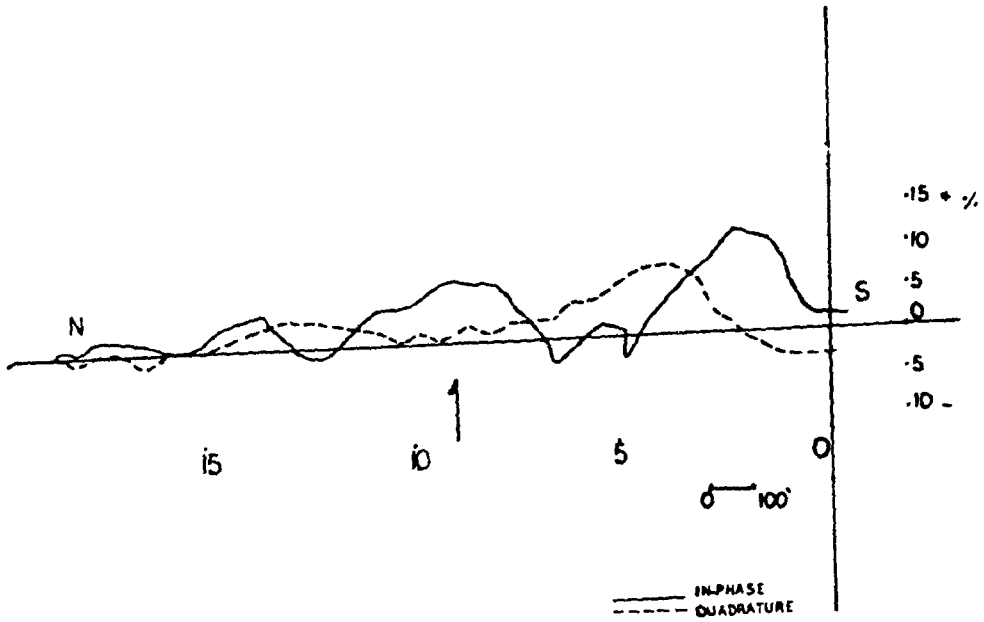

3.15 EM-16 Profile on Line 12+00W (Area I) .

3.6 EM-16R:

Fig. 3.2B shows the response of apparent resistivity and phase angle over a vertical contact model. The profiles are similar to those for DC resistivity across a vertical contact and indicate a changing lithology across the contact. The phase angle between E_y and H_x is greater on the conductive side of the contact than on the resistive side. It increases more rapidly, though, on the conductive side of the contact (see Jones, 1981).

From the above figure, however, the apparent resistivity contrast in the presence of overburden, is less than the true resistivity contrast between the bedrock on either side of the fault.

The presence of overburden generally decreases the phase angle (E_y-H_x) and lowers the apparent resistivity as well as the resistivity contrast across the fault.

Kisak (1976) gives a complete mathematical treatment of magnetotelluric responses over vertical contacts and topographic effects using finite element analysis.

3.6.1 Area I

Two traverses were made along the line 4+00E and line 4+00W with the EM-16R apparatus (see fig. 3.16 a,b) The results confirm the geologic information (Clark 1972, Globensky 1986) that the resistivity is considerably higher on the south side of the fault (Chazy limestone) and conductive on the north side of the fault (mostly shale).

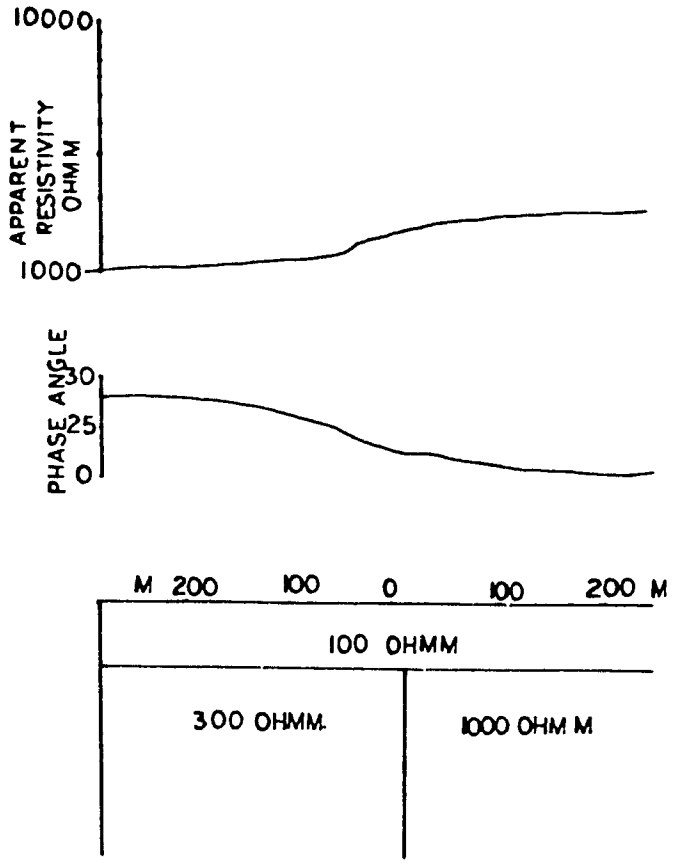

3.2B EM-16R theoretical profile Over Vertical Contact Model (D.Jones, 1981).

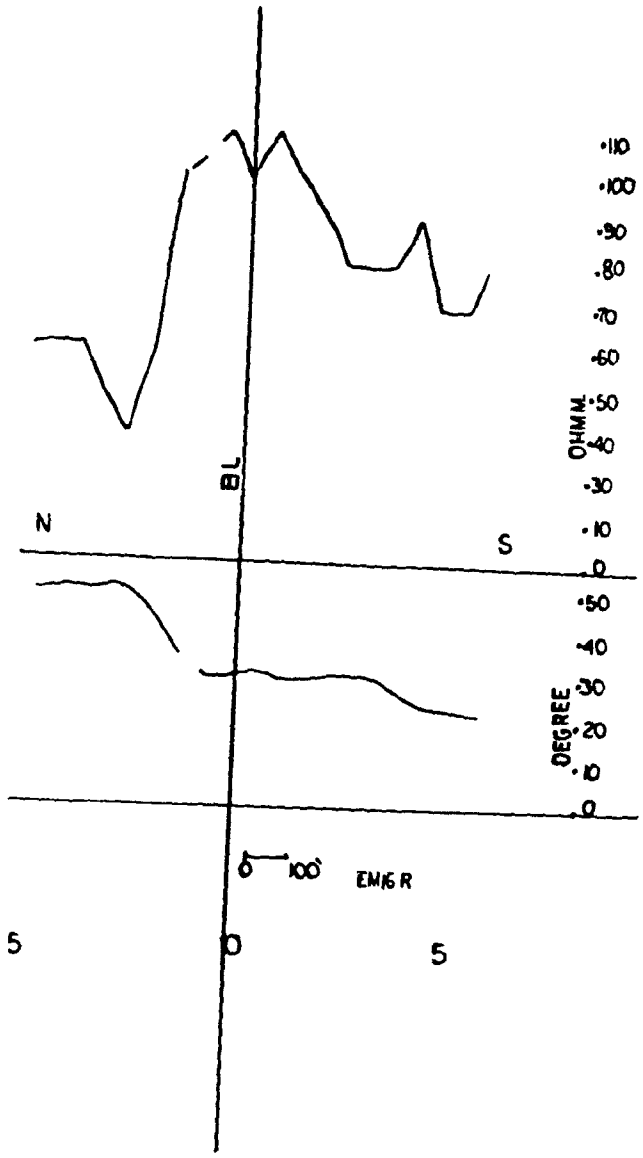

3.16A EM-16R Profile on Line 4+00E (Area I) .

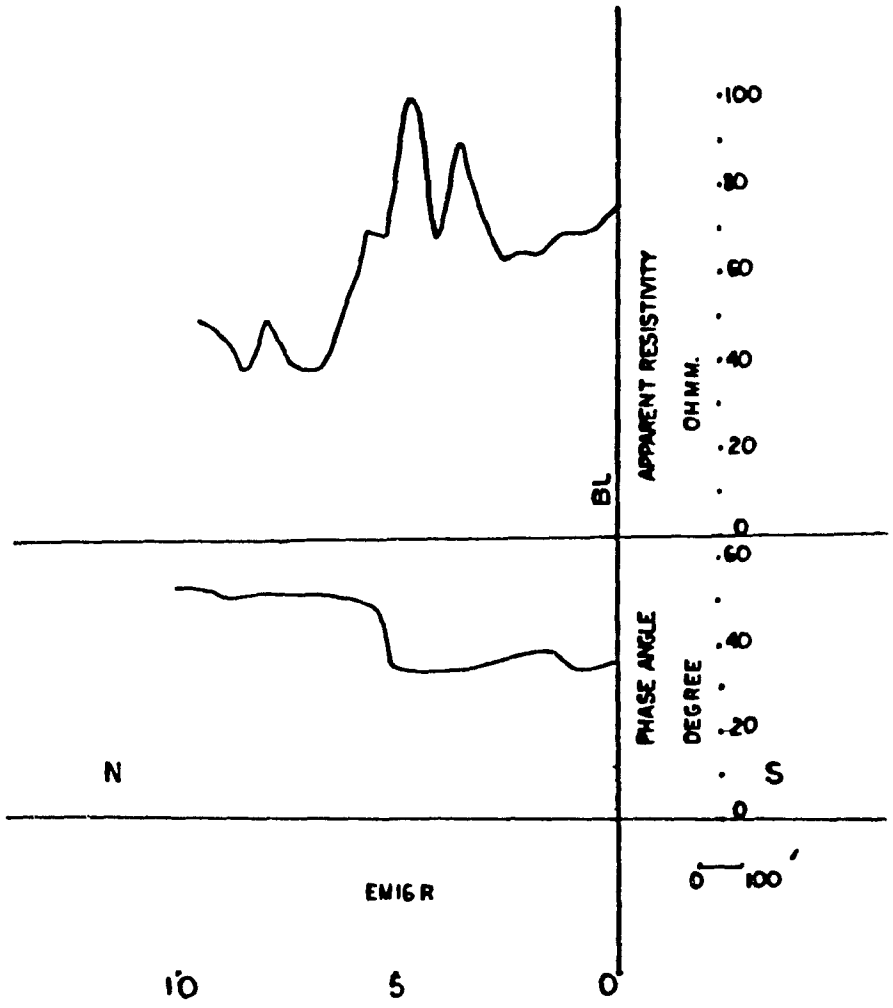

3.16B EM-16R Profile on Line 4+00W (Area I)

The EM-16R profiles approximately coincide with the EM-16 response (see fig. 3.17 a,b).

The abrupt changes in the apparent resistivity on line 4+00E between stations 2+00N and 2+25S may be due to bumps in the bedrock topography. This is also true between stations 5+50N and 2+25N of line 4+00W.

3.7 Area II : EM-16 and EM-16R Results

Figures 3.18-3.22 show the EM-16 profiles obtained by the traverses in the area II. Profile 1 was taken entirely along a path, while Profiles 3 and 4 were following roads ; and Profiles 2 and 5 were in farmland. The sharp cross-over between 5+00N and 5+00S (ie. when the road to St-Constant was crossed) was caused by a buried telephone and power line on the south side of the road. In fact, except for the anomalies caused by artificial objects there is no definite anomaly nor any anomalous response on these profiles.

Unfortunately, no more profiles could be done because the need to avoid houses and damage to crops. There were also a great deal of artificial objects such as power lines, telephone cables, etc. which accompany such densely populated areas.

Line 0+00 (path): (fig.3.18)

The large crossovers between 5+00N and 5+00S were caused by a buried telephone cable and a power line near station 0+00. According to Clark (1972), the fault should

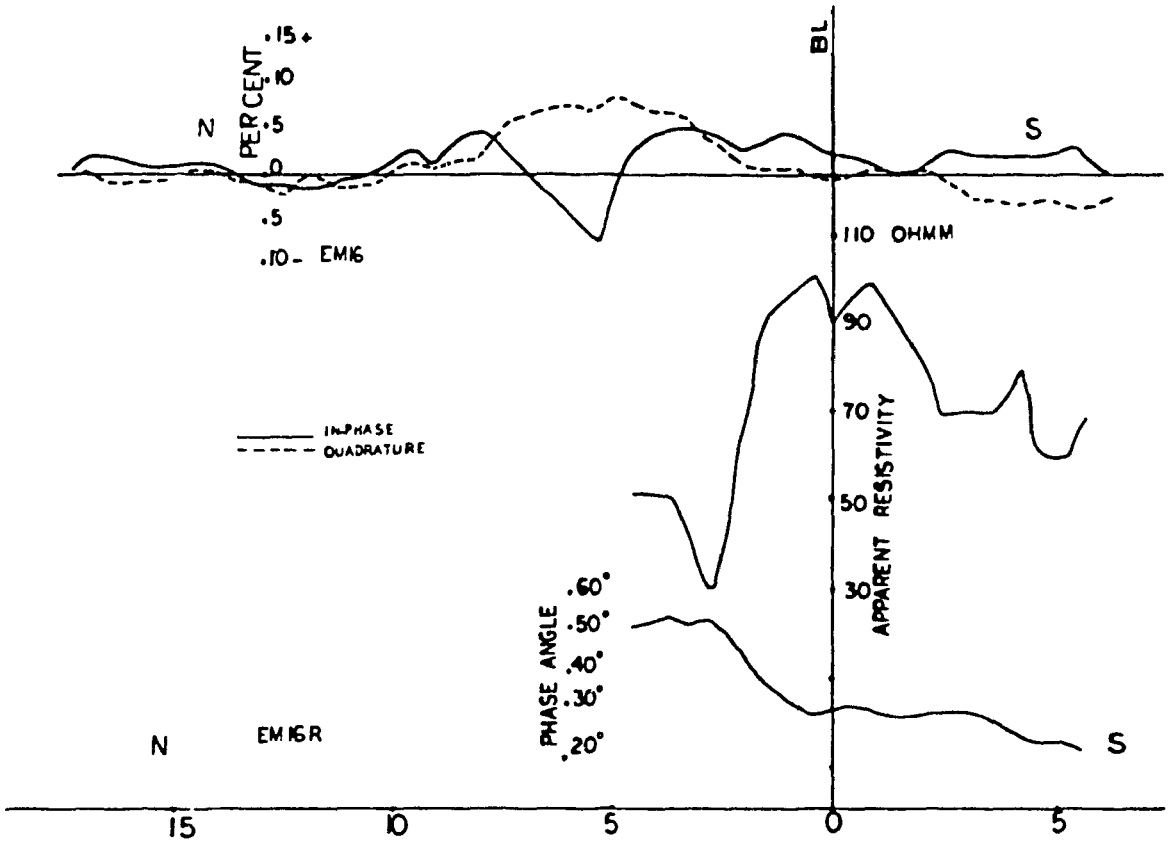

3.17A EM-16 and EM-16R Profiles on Line 4+00E (Area I) .

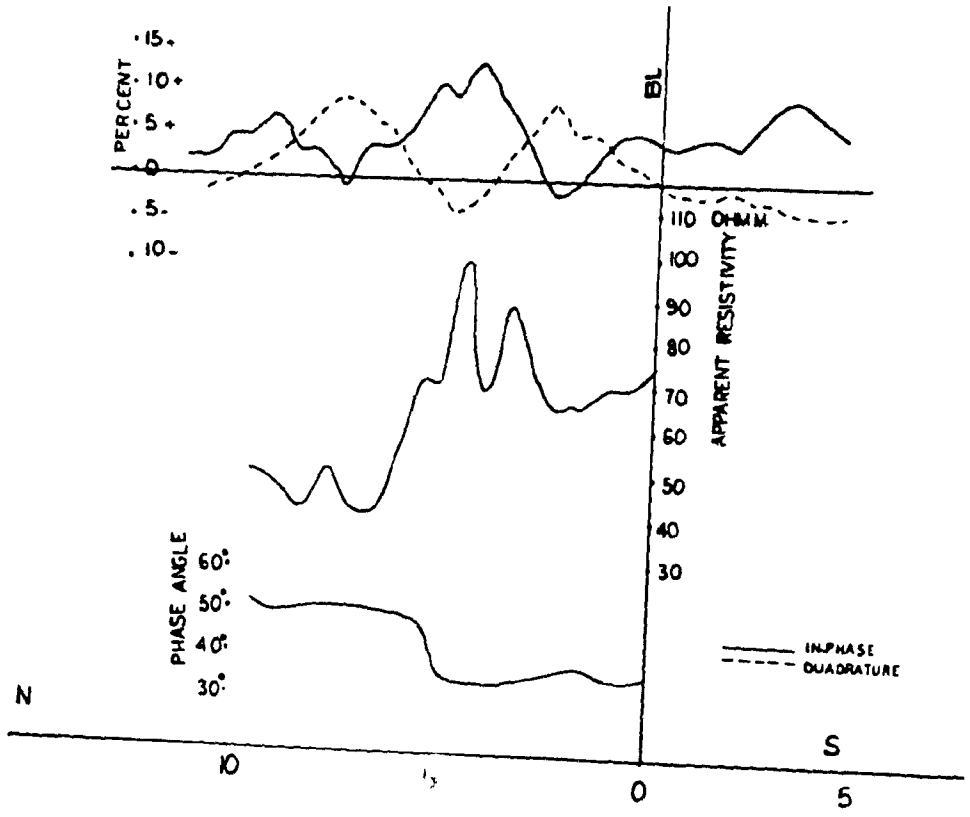

3.17B EM-16 and EM-16R Profiles on Line 4+00W (Area I) .

3.18 EM-16 Profile on Line 0+00 (Area II) .

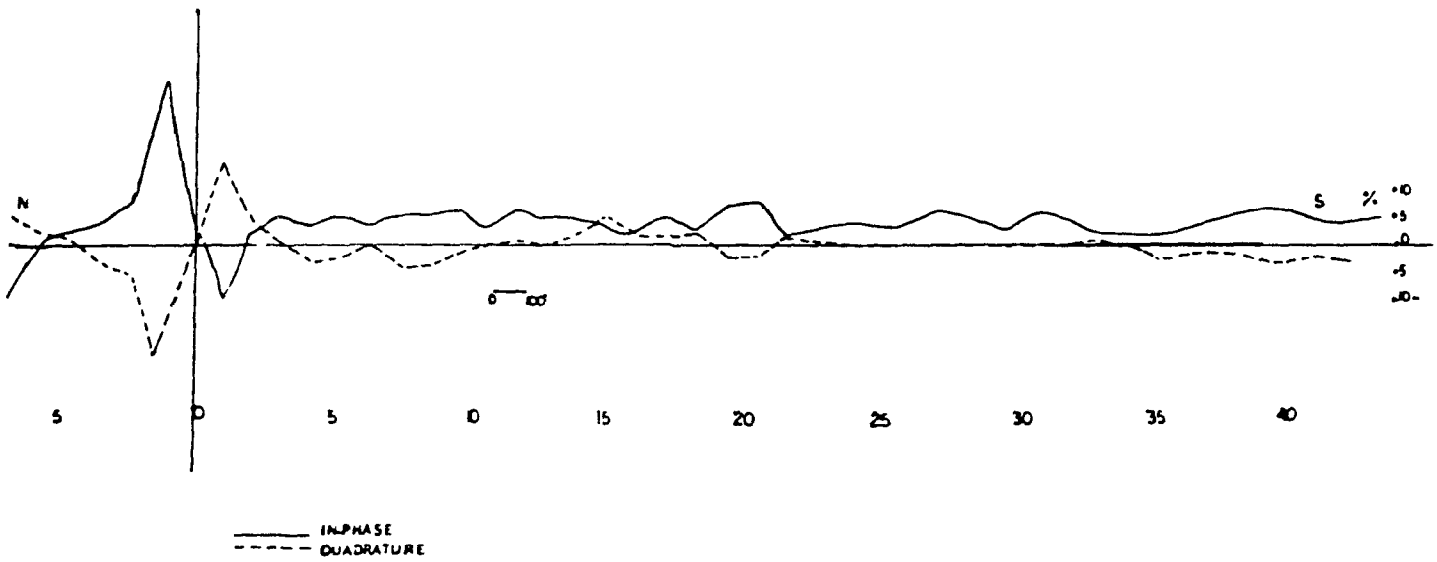

3.19 EM-16 Profile on Line 1+00E (Area II) .

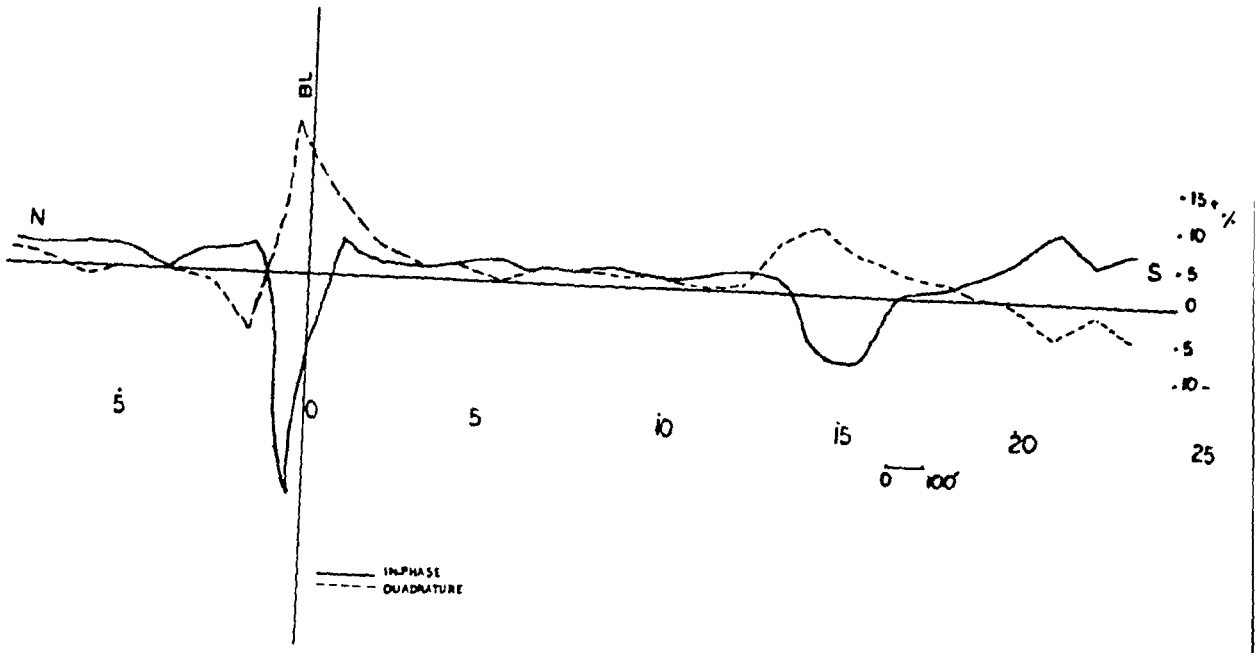

3.20 EM-16 Profile on Line 1+00W (Area II) .

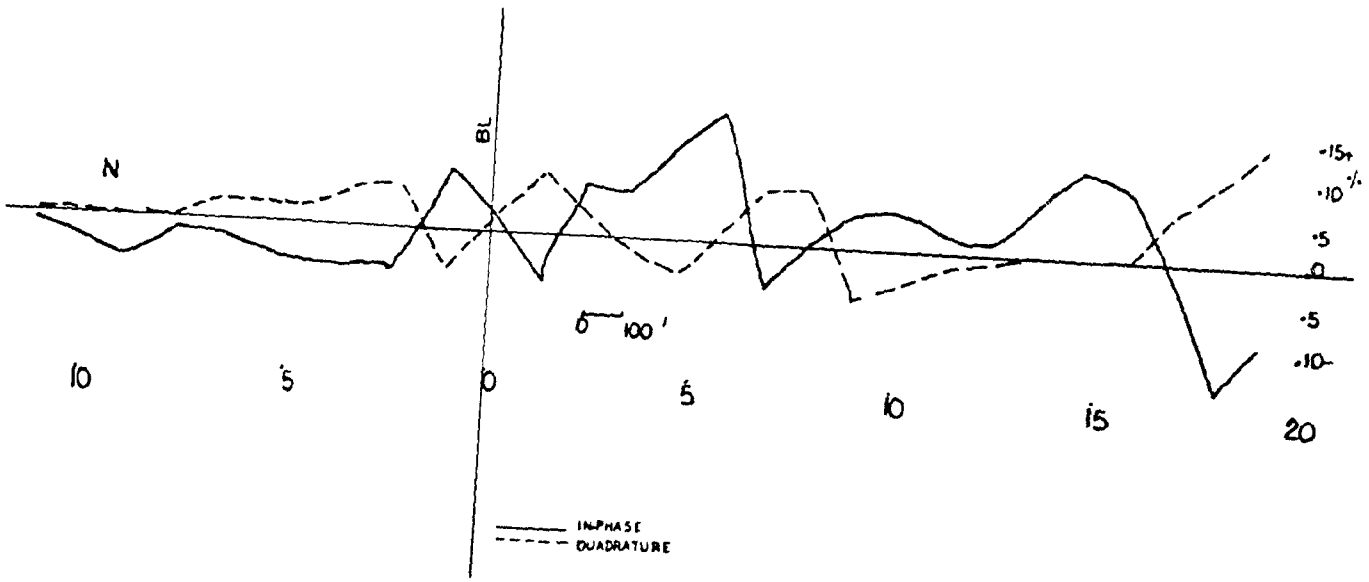

3.21 EM-16 Profile on Line 2+00E (Area II) .

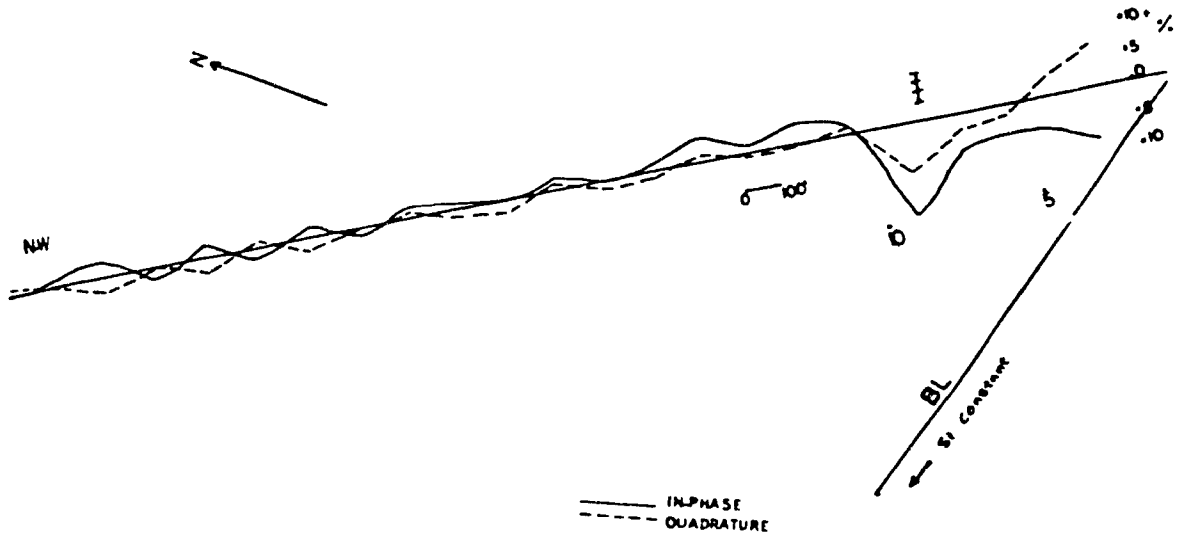

3.22 EM-16 Profile on Line 1+00NW (Area II) .

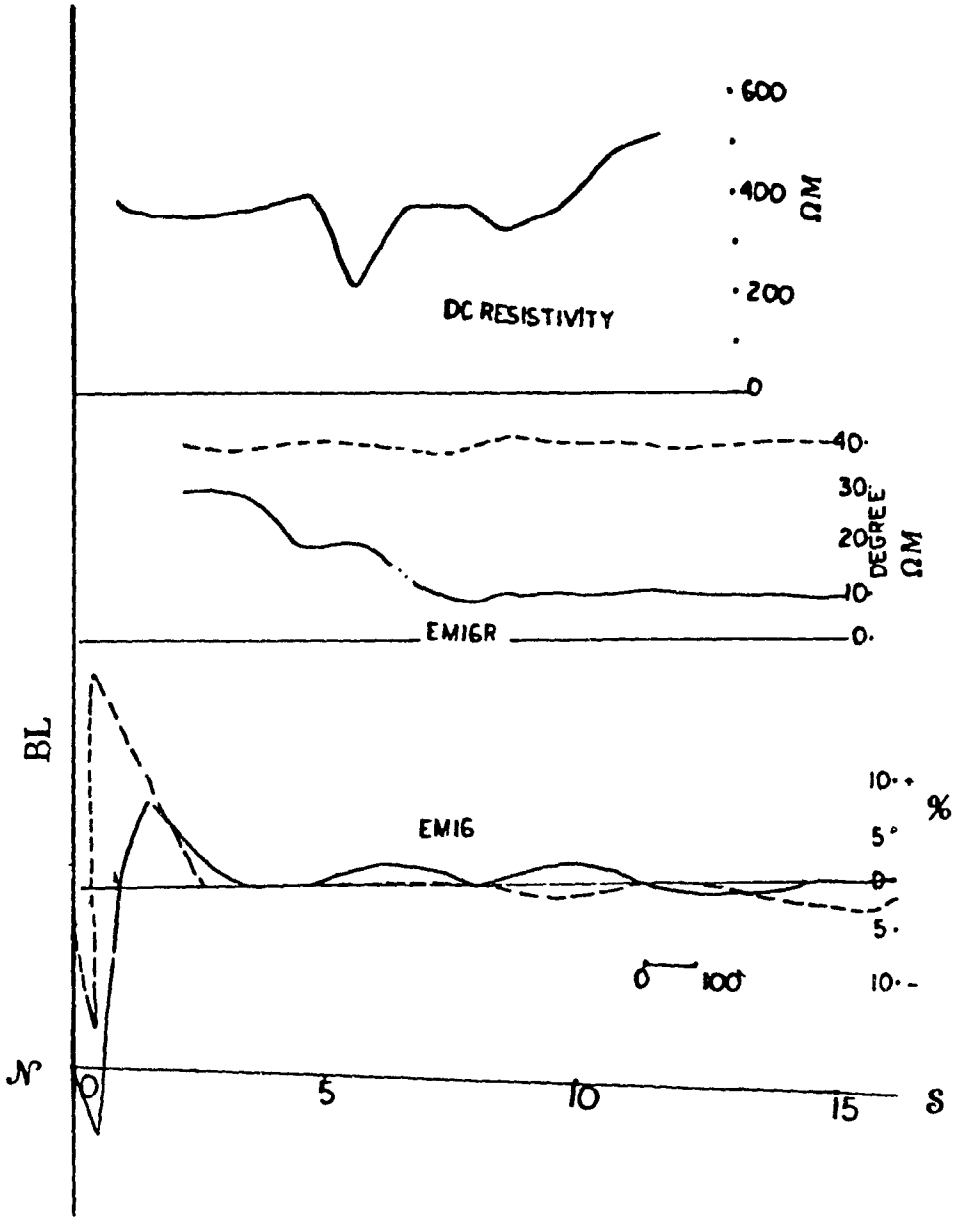

3.23 EM-16 and EM-16R Profiles on Line 0+00E (Area II)

have occurred in the vicinity of 12+00S on the profile. Globensky (1982) indicated that the fault strikes in the vicinity of station 17+00S. According to the EM-16 result, even though the fault is located on geological maps, it cannot be detected unless one assumes the bump in the vicinity of 6+00N to be a contact response. The EM-16R and DC resistivity results , on the other hand, show a contact type response in the vicinity of station 7+00S, while there was no such indication on the phase angle profile (see fig. 3.23).

The remainder of the profiles were generally noisy, especially line 2+00E because of the road and other man-made objects.

3.8 Area III: EM-16 and EM-16R Results

Figures 3.24-3.28A,B show the profiles obtained by traverses in area III. This area lies north-west of area II, where a contact between the Tetreauville formation and the Lachine formation occurs which strikes approximately north-south. According to Globensky (1982), this is a contact between limestone-shale in the east, and shale in the west. Four EM-16 east-west traverses were conducted in this area, the results gave similar profiles. Almost all profiles show a very slight bump on the in-phase and quadrature components between station 15+00E and station 20+00E, where the contact is expected to occur. This may be due to the low resistivity contrast between the formations or may also be due to the overlap of shale across the

contact. Resistivity results with DC and EM-16R support the geology by showing a contact type response at station 17+00E (see fig. 3.28 a, b). A fence on the east side of the road may have caused the high readings in the in-phase component at the beginning of the profiles. The profiles could not be extended any more to the east because of a power line and a fence.

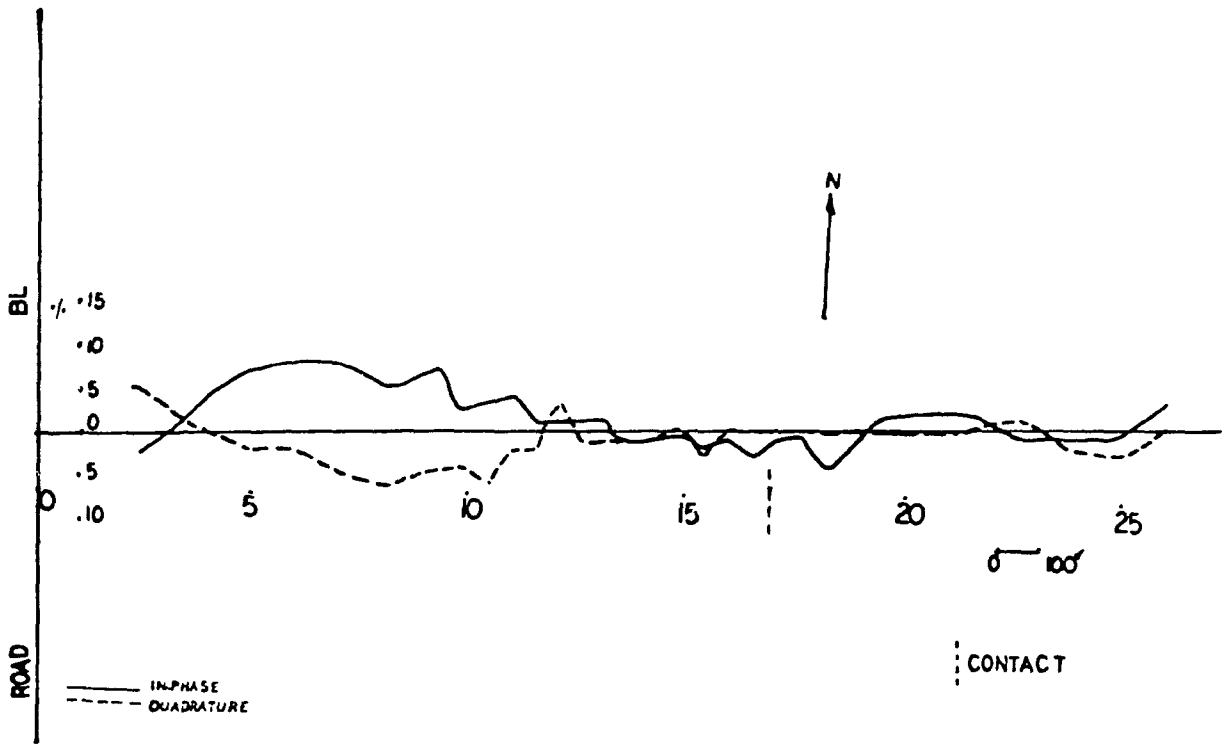

3.24 EM-16 Profile on Line 1+00E (Area III) .

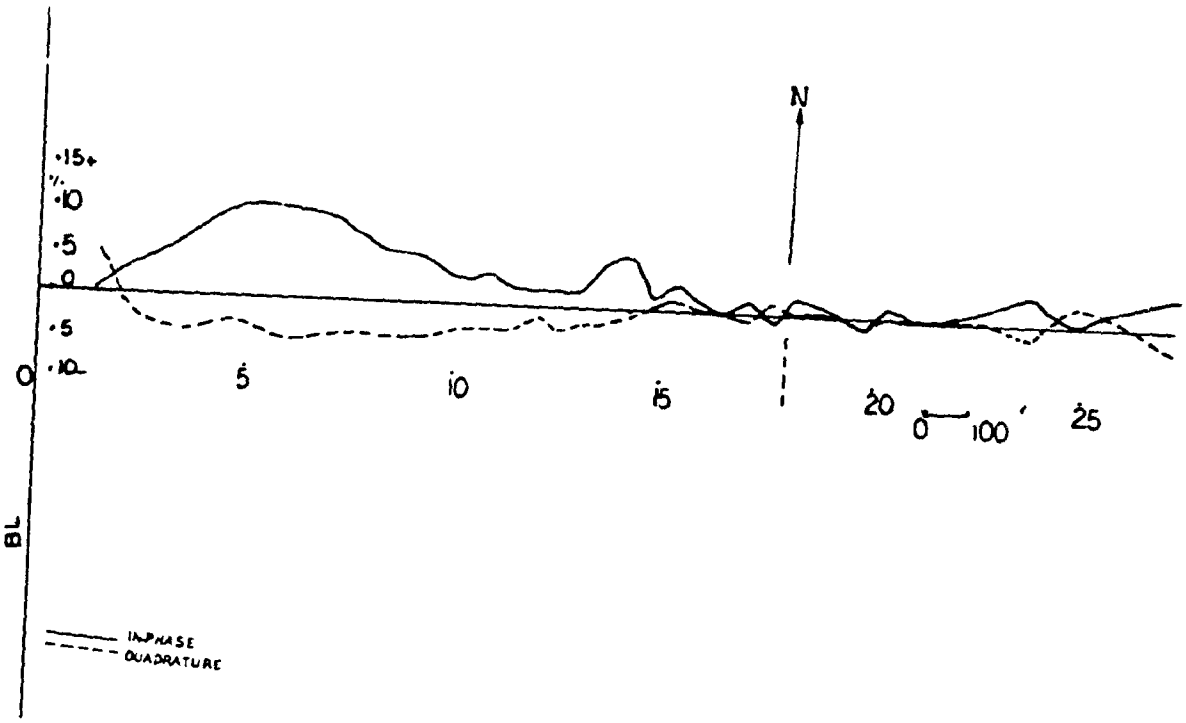

3.25 EM-16 Profile on Line 2+00E (Area III) .

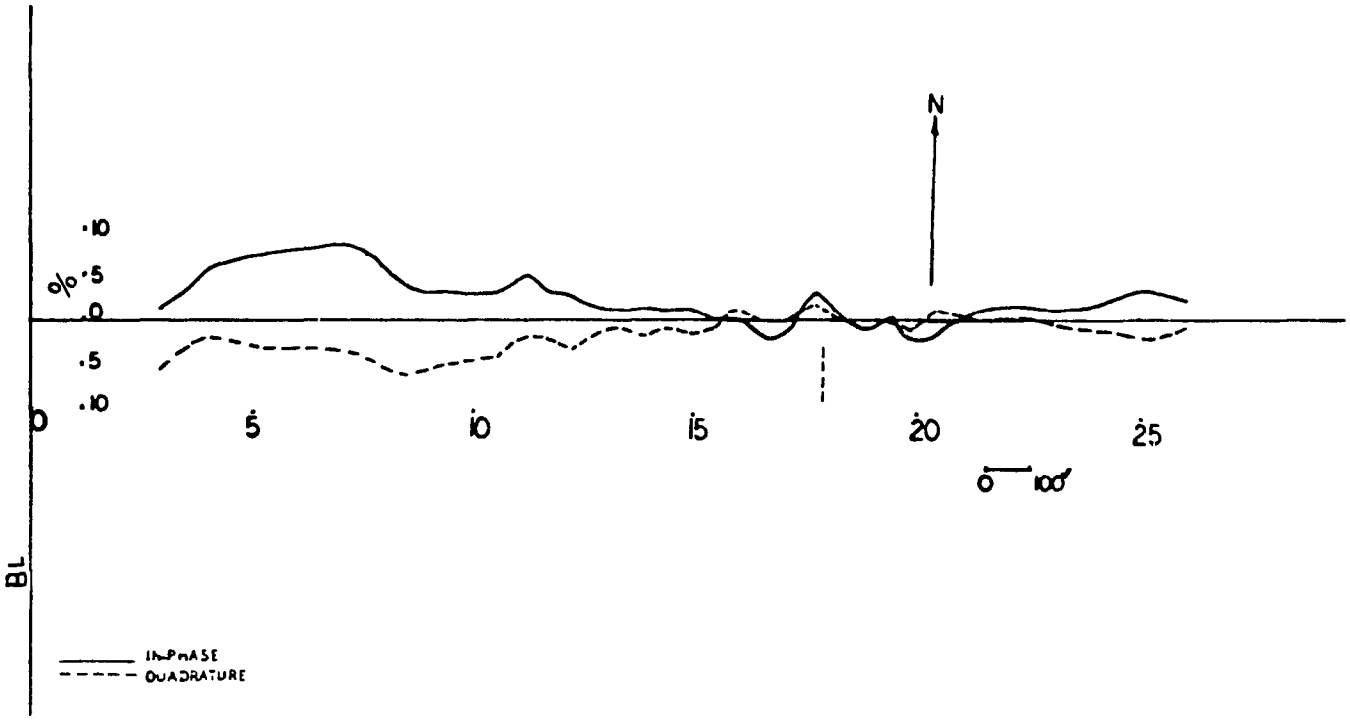

3.26 EM-16 Profile on Line 3+00E (Area III) .

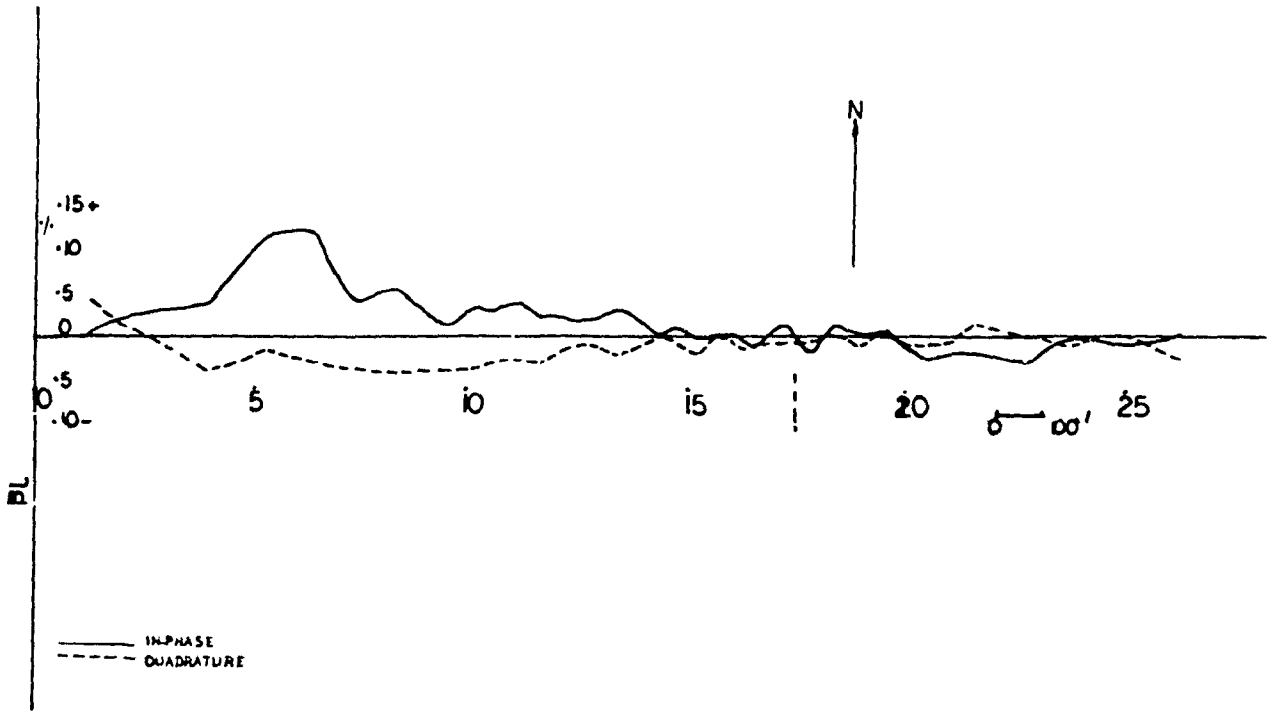

3.27 EM-16 Profile on Line 3+00E (Area III)

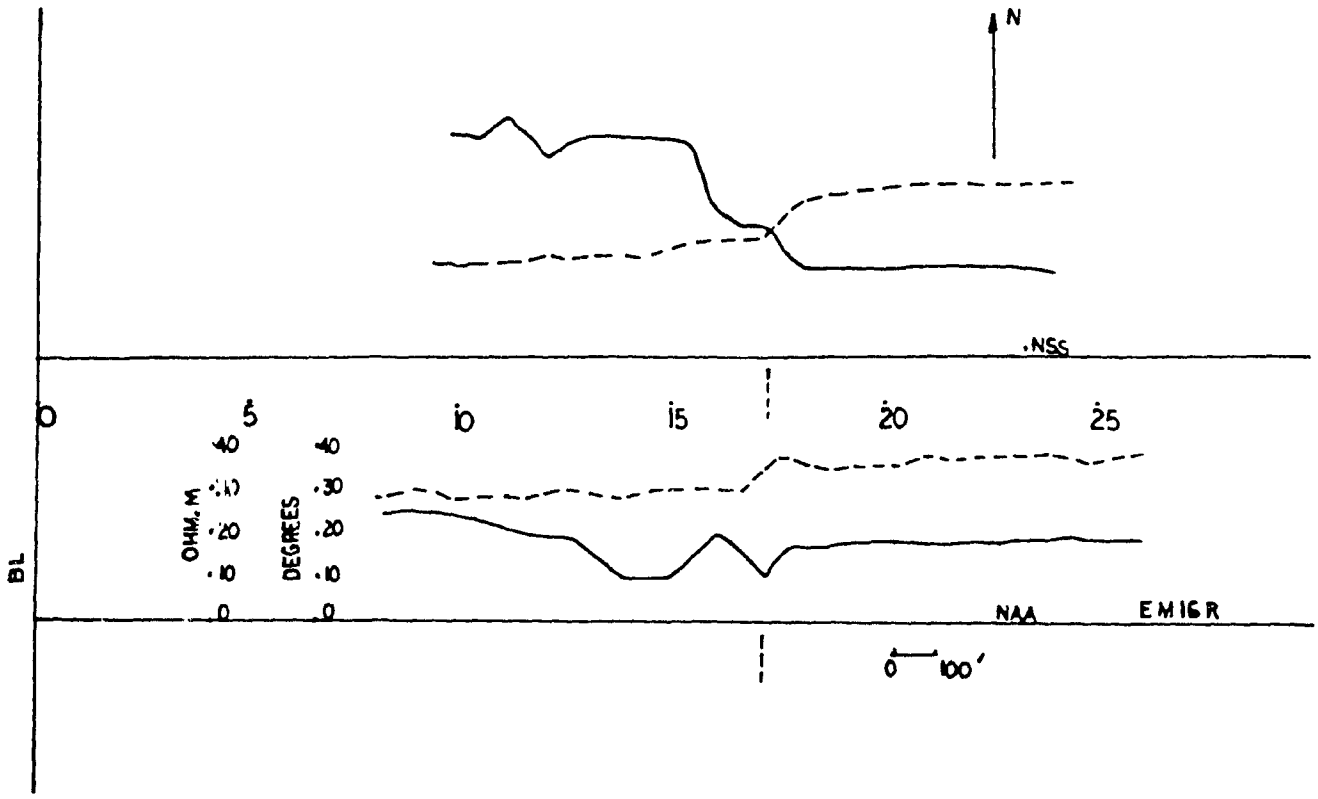

3.28A EM-16R Profile on Line 6+00E (Area III)

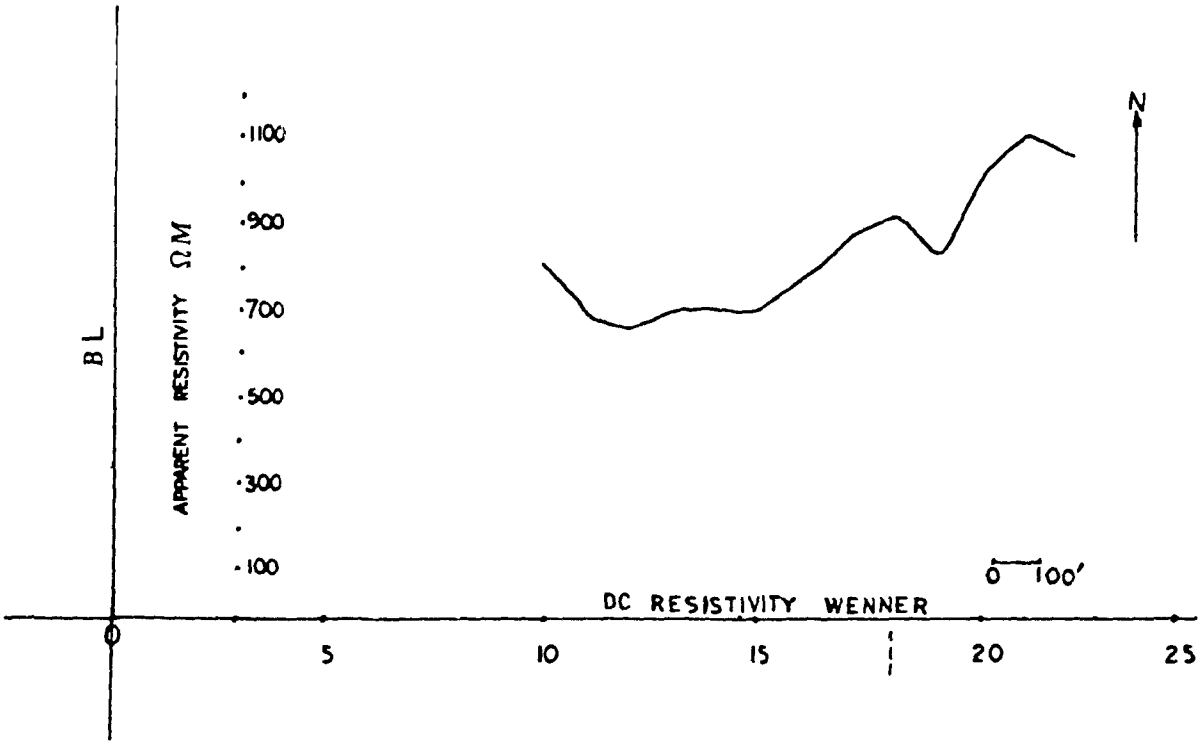

3.28B DC Wenner Resistivity Profile on Line 6+00E (Area III)

3.9 Interpretation of Joint EM16R Resistivity, Phase angle and DC Resistivities :

3.9.1 Introduction

All resistivity methods employ an artificial source of current which is introduced into the ground through point electrodes or long line contacts. The procedure then is to measure potentials at other electrodes in the vicinity of the current flow. In most cases the current is noted as well; it is then possible to determine an effective or apparent resistivity of the subsurface.

In the Wenner spread the electrodes are uniformly spaced in a line (see fig.3.29). The apparent resistivity is :

$$\rho a = 2\pi a \, (\nabla V/I) \qquad (\Omega.m)$$

Wenner spread (depth sounding) and Wenner profiling (mapping) were used in this study.

For depth exploration using the Wenner spread,the electrodes are expanded about a fixed centre, increasing the spacing a in steps (see results in appendix I). For lateral exploration, the spacing remains constant and all four electrodes are moved along the line, then along another line, and so on. In lateral exploration the

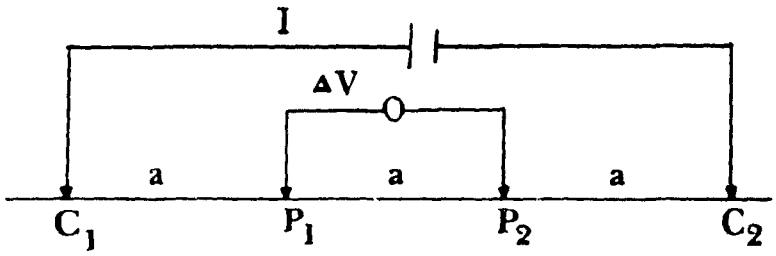

3.29 Wenner Array .

apparent resistivity for each array position is plotted again the centre of the spread. In this study a = 100 feet (≈30.5 m).

3.9.2 Resistivity Inversion

The inversion of geophysical field data involves two steps. The first step is solving the forward problem, i.e calculating the response of an assumed model. The second step is the inverse problem, which is mathematical adjustment of the model so that the response fits the field data as closely as possible. Complete treatment of inversion of geophysical field data will be discussed in the magnetic data inversion in chapter 5.

The program used was developed and written by Philip A. Davis at the University of Minnesota. This program contains two parts; program Resist to yield the theoretical apparent resistivity values from a specified layered earth model. The original concept for this methode of computing apparent resistivity is due to Ghosh (1971). The second part of this program is Inverse to yield apossible layered earth model from field measurements of apparent resistivity. The program is based upon a concept presented by N.P. Merrick (1977). The purpose of the program is to compute a layered earth model whose theoretical apparent resistivities agree as closely as possible (in a least-squares sense) with the field ones. The program may be applied to a wide slection of field electrode

arrangements. These include the Schlumberger, Wenner, dipole-dipole, Wennerbeta, Wennergamma, and bipole-bipole .

3.9.3 VLF-EM16R Interpretation

Two-layer Model - Master Curves: Knowing (ρ_2/ρ_1):

This interpretation is based on Mathieson and Crossley (1981) at the Department of Geological Sciences, McGill University, Montreal. Interpretation of any two layer model can be done with the use of the master curves (see appendix II). In this case we assume the Earth has two layers, the upper with thickness h1, resistivity ρ_1 and the lower with resistivity ρ_2 and free-space values of μ , ϵ , are assumed throughout.

The interpretations procedure is as following :

(ρ_2 / ρ_1) is known from DC resistivity inversion

1-compute ρ_1 from $\rho_1 = \rho_a / |Q|$ (Ω m).

2-compute ρ_2 from $\rho_2 = \beta^2 \rho_1$ (Ω m).

3-compute h1 from $h1 = \alpha / \sqrt{w\mu/\rho_1}$ m.

Where α , β and Q can be located from the curves, whereas ρ_a , Φ are measured in the field.

3.10 Results:

The geoelectric 2-layer sections obtained by DC resistivity inversion and EM16R curves are presented here.

3.10.1 Area I: Line 4+00 E

A: DC resistivity inversion results :

ρ_1 = 25.9 ohm.m

h1 = 3.9 m

ρ_2 = 308 ohm.m

B: EM16R-Master curves results :

ρ_1 = 12 ohm.m

h1 = 2.1 m

ρ_2 = 142 ohm.m

3.10.2 Area II: Line 0+00 (path)

A: DC Resistivity inversion results :

ρ_1 = 17.9 ohm.m

h1 = 3.2 m

ρ_2 = 177.3 ohm.m

B: EM16R-Master curves results :

ρ_1 = 1.15 ohm.m

h1 = 0.15 m

ρ_2 = 11.4 ohm.m

The calculated data for both resistivity inversion and master curves are presented in appendix (I).

Chapter 4: Radioactive Survey : Radon Emanation
: Gamma-Ray

Chpter 4: Radioactive Methods

A:Radon Emanation Survey

4.1A General Theory

The conventional geophysical techniques (which include electrical, gravity, magnetic, seismic, and self-potential methods) depend on variations in the mechanical, chemical, electrical, or magnetic properties of rocks and minerals. In these methods the anomalies are usually caused by the contrast in properties such as electrical conductivity, density, susceptibility, and elasticity between rocks or between ore bodies and rocks.

In the case of a fault, for example, the anomaly is usually caused by the contrast in these properties on opposite sides of the fault zone or contact. However, in some cases a property change associated with the fault zone itself is principally responsible . For example, in the radon emanation method, the anomalies are usually believed to be associated with the fault zone itself, which provides channels for the transport of radon generated at a depth (Abdoh, A., 1985). In the present field area, both types of anomalies are expected, where shale and limestone are in fault contact, because of the greater uranium content of shale.

According to this, the method may be considered as a

very important tool in areas such as the Montreal region, which have a complex geology.

4.1.1A Radioactive Disintegration

According to the Law of Radioactive Disintegration:

$$\int_{No}^{N} \frac{dN}{N} = -\lambda \int_{0}^{t} dt \qquad 4.1\ (a)$$

or $$N = N_o\, e^{-\lambda t}$$

where N_o = Number if radioactive nuclei at t = 0
N = Number of radioactive nuclei at time t
λ = Decay constant of radioactive species

any radioactive element in its decay will generally emit alpha beta particles and gamma radiation. The decay rates of radioactive species are often expressed in terms of half-life, $t_{\frac{1}{2}}$: the time required for half the initial number of parent nuclei to disintegrate.

$$N/N_o = e^{-\lambda t_{\frac{1}{2}}} = \tfrac{1}{2}$$

or $$t_{\frac{1}{2}} = \ln(2)/\lambda$$

The unit used to express the amount of radioactivity produced by a radioactive element is "Curie" (see Telford et al., 1976).

Table 4.1a,b,c taken from Abdoh's thesis (1985) gives the nuclides of the decay chains for Uranium 238, Uranium 235, and Thorium 232.

Among these are the three radon isotopes Rn^{222}, Rn^{220} and Rn^{219} which are members of the Uranium 238, Thorium 232, and Uranium 235 respectively. All three radon isotopes are gases at standard temperature and pressure and are soluble in water.

4.1A THE DECAY SERIES OF URANIUM 238

Element		Half-life	Decay constant sec^{-1}	Radiation
Uranium	92 U^{238}	4.51×10^{9} yr	4.9×10^{-18}	α, SF*, γ
Thorium	90 Th^{234}	24.1 d	3.3×10^{-7}	β, γ
Protoact.	91 Pa^{234}	6.7 hr	2.84×10^{-5}	β, γ
Uranium	89 U^{234}	2.48×10^{5} yr	8.9×10^{-14}	α, SF*, γ
Thorium	90 Th^{230}	8×10^{4} yr	2.75×10^{-10}	α, γ
Radium	88 Ra^{226}	1622 yr	1.35×10^{-11}	α, γ
Radon	86 Rn^{222}	3.82 d	2.07×10^{-6}	α, γ
Polonium	84 Po^{218}	3.05 m	3.8×10^{-3}	α, β
Astatine	85 At^{218}	1.35 s	0.51	α
Radon	86 Rn^{218}	0.03 s	----	α
Bismuth	83 Bi^{214}	19.7 m	5.85×10^{-4}	β, α, γ
Polonium	84 Po^{214}	1.64×10^{-4} S	4.2×10^{-3}	α
Lead	82 Pb^{214}	26.8 m	4.3×10^{-4}	β, γ
Lead	82 Pb^{210}	21 yr	1.05×10^{-9}	β, γ
Bismuth	83 Bi^{210}	5 d	1.58×10^{-6}	β
Polonium	84 Po^{210}	138.4 d	5.7×10^{-8}	α, γ
Thallium	81 Tl^{210}	1.3 m	8.85×10^{-3}	β, γ
Thallium	82 Tl^{206}	4.2 m	----	β
Lead	82 Pb^{206}	stable		

Abbreviations: yr = year, d = day, hr = hour, m = minute, s = second

4.1 A The Decay Series of Uranium 238, Uranium 235, and Thorium 232 .

4.1B THE DECAY SERIES OF URANIUM 235

Element		Half-life	Decay constant SEC^{-1}	Radiation
Uranium	92 U^{235}	7.1×10^{-8} yr	3.1×10^{-17}	α, SF*, γ
Thorium	90 Th^{231}	25.6 hr	7.4×10^{-6}	β, γ
Protoact.	91 Pr^{231}	3.4×10^{4} yr	6.5×10^{-13}	α, γ
Actinium	89 Ac^{237}	21.6 yr	10^{-9}	β, α, γ
Thorium	90 Th^{227}	18.2 d	4.35×10^{-7}	α, γ
Francium	87 Fr^{223}	22 m	5.2×10^{-4}	β, α, γ
Radium	88 Ra^{223}	11.7 d	6.76×10^{-7}	α, γ
Radon	86 Rn^{219}	4 s	0.17	α, γ
Astatine	85 At^{219}	54 s	1.28×10^{-2}	α, β
Polonium	84 Po^{215}	1.8×10^{-3} s	3.8×10^{2}	α, β
Astatine	85 At^{215}	10^{-4} s	6.9×10^{3}	α
Bismuth	83 Bi^{215}	8 m	1.44×10^{-3}	β
Bismuth	83 Bi^{211}	2.15 m	5.35×10^{-3}	β, α, γ
Polonium	84 Po^{211}	0.52 s	1.32	α, γ
Lead	82 Pb^{211}	36 m	3.2×10^{-4}	β, γ
Thallium	81 Tl^{207}	4.8 m	2.4×10^{-3}	β, γ
Lead	82 Pb^{207}	stable		

For abbreviations, refer to Table 4.1.a

SF* = spontaneous fission

4.1C THE DECAY SERIES OF THORIUM 232

Element		Half-life	Decay constant SEC^{-1}	Radiation
Thorium	90 Th^{232}	1.4×10^{10} yr	1.58×10^{-18}	α, SF*, γ
Radium	88 Ra^{228}	6.7 yr	3.3×10^{-9}	β, γ
Actinium	89 Ac^{228}	6.1 hr	3.1×10^{-4}	β, γ
Thorium	90 Th^{228}	1.91 yr	1.15×10^{-8}	α, γ
Radium	88 Ra^{224}	3.64 d	2.2×10^{-6}	α, γ
Radon	86 Rn^{220}	54.5 s	1.3×10^{-2}	α, γ
Polonium	84 Po^{216}	0.16 s	4.3	α
Lead	82 Pb^{212}	10.6 hr	1.8×10^{-5}	β, γ
Bismuth	83 Bi^{212}	60.6 m	1.9×10^{-4}	β, α, γ
Polonium	84 Po^{212}	0.3×10^{-6} s	2.3×10^{6}	α
Thallium	81 Ti^{208}	3.1 m	3.7×10^{-3}	β, γ
Lead	82 Pb^{208}	stable		

For abbreviations, refer to Table 4.1.a

SF* = spontaneous fission

Being noble gases, their transport by gaseous diffusion and gas flow is permitted through pore spaces in rocks and soils or surface waters. (For more details about formation, transport, exhalation, and factors affecting them see Fleischer et al., 1980, Tanner 1964, and Abdoh 1985.)

4.1.2A Formation of Radon 222 over Faults

Only radon 222 and radon 220 have sufficiently long half-lives to undergo significant transport in the soil from their site of formation. In fact, only radon 222 is widely used for geophysical applications because it has a half-life of about 3.82 days (see table 4.1).

According to Abdoh (1985), any subsurface variation in permeability can affect the vertical migration of radioactive gases thus altering the surface radiation pattern. Therefore, in the fault zone, the migration of radon 222 from the bedrock to the fault level is more rapid causing the radon 222 concentration to be higher over a fault zone.

However, the radon emanation method can only be used for mapping fault zones when the depth of overburden is not too great.

4.2A Ionization Chamber Method (Emanometer)

Most current instruments designed to detect radon gases drawn from the ground emanometers work by measuring the level of alpha radiation through an alpha detector using the principle that radon gases emit alpha particles when they undergo radioactive disintegration.

In this study, field measurements of the radon 222 content of the soil gases were made using the ETR-1 pump type emanometer designed and developed by Scintrex Ltd., Toronto.

The accuracy of the instrument is between 5 and 15% and the operating temperature range is from -10°C to 50°C.

The operation of this emanometer is as follows: a 60 cm hole is made in the ground by means of a pointed steel rod about 2 cm in diameter and a 5 kg sledgehammer. Immediately after the rod is withdrawn from the ground a probe is inserted, and the hole is sealed by pressing down on a sealing cone concentric with the probe which isolates the soil from atmospheric air. The concentration measurements begin immediately after the soil gas has been pumped into the chamber. These readings are carried out starting one minute after the air has been sampled. By that time most of the short-lived radon 220 has disintegrated so that the readings can be attributed mainly to radon 222. If another hole is needed at the same station, a new sampling hole should be located at least 30cm from the previous one, so that the new readings would not be distorted by the

soil's having been disturbed during the making of the previous hole. The Radon field operations is physically demanding and not more than 5 hours of work could be done in a single day.

For this field work, profiles were spaced 200 feet apart perpendicular to the fault strike. If in-between profiles were needed then the spacing was 100 feet apart.

The profiles had almost N-S strike and 8 m was the distance between stations.

4B : Gamma-ray Survey

Contrasts in radioactivity arising from variations in rock types and from radon diffusion can produce variations in gamma radiations at the soil surface. The variations can best be investigated using a scintillometer.

Telford (1976,p.749-750) gives an explanation and description of the scintillometer used for the detection of gamma rays .

A total of four profiles were measured in area I and area II. The result obtained will be discussed in the next chapter.

4.1B Radioactivity of Rocks and Minerals

Table 4.2 shows the background radioactivity in rocks and water. In general, the activity in sedimentary rocks and metamorphosed sediments is higher than that in igneous and other metamorphic types, with the exception of potassium rich granites (Telford et al., 1977, p.745).

Table 4.2: Background Radioactivity in Rocks and Waters

Rock	Curies/gm ($x10^{-12}$)	K (ppm)	Th (ppm)	U (ppm)
Hornblende	1.2			
Granite	0.7-4.8	35,000	15	4
Basalts	0.5	9000	2	0.6
Olivine	0.33			
Ultramafics		10	0.2	0.05
Marble	1.9			
Quartzite	5.0			
Sandstone	2-4			
Slates	3-8			
Dolomites	8			
Chalk	0-4			
Chondrites		850	0.08	0.02
Iron Meteor			0.015	0.04

Water	Curies/gm ($x10^{-12}$)
Saratoga, N.Y.	0.01-0.1
Bath, England	0.14
Carlsbad, Czech.	0.04-0.1
St-Lawrence River	0.00025
Valdemorillo, Spain	0.02
Aix-les-bains, France	0.002
Manitou, Colorado	0.003
Hot Springs, Ark.	0.0009
Atlantic Ocean	0.014-0.034
Indian Ocean	0.007

4.3 Results

4.3.1 Emanometer Method

Area II was not surveyed with the emanometer because the preliminary survey with the scintillation meter was not positive. Figures 4.1-4.6 are the results of traversing in area I with the emanometer. During the field work, the average background reading for all the stations was approximately ≈2 emans, where 1 eman is equal to 10 Curies per liter and the country rock (bedrock) was never reached when preparing sample holes.

From the above observations it can generally be concluded that except for two definite anomalies (one in line 2+00E, at station 9+00N fig. 4.1, and the other in line 1+00W, fig. 4.5, at stations 6+50N and 4+50N with values of ≈11.5 emans and 10 emans respectively) it was difficult to see any significant anomalies.

Generally, it may be stated that there is a trend in most of the profiles from higher readings in the north to lower readings in the south. The high trend could be from the shale content in the north, which may be considered more active than the limestone in the south.

4.3.2 Scintillation Meter Method (Area I & II):

Figures 4.7-4.8 show the results of traversing with the scintillation meter in area I and area II. Again, there were few definite high anomalies in the profiles, but the trend of the high readings from the north to the lower

readings in the south is very evident. The average readings in both areas were approximately 15 counts/minute.

There is a high reading in the vicinity of station 5+00S in line 2+00E in area I, but the reason for this anomaly is unknown.

Generally, the profiles fluctuate where the fault zone is expected to occur (see for example Line 2+00E and Line 1+00W, fig. 4.7 between stations 1+00N and 6+00N).

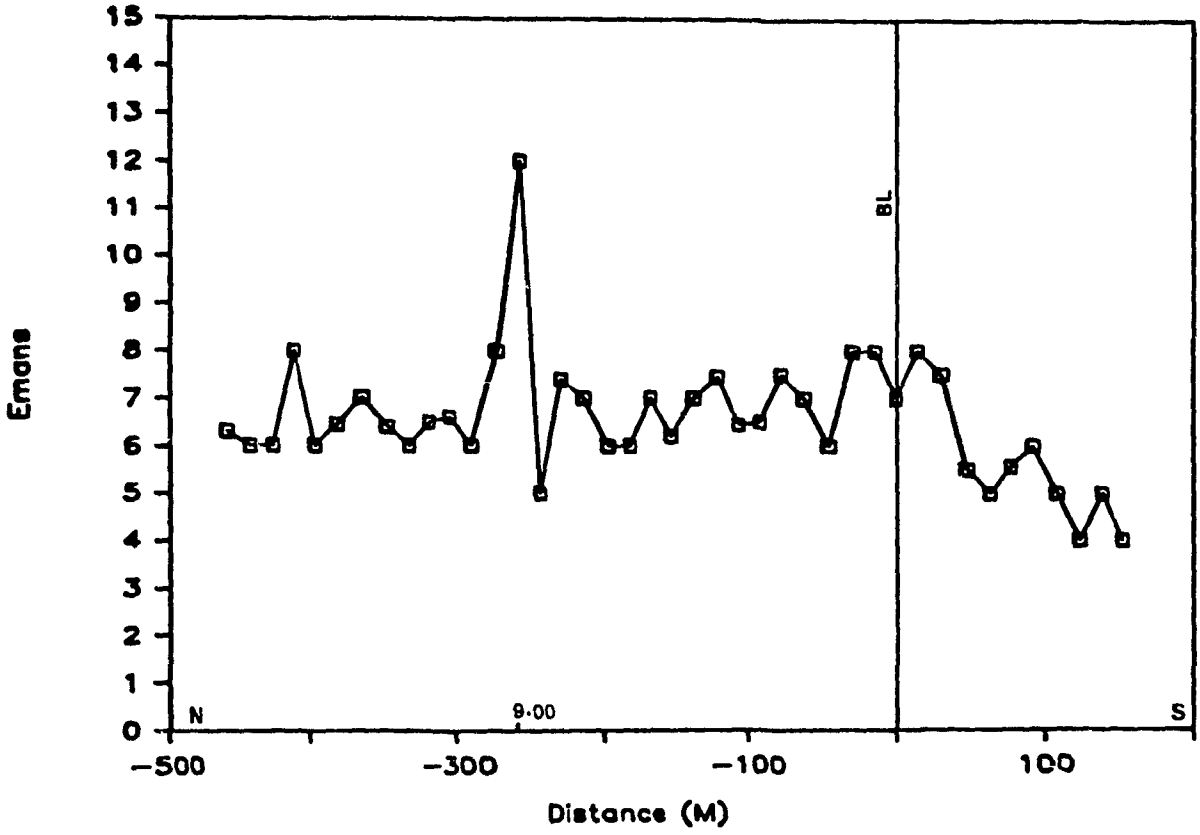

4.1 Radon 222 Profile on Line 2+00E (Area I) .

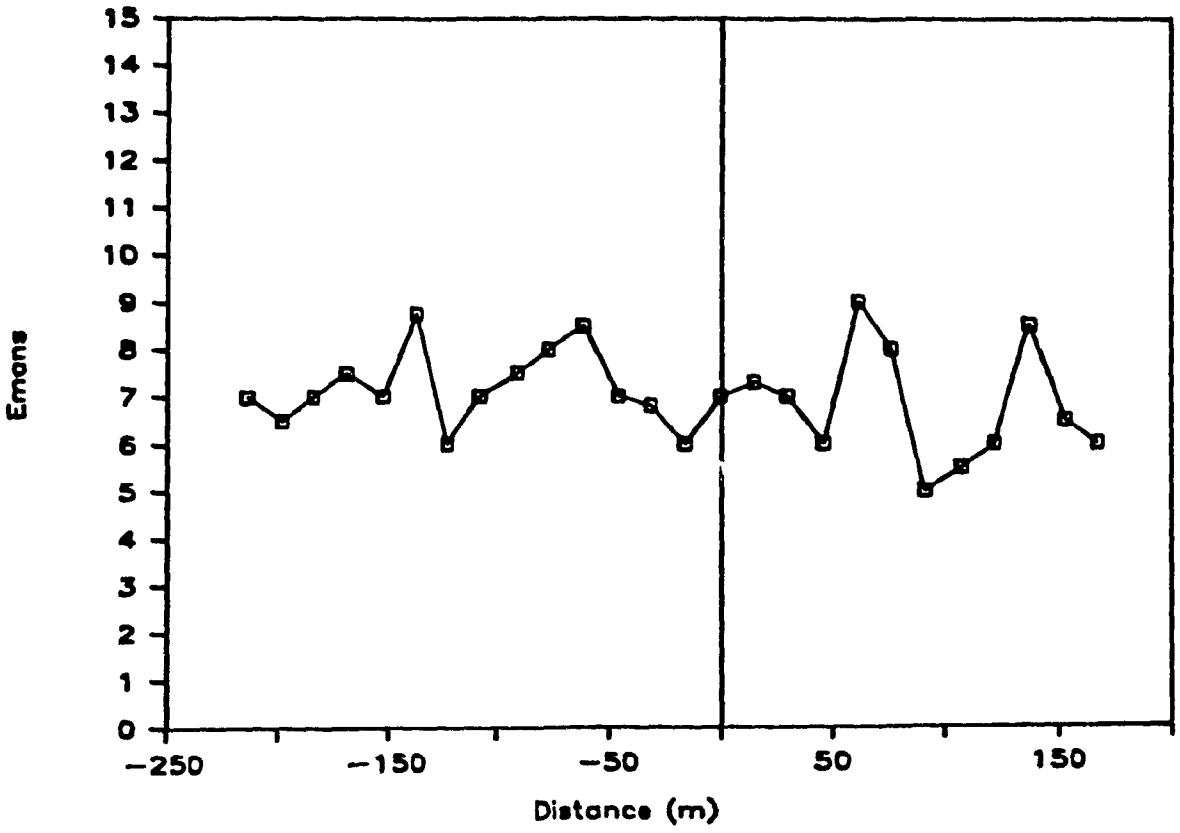

4.2 Radon 222 Profile on Line 6+00E (Area I) .

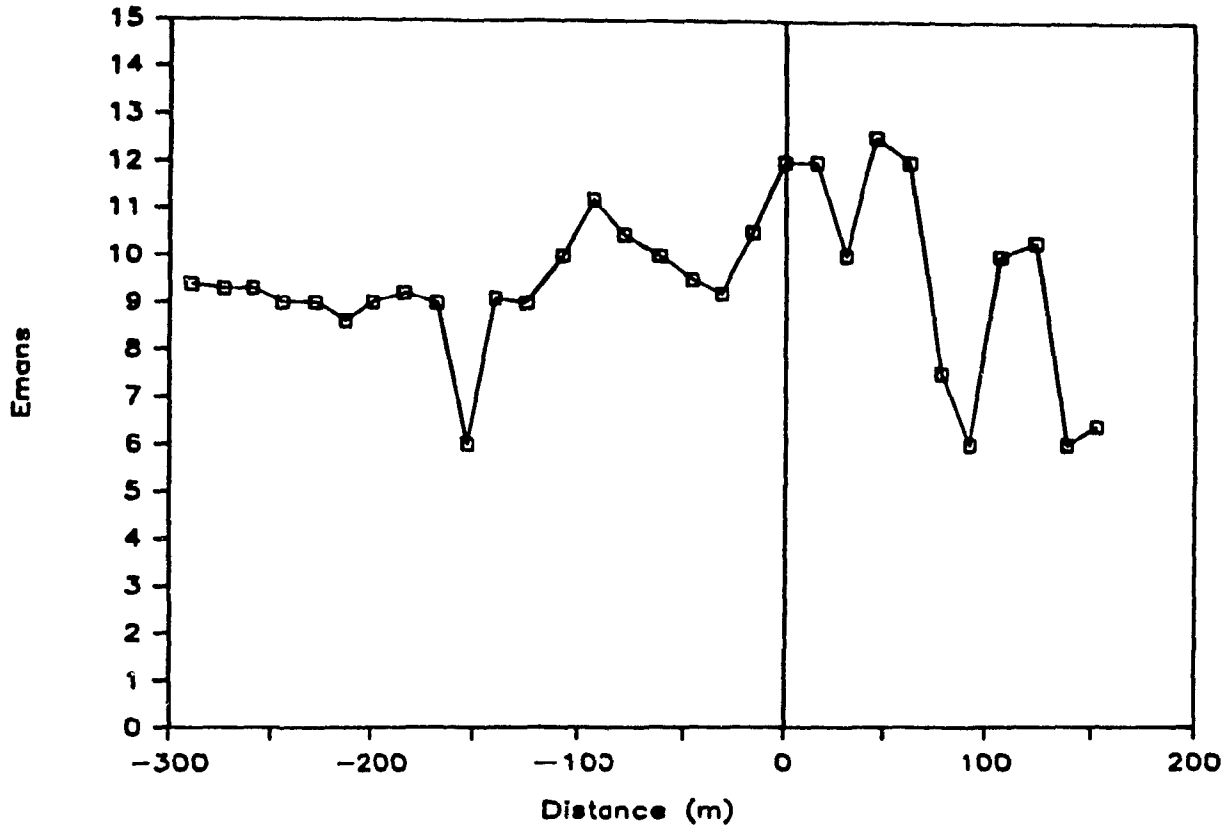

4.3 Radon 222 Profile on Line 7+00E (Area I) .

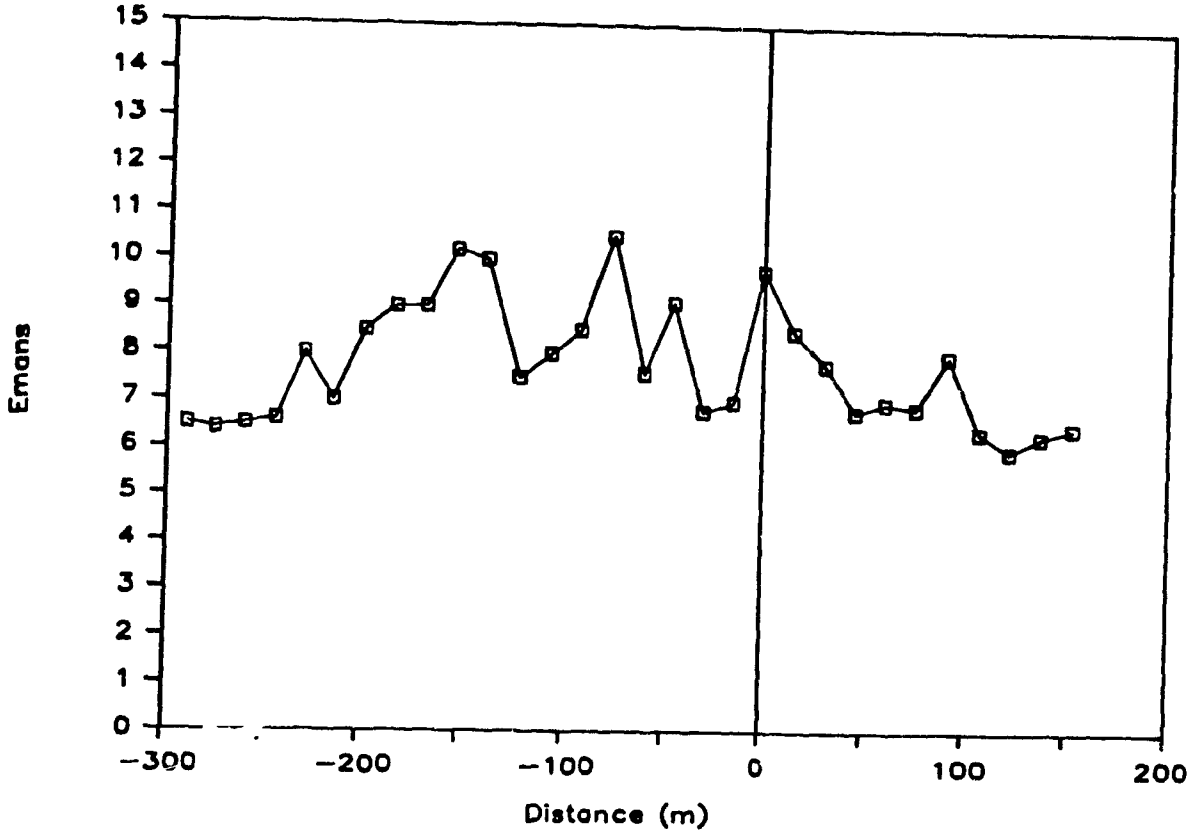

4.4 Radon 222 Profile on Line 8+00E (Area I) .

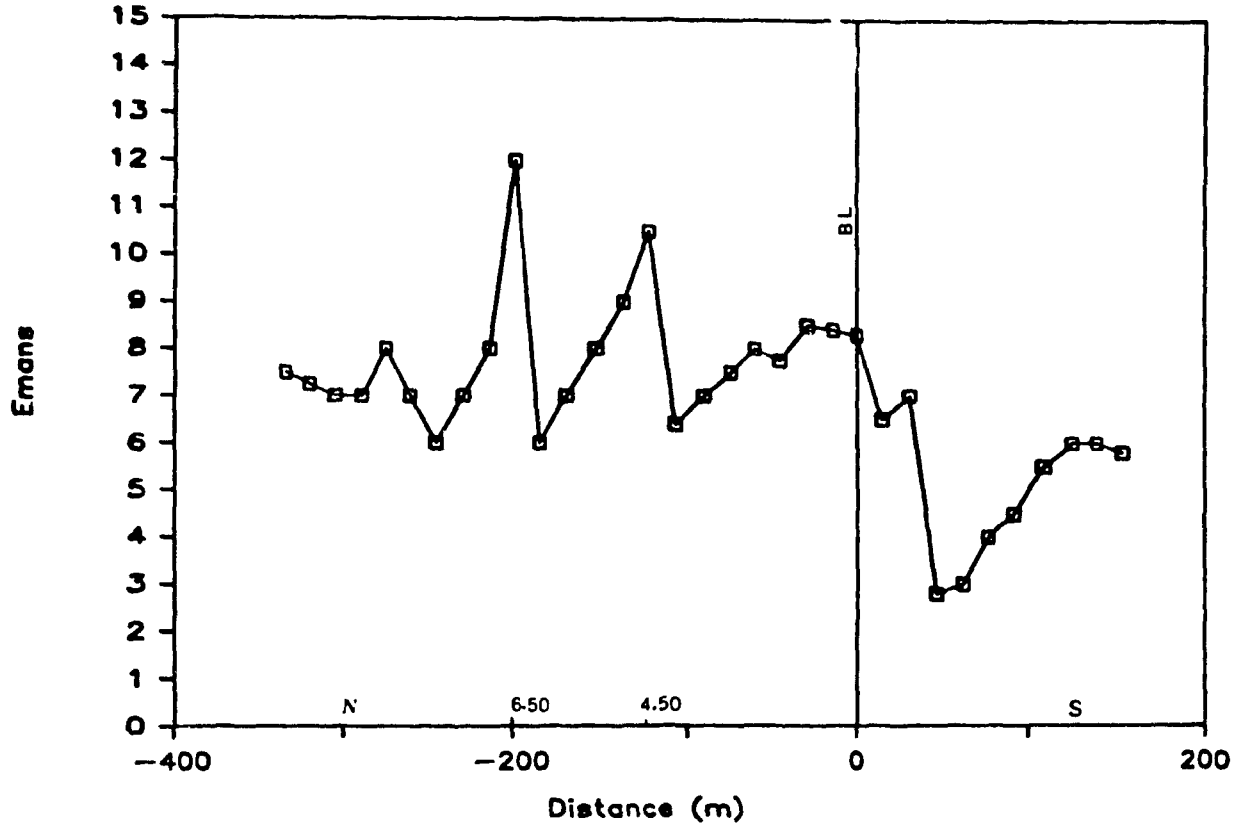

4.5 Radon 222 Profile on Line 1+00W (Area I)

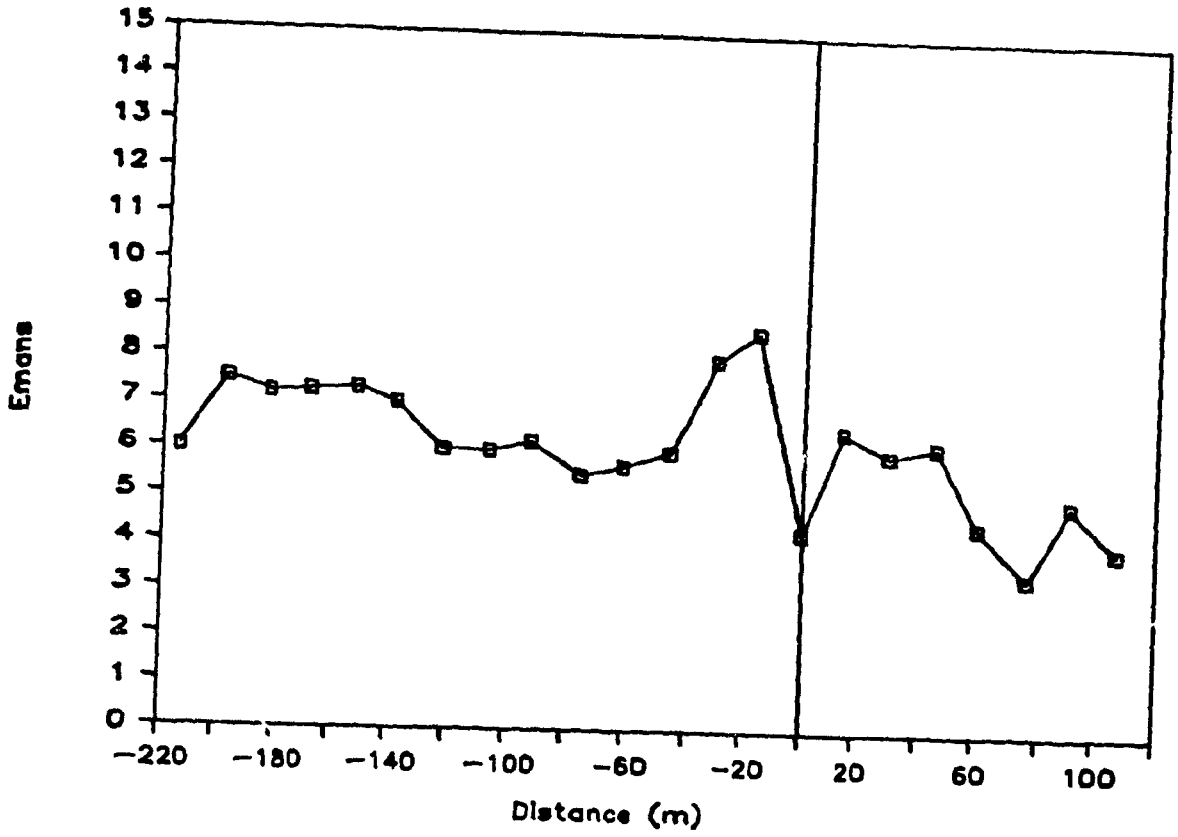

4.6 Radon 222 Profile on Line 2+00W (Area I) . .

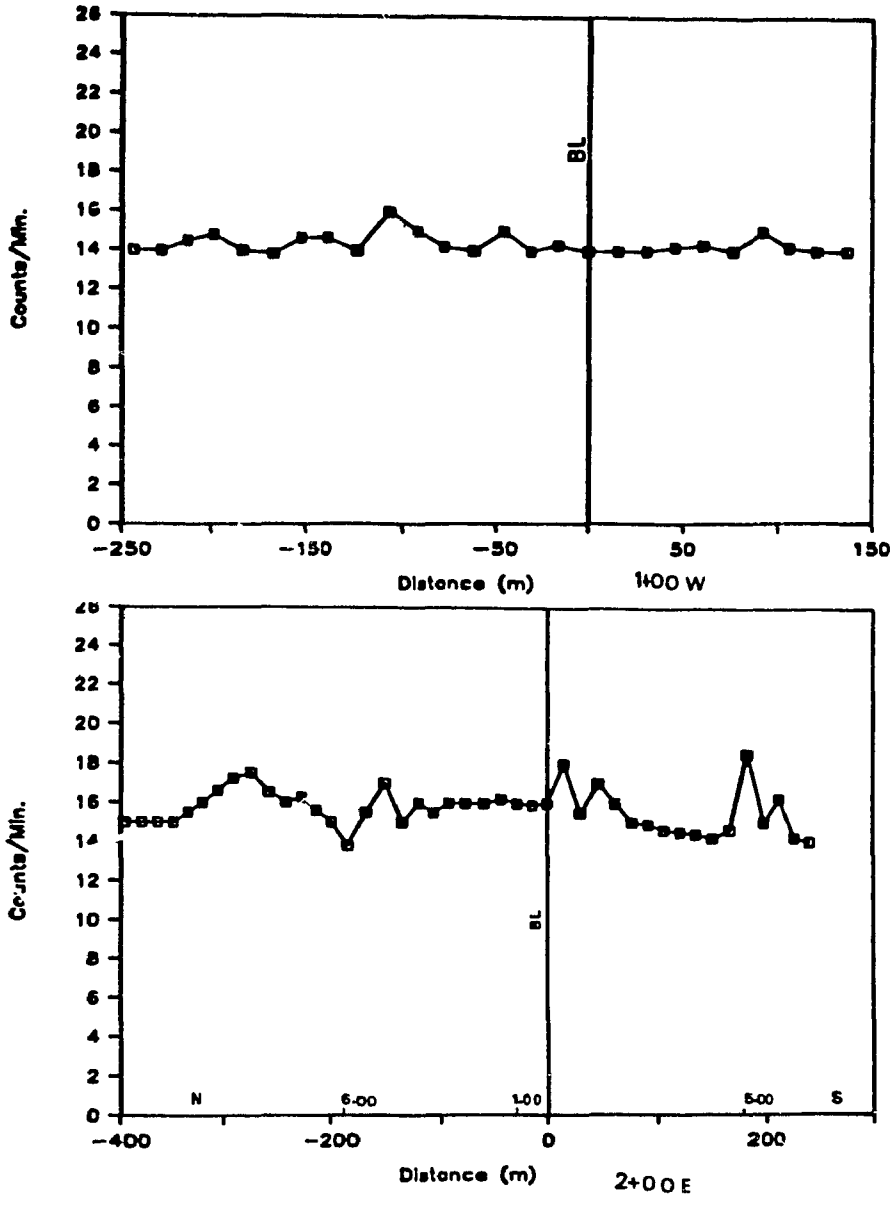

4.7 Scintillometer Profiles on Line 2+00E & 1+00W (Area I)

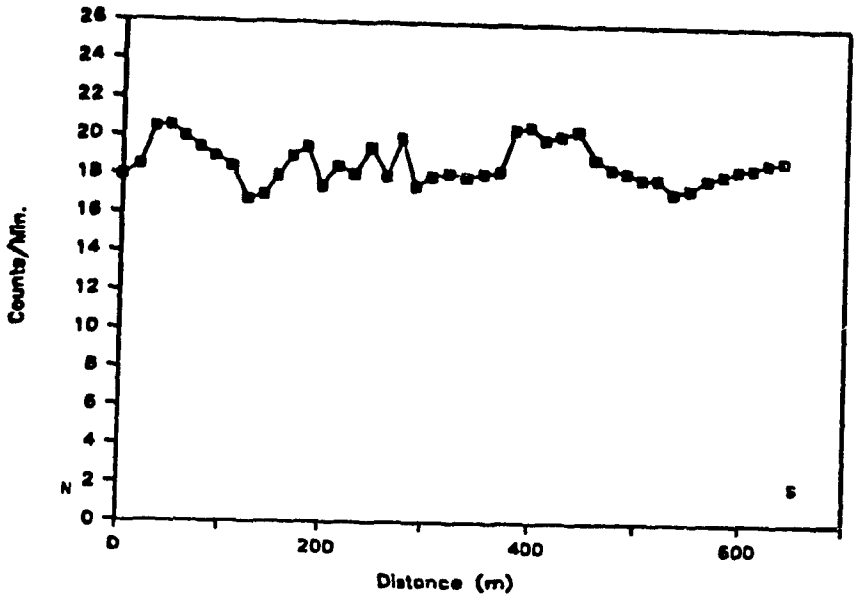

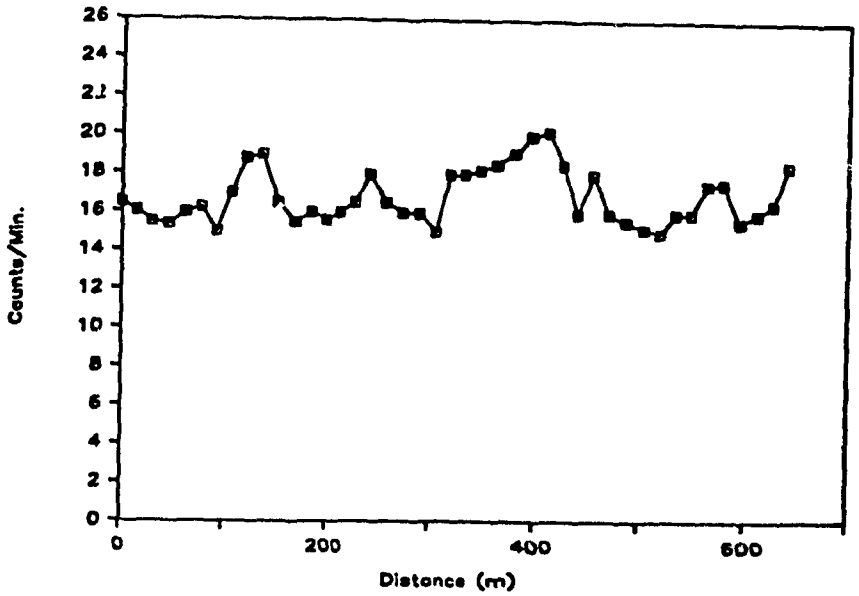

4.8 Scintillometer Profiles on Line 0+00 & 1+00E (Area II)

Chapter 5: Magnetic Survey

Chapter 5: Magnetic Survey

5.1 Equipment and Field Operations :

The magnetic survey was carried out in both areas I and II using a Sharp MF-1 flux-gate magnetometer with a sensitivity of 10 (nT). The instrument measures the vertical component of the magnetic field at every station.

Both areas were surveyed at stations 30 m apart and in-between stations were taken when there was a big change in the magnetic readings. The distance between the traverses was always 200 feet (≈65m) for area I.

According to Veinberg (1967) the two most important pieces of information which a magnetic survey produces are:

(1) Discovery of anomalous bodies characterized by a high magnetization.

(2) Mapping of different types of faults and other tectonic dislocations.

However, the ferromagnetic minerals, particularly magnetite, are the main source of local magnetic anomalies. Table 5.1 a and b show magnetic susceptibilities of some rock samples and various minerals (Telford et al., 1977, p.121).

The vertical magnetic intensity measured is produced by a combination of two vector sums of magnetization in the rock: remanant magnetization and induced magnetization. The remanant magnetization is determined by the geological

Table 5.1A: Magnetic Susceptibilities of Various Rocks

Type Susceptibility	Range	Average
Sedimentary		
Dolomite	0-75	10
Limestones	2-280	25
Sandstones	0-1660	30
Shales	5-1480	50
Av. Var. Sed. (48)	0-4000	75
Metamorphic		
Amphibolite		60
Schist	25-240	120
Phyllite		130
Gneiss	10-2000	
Quartzite		350
Serpentine	250-1400	
Slate	0-3000	500
Av. Var. Met. (61)	0-5800	350
Igneous		
Granite	0-4000	200
Rhyolite	20-3000	
Dolerite	100-3000	1400
Augite-Syenite	2700-3600	
Olivine-Diabase		2000
Diabase	80-13,000	4500
Porphyry	20-16,700	5000
Gabbro	80-7200	6000
Basalts	20-14,500	6000
Diorite	50-10,000	7000
Pyroxenite		10,500
Peridotite	7600-15,600	13,000
Andesite		13,500
Av. acid Ign.	3-6530	650
Av. basic Ign.	44-9710	2600

Table 5.1B: Magnetic Susceptibilities of Various Minerals

Type	Susceptibility Range	$x10^6$ emu Average
Graphite		-8
Quartz		-1
Rock Salt		-1
Anhydrite, Gypsum		-1
Calcite	-0.6--1	
Coal		2
Clays		20
Chalcopyrite		32
Sphalerite		60
Cassiterite		90
Siderite	100-310	
Pyrite	4-420	130
Limonite		220
Arsenopyrite		240
Hematite	40-3000	550
Chromite	240-9400	600
Franklinite		36,000
Pyrrhotite	$100-5x10^5$	125,000
Ilmenite	$2.5x10^4-3x10^5$	$1.5x10^5$
Magnetite	$10^5-1.6x10^6$	$5x10^5$

history and formation of the rocks, whereas induced magnetization depends primarily upon the magnetic susceptibility and the magnetic field.

Taking these into account and correlating them with the geology of the area, it should be easier to establish the sources of the magnetic anomalies.

5.2 Results

5.2.1 Qualitative Interpretation :

5.2.1.1 Area I :

The magnetic results for area I and area II are displayed as profiles. All the profiles in area I display clearly a well defined magnetic anomaly, having a maximum intensity of about ≈700 (nT). Obviously, all the anomalies are similar, having the same strike direction and dip .

The postulated source shapes (which are elongated in the form of a thin vertical sheet) are similar. The major magnetic anomalies are almost parallel to the baseline (see figs. 5.1-5.8).

Line 6+00E (fig. 5.4) and line 8+00E (fig. 5.5) show a split of the postulated thin-sheet into two, while line 4+00E and line 1+00W show a split of the same sheet possibly into three (see fig. 5.3 and 5.6).

There is a very weak response in the vicinity of the fault where Utica shale in the north contacts Trenton limestone in the south (see station 2+00N in fig. 5.1, station 2+50N in fig. 5.2, station 3+00N in fig. 5.3, station 0+00 in fig. 5.4, 3+25N in fig. 5.6, and station

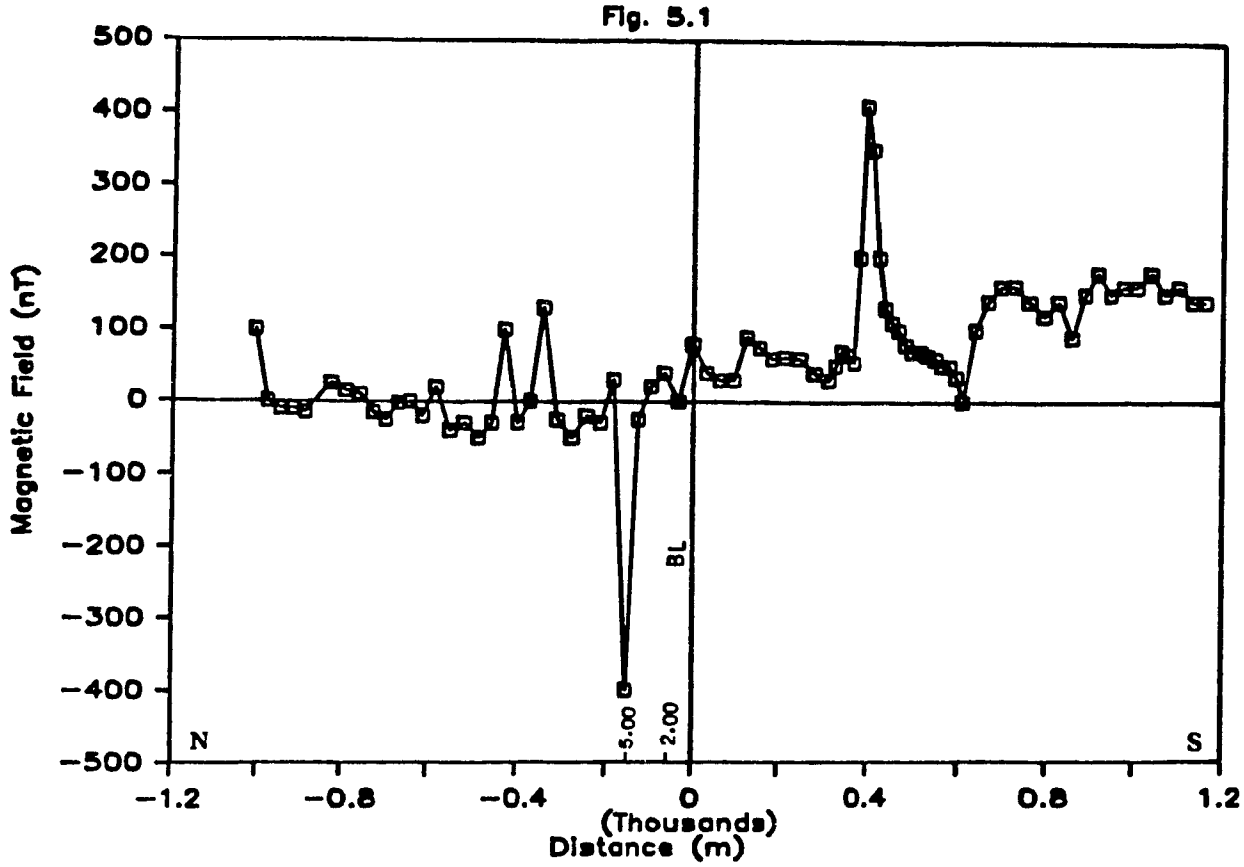

5.1 Magnetic Profile on Line 1+00E (Area I) .

Fig. 5.2

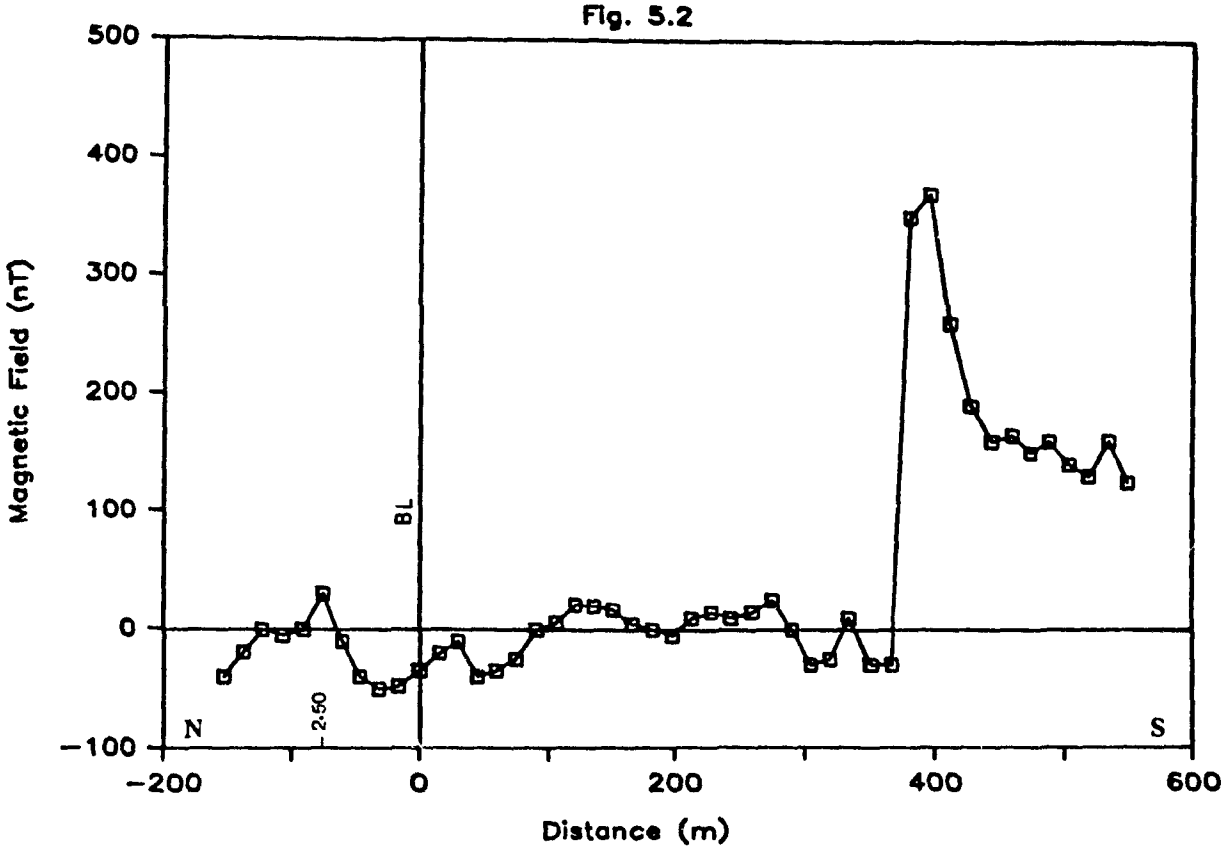

5.2 Magnetic Profile on Line 2+00E (Area I) . . .

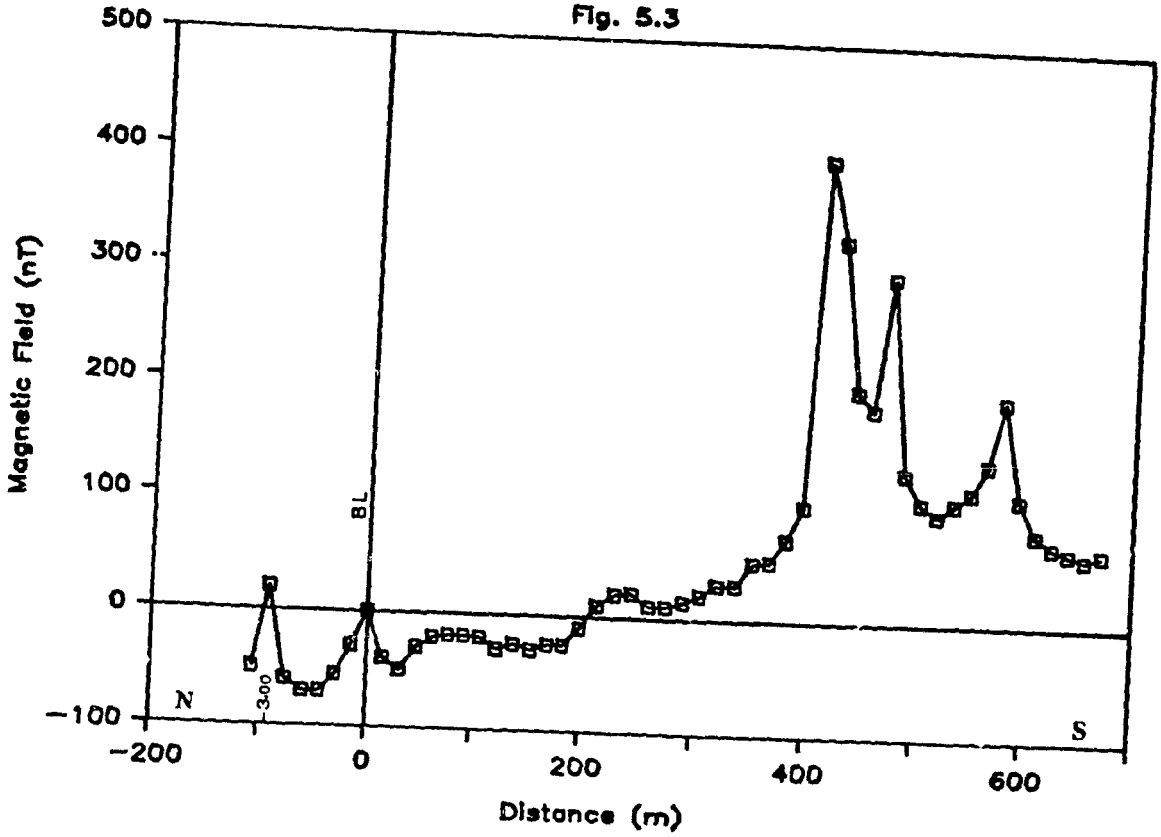

5.3 Magnetic Profile on Line 4+00E (Area I) .

Fig. 5.4

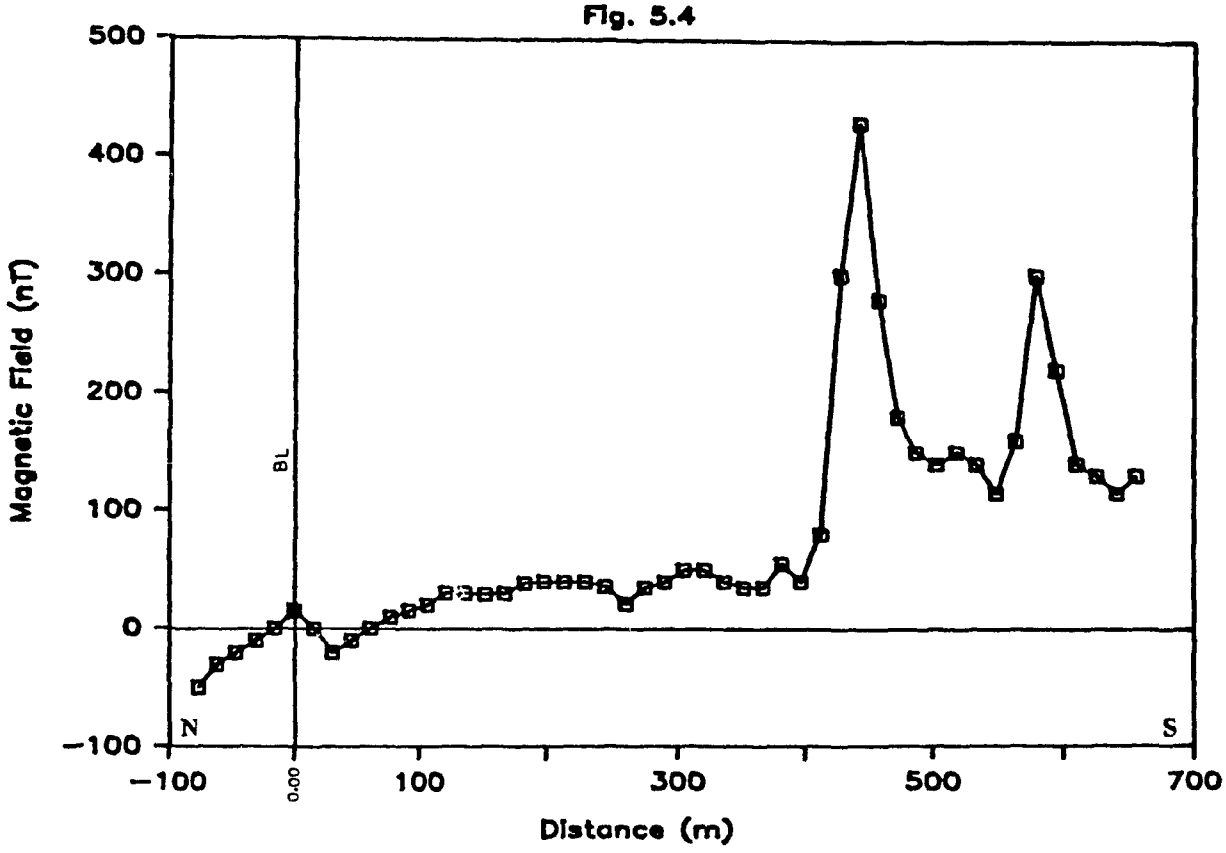

5.4 Magnetic Profile on Line 6+00E (Area I) . . .

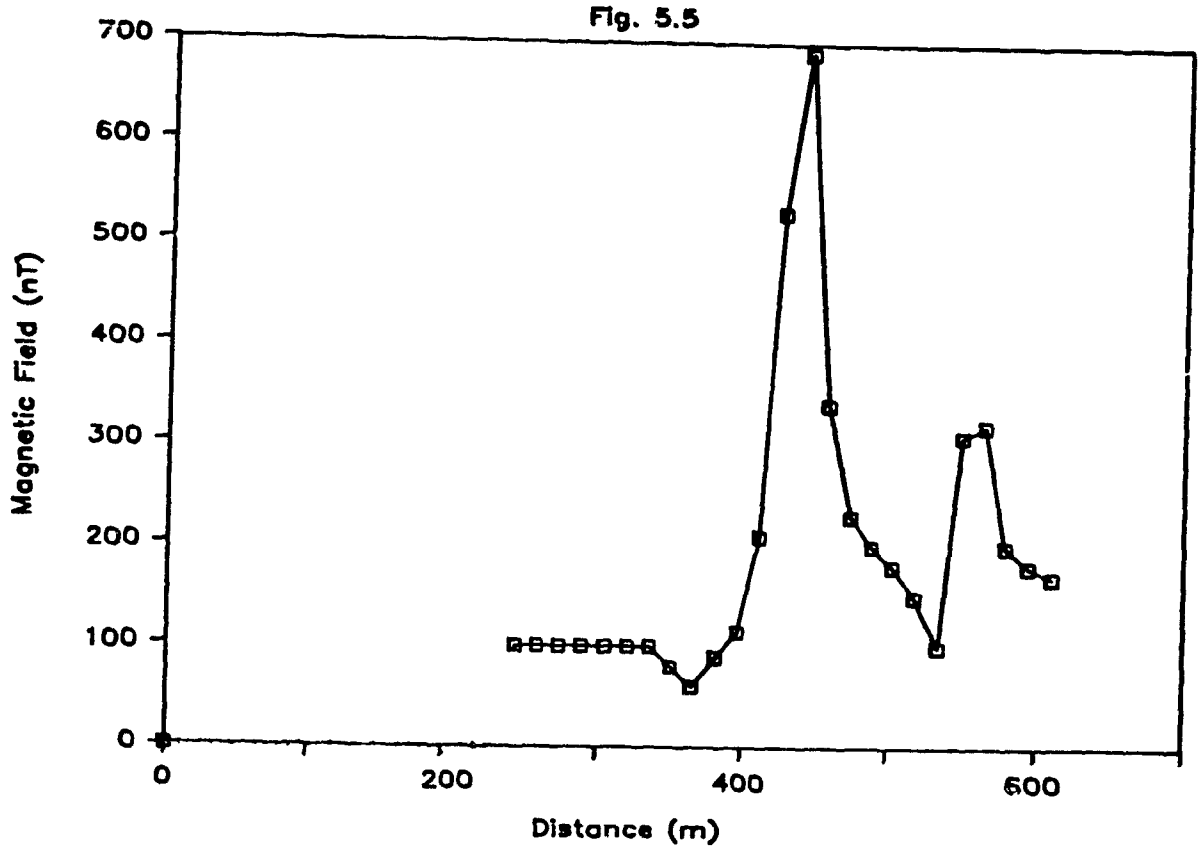

5.5 Magnetic Profile on Line 8+00E (Area I) .

Fig. 5.6

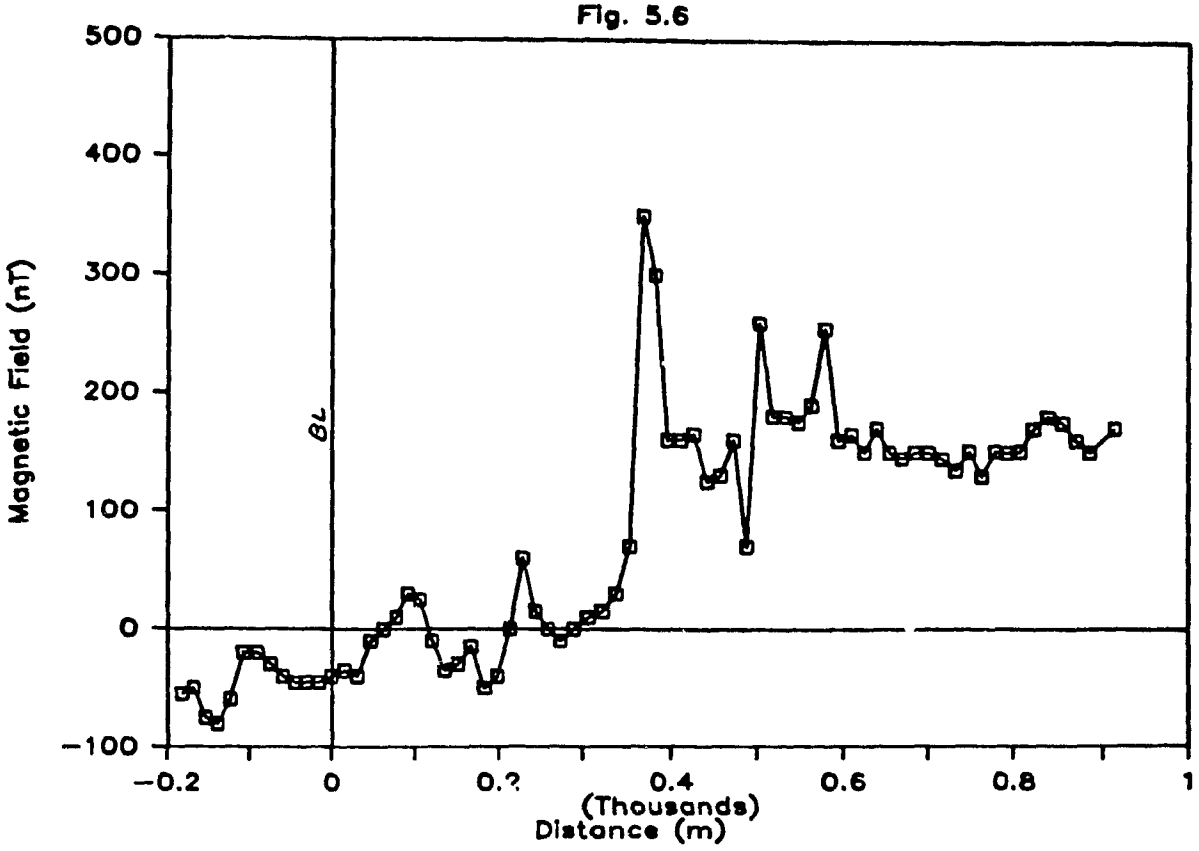

5.6 Magnetic Profile on Line 1+00W (Area I)

Fig. 5.7

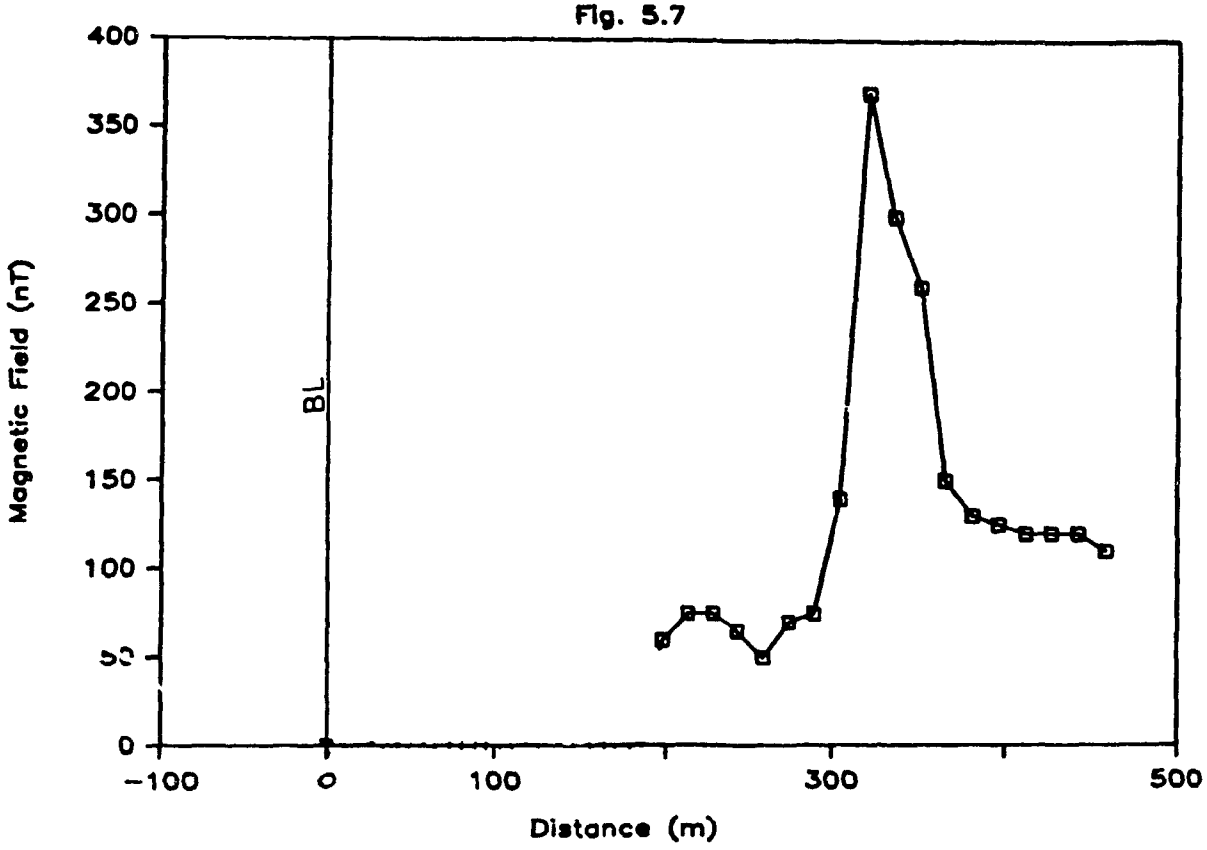

5.7 Magnetic Profile on Line 2+00W (Area I)

Fig. 5.8

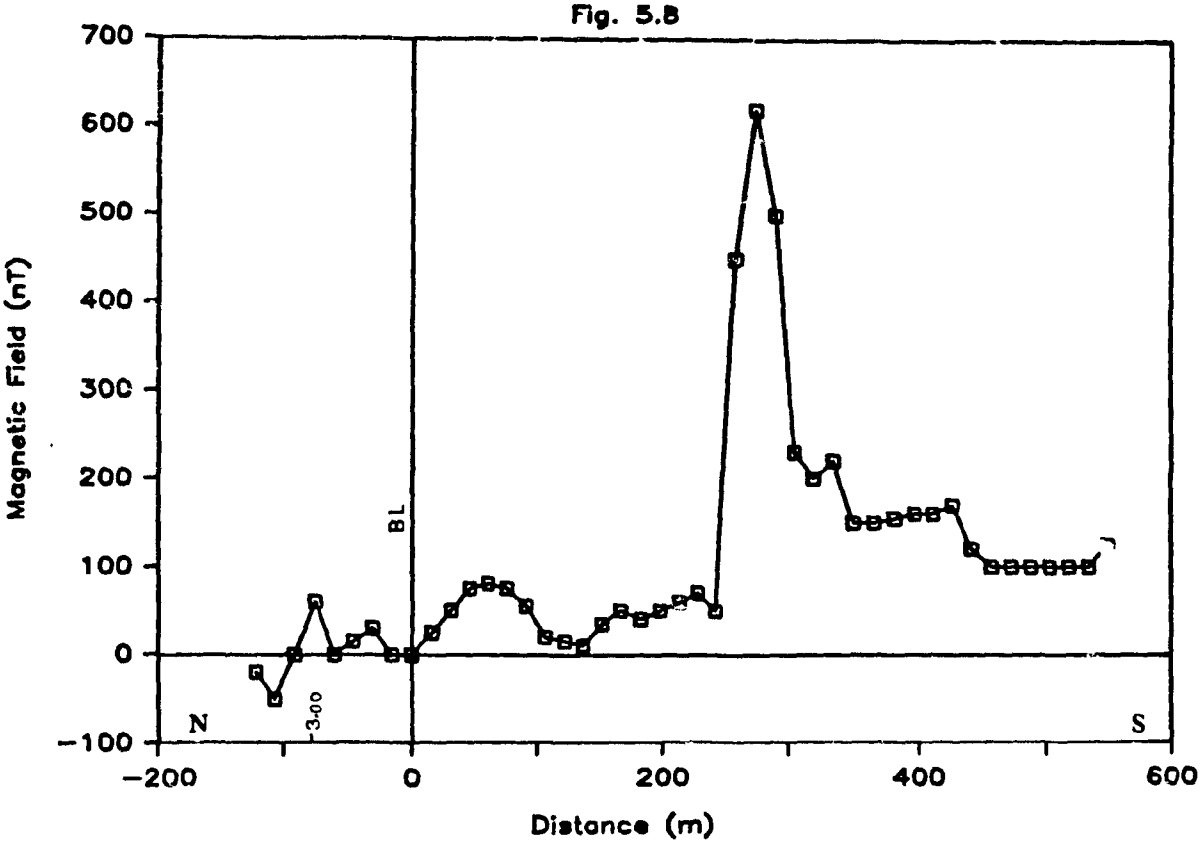

5.8 Magnetic Profile on Line 12+00W (Area I) .

3+00N in fig. 5.8). This may be due to the small susceptibility contrast between the two formations.

The other anomalies on line 1+00W and 1+00E (fig. 5.1 and 5.6) are caused by man-made objects. For example, the negative anomaly at station 5+00N line 1+00E (fig.5.1) is caused by a traffic sign on the east side of the highway.

5.2.1.2 Area II

Figure 5.9 shows traverses in area II, using fluxgate magnetometer. The results are displayed in profiles (fig. 5.10-5.12). Profile 1 (fig. 5.10) is in path, while profile 2 is 100 feet (≈30.5m) west of Lasaline Road. Profile 3 follows St-Pierre Road (see fig. 5.9).

Profile 1 (fig. 5.10) clearly displays two well defined magnetic anomalies with maximum value ≈600 (nT) at stations 34+00s and 44+00s respectively. The sharp negative anomaly at station 9+00s is caused by a thin metal drainage pipe crossing under the path. Profile 2 (fig. 5.11) displays a well defined magnetic anomaly at station 37+00s with maximum value ≈450 (nT), while profile 3 (fig. 5.12) is very noisy. It was very difficult to distinguish any definite anomaly because of the effect of some artificial metal objects such as traffic signs, fences, telephone cables, etc (see stations 35+00s and 46+00s).

5. 9 Index Map Showing the Magnetic Profiles in Area II .

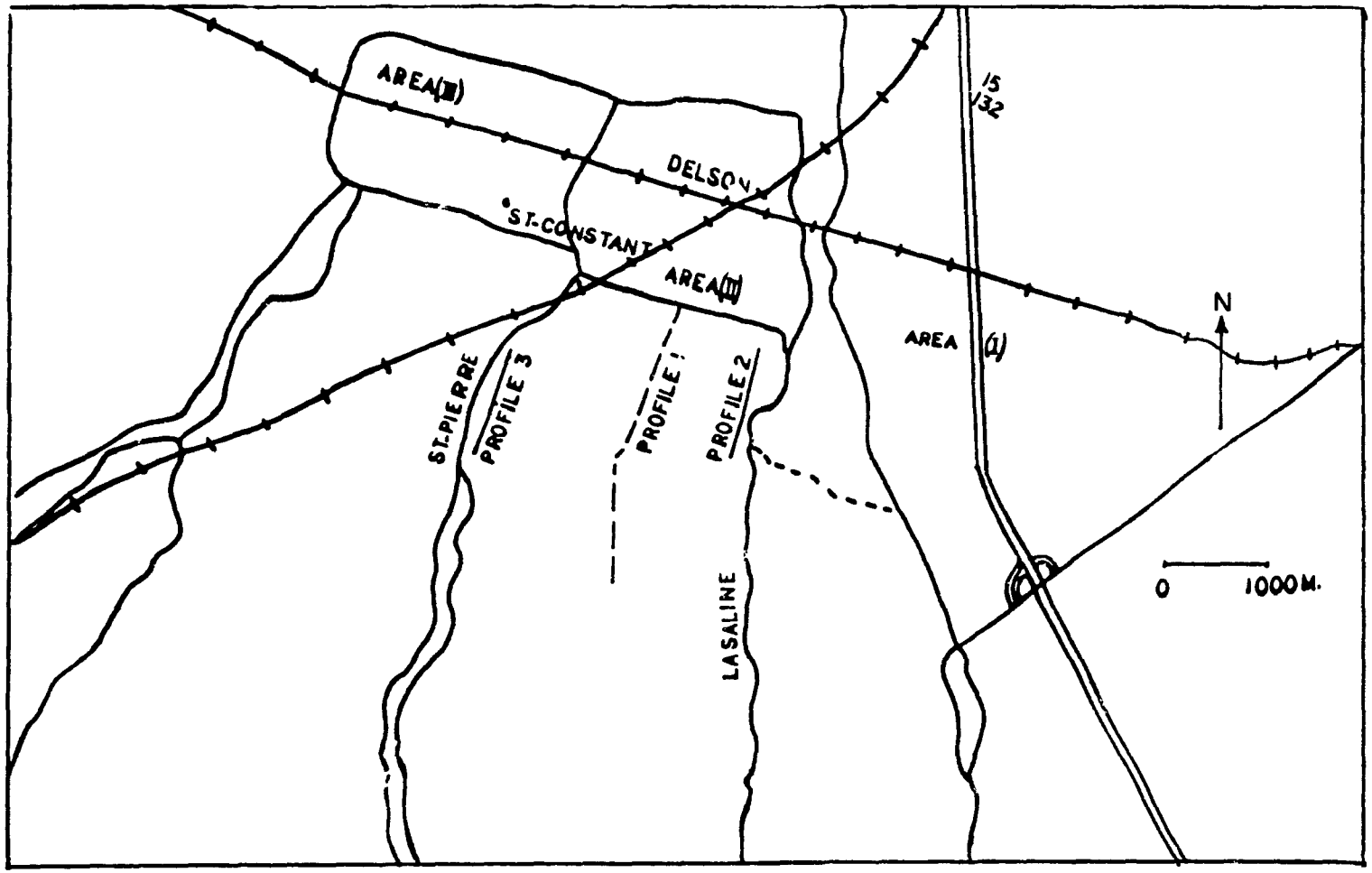

Fig. 5.10

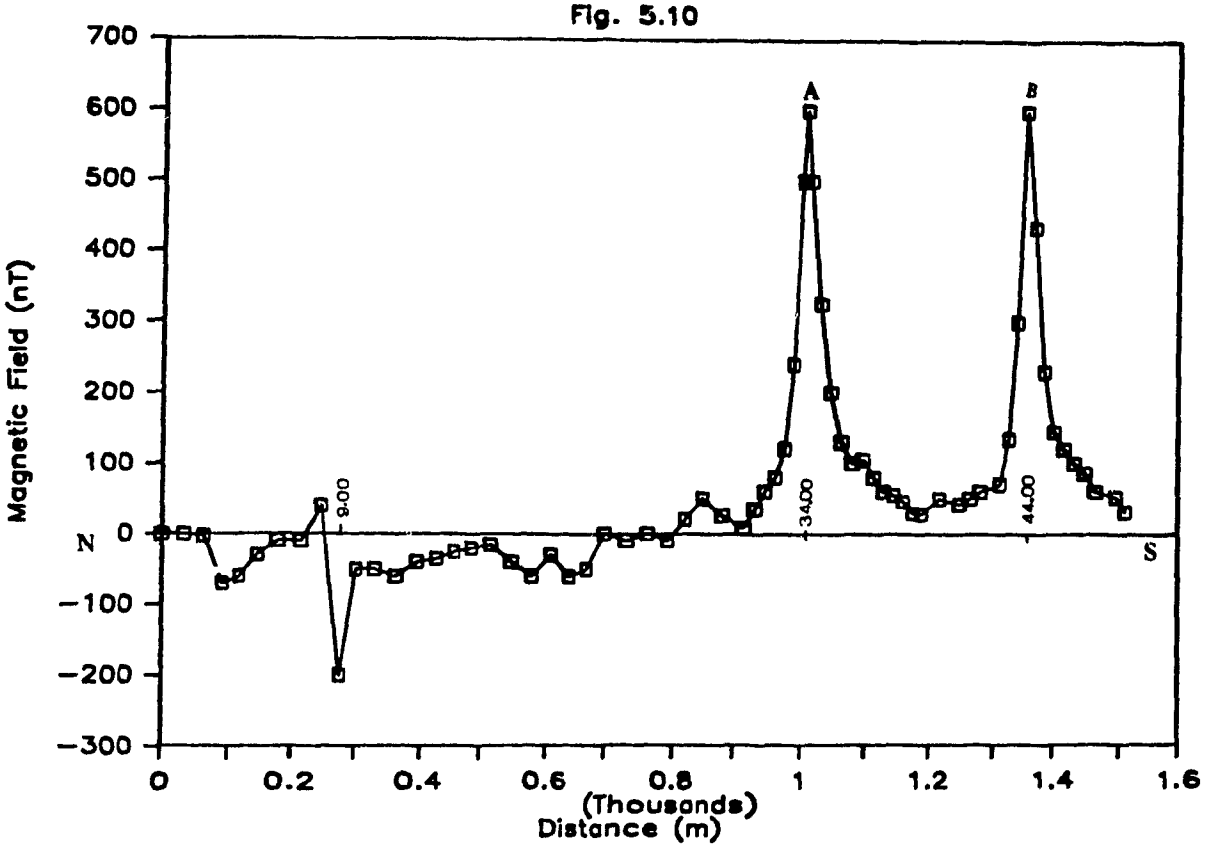

5.10 Magnetic Profile on Line 0+00, Profile 1, Area II .

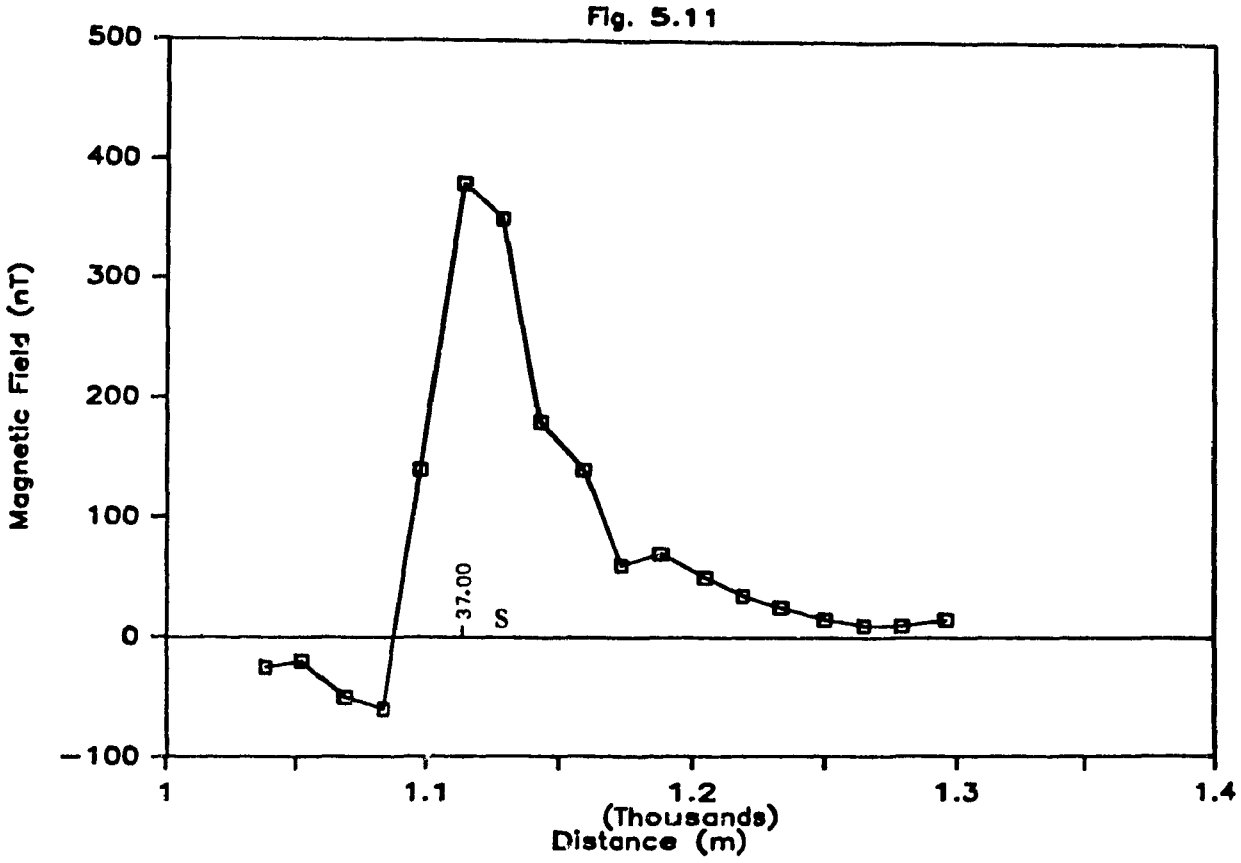

5.11 Magnetic Profile on Line 2, Area II .

Fig. 5.12

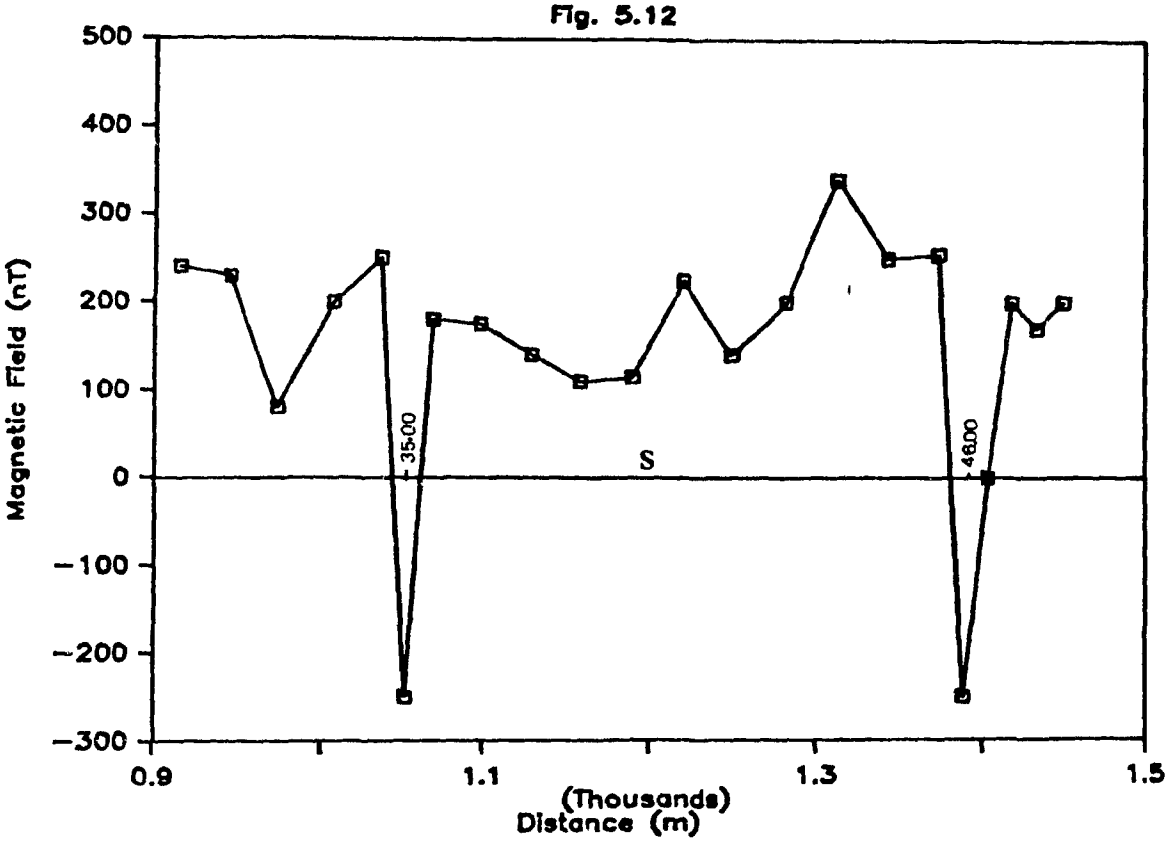

5.12 Magnetic Profile on Line 3, Area II . . .

The magnetic anomalies discovered in this area are similar to those discovered in area I and can be considered as the continuation of the same anomaly (thin vertical sheet).

5.3 Quantitative Interpretation

The ultimate objective of magnetic interpretation is to deduce the geometry of the magnetic bodies which cause a given set of anomalies. In this solution, estimates of parameters (such as depth of overburden, length of the strike, dip, depth extent and width, as well as magnetic susceptibility play very important roles in the computation of magnetic profiles. Estimates of these parameters depend on the observed anomaly and on the shape of the profiles.

Matching of field anomalies with simple geometrical shapes is the most common method of interpretation when enough geological information is available.

Using a combination of inverse and forward modelling (which refers to any procedure in which a model anomaly curve is calculated for an arbitrarily shaped source) the discovered igneous intrusion will be modelled as a vertical thin sheet having an extreme depth of extent (see fig. 5.13). Unfortunately, the use of modelling procedures to interpret magnetic anomalies cannot assure a unique solution because of ambiguity (see Skeels, 1947; Roy, 1970; and Dobrin, 1976 pp 458-463, 554-555), the effect of remanent magnetization and the dipole character of magnetism.

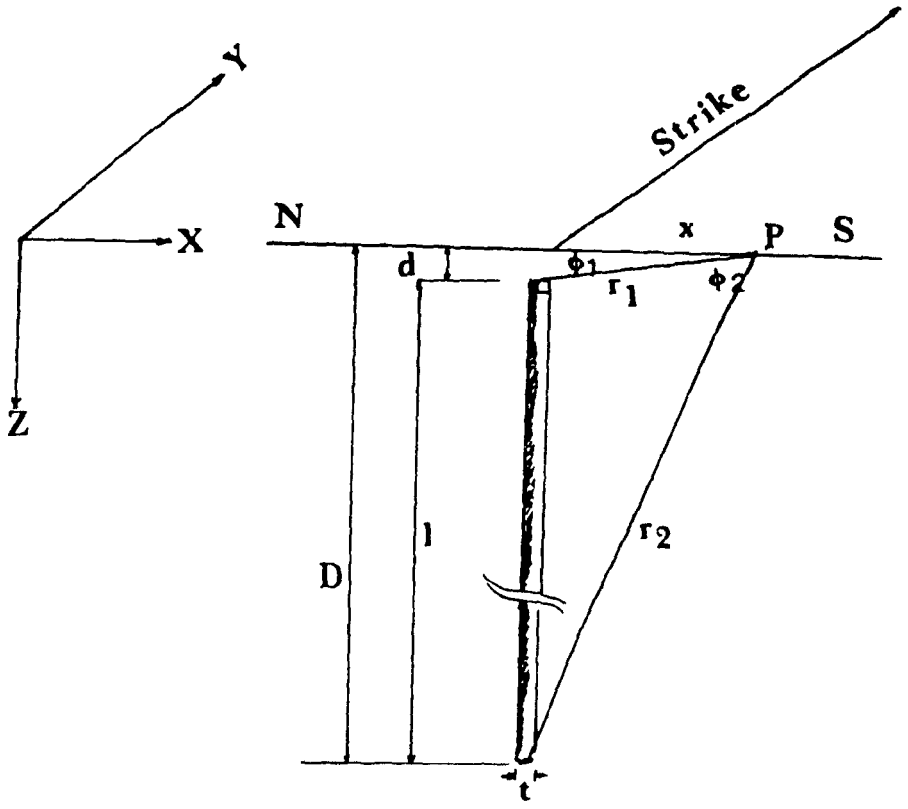

5.13 Geometry of a Vertical Thin Sheet Striking E-W.

5.3.1 Inversion of Space Domain Field Magnetic Data:

An attempt has been made to carry out inversion of the ground magnetic data over a discovered anomaly (which is assumed a vertical thin sheet). A simple vertical thin sheet striking 46^{o}, 47^{o}, and 48^{o} degrees magnetic east and specified sucsceptibility and thickness depth extent and depth to the top was used to derive a forward solution. Then a set of initial parameters for the model was used to tackle the inverse problem. The initial parameters are determined by profile analysis, experimentally and by the existing geological information .

In the modelling process we used the techniques of inversion theory to predict those parameters when given a set of ground magnetic data.

In the present study, ridge regression technique, as extended in Marquardt (1963) to nonlinear problems, was applied to an overdetermined and complete inverse problem. The technique of singular value decomposition (SVD) has also been used to study the properties of the problem matrix for the inversion procedures. The presence of nearly zero eigenvalues indicates that some of the parameters are linearly dependent and do not contribute significantly to the shape of the profile. This problem of presence of certain parameters, which are poorly determined in the data, destroys the orthogonality of the problem and causes the system matrix to be nearly singular. The cutoff point

between significant and insignificant eigenvalues was performed experimentally. The removal of extremely small eigenvalues adds stability to the inversion process. In general the most significant physical parameters for this problem are the angle of strike and depth to the top.

In the inversion process, Marquardt factor (MF) starts out being 10^{-6} and increases or decreases according to a goodness of fit criterion called reduced chi-squared (X). If chi-squared decreases after new parameters are calculated, then the Maquardt factor is decreased to MF/10 . If chi-squared increases, then MF is increased to MF x 10

In this inversion technique also, fixing of certain model parameters is based on existing geological information as angle of strike and then on the (SVD) analysis as explained before. However, lack of exposure prohibits direct susceptibility measurements in the field.

It was observed that in this particular inverse problem there was difficulty in converging to a suitable solution without setting some preconditions. These conditions are :

1- The A matrix whose elements are the first partial derivatives of the forward functional with respect to the parameter had to be updated at every iteration in order for it to be stable.

2- Parameters corresponding to near zero eigenvalues were fixed in the inversion process.

3- A specified percentage of the value of the parameter given by the preceding iteration had to

be set as the limit Dpj, if the latter happened to be too large (Inman et al, 1973).

5.3.1.1 Theory

The forward problem for a vertical thin-sheet of infinite strike length, as shown in fig. 5.13, is given by equation 1, (Telford et al, 1976). Cook (1956), gives a comprehensive description of magnetic interpretation over veins. Assuming the material comprising the magnetic body is homogeneous and has a true magnetic susceptibility k.

$$V_z = 2kt\ \{(H_o \times \sin\beta - Z_o\ D)/(r2)^2 - (H_o \times \sin\beta - Z_o\ d)/(r1)^2\ \}$$

.....(1)

where I: inclination of the earth's magnetic field (≈75° in Montreal).

H_t= Total earth magnetic field $60x10^3$ (nT)

H_c= H_t cos I = 15529 (nT) (horizontal component)

Z_o= H_t sin I = 57956 (nT) (vertical component)

where $\Phi_1 = \tan^{-1}\left(\frac{d}{X}\right)$

$\Phi_2 = \tan^{-1}\left(\frac{D}{X}\right)$

$r_1 = \sqrt{[(X)^2 + d^2]}$

$r2 = \sqrt{[(X)^2 + D^2]}$

V_z= vertical components of anomaly at P

Z_o= vertical component of the earth's normal magnetic field (≈57956 nT)

H_o= Horizontal component of the earth's normal magnetic field (≈15529 nT)

d = depth to the top (overburden) (m)

β = angle of strike

D = depth to the bottom (m)

5.3.1.2 Inverse Problem

In tackling an inverse problem, we first choose a model, assign to it model parameters and then predict the data using the following forward problem equation :

$$Y = A\ (p,x) \qquad (2)$$

where

Y = Computed value of some geophysical quantity

A = Functional of some known parameter

p = Vector containing unknown model parameters

x = Vector containing the known system parameters

Since most inverse problems encountered in geophysics are nonlinear, the next stage is to linearize equation (2) by expanding it in a Taylor's series and dropping all terms of order higher than the first.

In the matrix notation equation (2) becomes

$$Y_i = A_{ij}\ P_j \qquad (3)$$

where

A_{ij} is an (n,m) matrix whose elements are

$[A]_{ij} = (d\ A(x,p)/\ d\ P_j\ ),\ p = p_0\ -\ x = x_0$

The least-squares solution for the parameter increment vector is

$$Dp = (A^T A)^{-1} A^T Dy \quad (4)$$

where

A^T = The transpose of A.

The ridge regression form of equation (4) is

$$Dp = (A^T A + MF\ I)^{-1} A^T Dy$$

where

MF = Marquardt factor

I = The identity matrix

Dy = Observed data - Calculated data

The matrix A can be decomposed into eigenvalues and eigenvectors when it becomes

$$A(n,m) = U(n,m) \times S(m,m) \times V(m,m)$$

where

S(m)= diagonal matrix of eigenvalues

V,U = matrices of eigenvectors associated with the parameters and observations respectively.

5.3.1.3 Profile processing

The interpretation process begins with the selection of a profile which intersects the anomaly one wishes tc analyse. The profiles selected should be perpendicular to the strike of an anomalous feature, but care must be taken to avoid as much as possible interfering anomalies resulting from either local inhomogenieties or neibouring sources. However, almost all the profiles especially those in area (I) have interfering anomalies in the south side resulting from either local inhomogenities or neighbouring sources (see, for example, figs. 5.3, 5.6, 5.8). The selected profiles are digitized at 25 feet (≈7.6 m.).

Since the anomalies of interest have distinctly different characteristics from any noise or other anomalies the filtering process was designed solely to remove noise and no other filters were tried, such as upward continuation, to isolate anomalies of interest.

The smoothing was applied manually and by using Hanning 3-point filter (i.e. low pass filter).

Let [A1 A2 A3 A4 .....An] be magnetometer readings, then for the simple Hanning 3-point filter :

$$A'_i = (A_{i-1} + A_i \times 2 + A_{i+1})/ 4$$

The obtained filtered data in area I were contoured on a map (see fig.5.14).

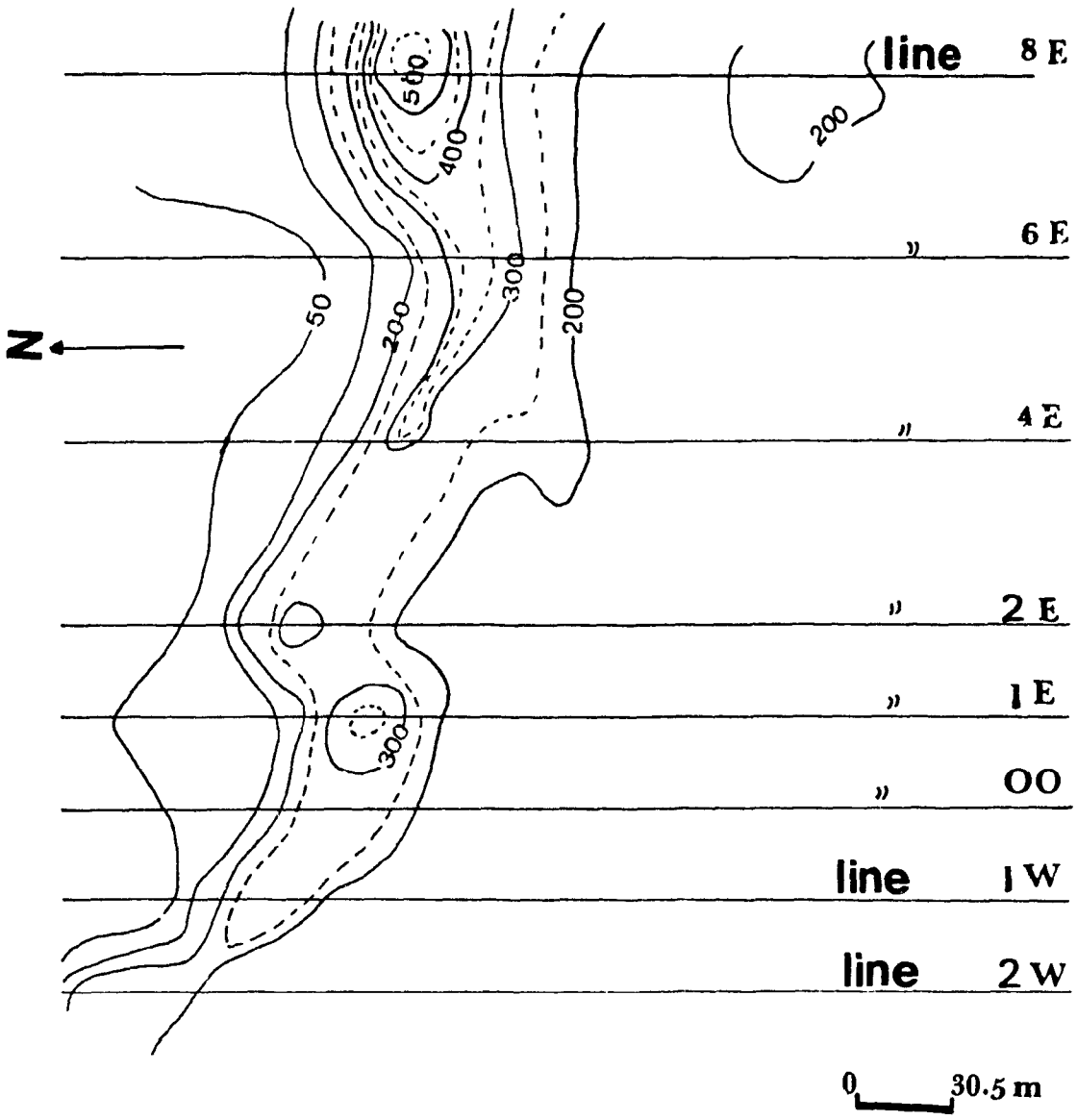

5.14 Magnetic Contour Map (Area I).

5.3.1.4 Profile Inversion

The inversion technique applied here was, to fix certain model parameters based on existing geological information and on (SVD) analysis, then iterate to a satisfied solution allowing only a few of the parameters to vary.

Inversion processing is performed on prepared data based on the forward model adopted. Profiles used did not undergo heavy filtering for the inversion process, but only the described smoothing stage.

The anomalies used for the inversion were:

1- the anomaly on line 8+00E area I (fig. 5.5).

2- anomaly (a) on line 0+00 (path) area II. (fig. 5.10).

3- anomaly (b) on line 0+00 (path) area II. (fig. 5.10).

4- the anomaly on line 1+00E area I (fig. 5.1).

5.3.2 Results:

Table 5.2(a,b,c,d) shows the results of the calculated model parameters P(m), eigenvalues S(m), the resolution matrix RS (m,m) and the standard deviation for the parameters SP(m). (see Leite and Leao, P.1298, 1985).

Table 5.2a - (fig. 5.15a):

1- Calculated parameters P(m) :

(a): strike angle (β)= 48 (degrees)

(b): depth to the top (d)= 85.64 feet (26.12 m)

(c): depth to the bottom (D)= 4192.69 feet (1278.8 m)

**(d): thickness * susceptibility (tk)= 0.350

(e): length of the magnetic body (L)= 4107.05 feet (1252.65 m)

2-Eigenvalues S(m):

(a): 3064.44

(b): 160.95

(c): 6.14

(d): 0.00536

3-Covariance CM(m,m):

.0542	-.0001	-.0450	-.0201
-.0001	.0001	-.0058	.0001
-.0450	-.0058	15.6028	.0104
-.0201	.0001	.0104	.0130

4-Standard deviation for the parameters SP(m):

(a): 0.239

(b): 0.009

(c): 3.95

(d): 0.114

5-Resolution matrix RM(m,m):

1.000	0.000	0.000	0.000
0.000	1.000	0.000	0.000
0.000	0.000	1.000	0.000
0.000	0.000	0.000	1.000

** It is assumed that the magnetic susceptibility of the magnetic body is constant and equal to 0.0055 emu. (i.e. in the range of the gabbro 0.004 - 0.006 emu).

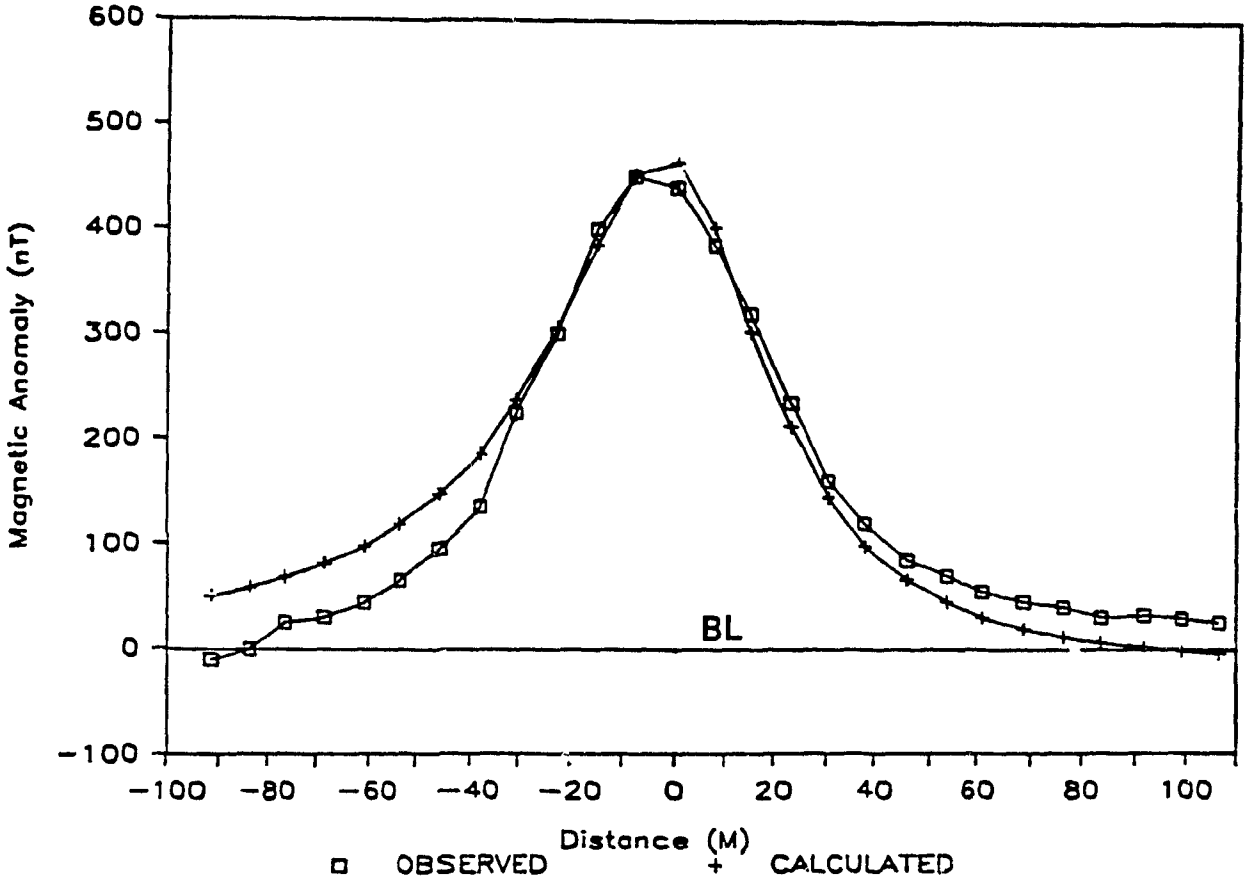

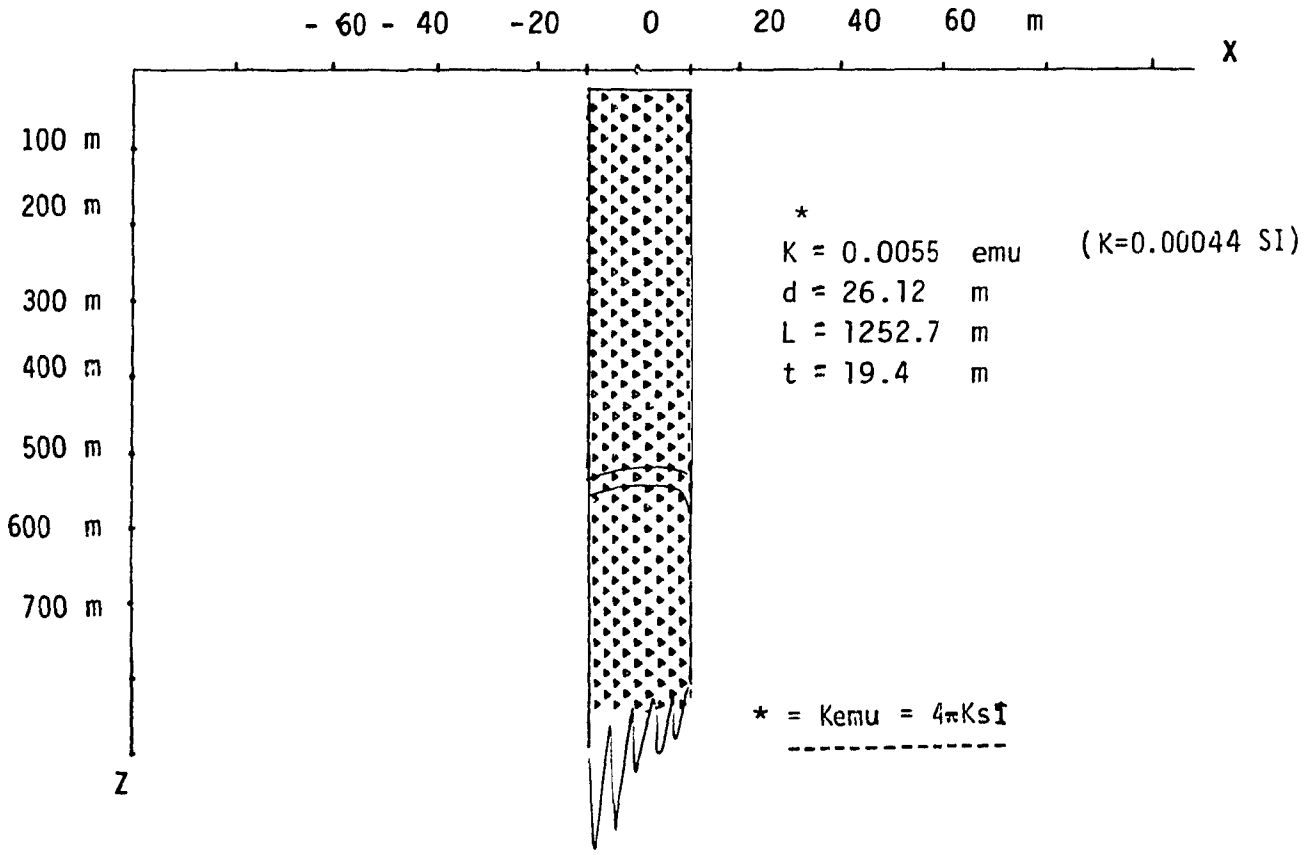

5.15a Observed and Model Curves on Line 0+00 (Anomaly (A) Area II).

Table (5.2b)- (fig. 5.15b) :

1- Calculated parameter P(m):

(a): strike angle (β)= 47 degrees

(b): depth to the top (d)= 75.7 feet (23.1 m).

(c): depth to the bottom (D)= 5273.73 feet (1608.5 m).

(d): thickness * susceptibility (tk)= 0.300

(e): lenght of the magnetic body (L)= 5198.03 feet (1585.4 m).

2- Eigenvalues S(m):

(a): 3294.67

(b): 153.25

(c): 6.43

(d): 0.003

3- Covariance matrix CM(m,m):

.0679	-.0002	-.0518	-.0221
-.0002	.0001	-.0052	.0001
-.0518	-.0052	16.6244	.0113
-.0221	.0001	.0113	.0126

4- Resolution matrix RM (m,m):

1.000	0.000	0.000	0.000
0.000	1.000	0.000	0.000
0.000	0.000	1.000	0.000
0.000	0.000	0.000	1.000

5- Standared deviation for the parameters SP(m):

(a): 0.26053

(b): 0.00874

(c): 4.07729

(d): 0.11242

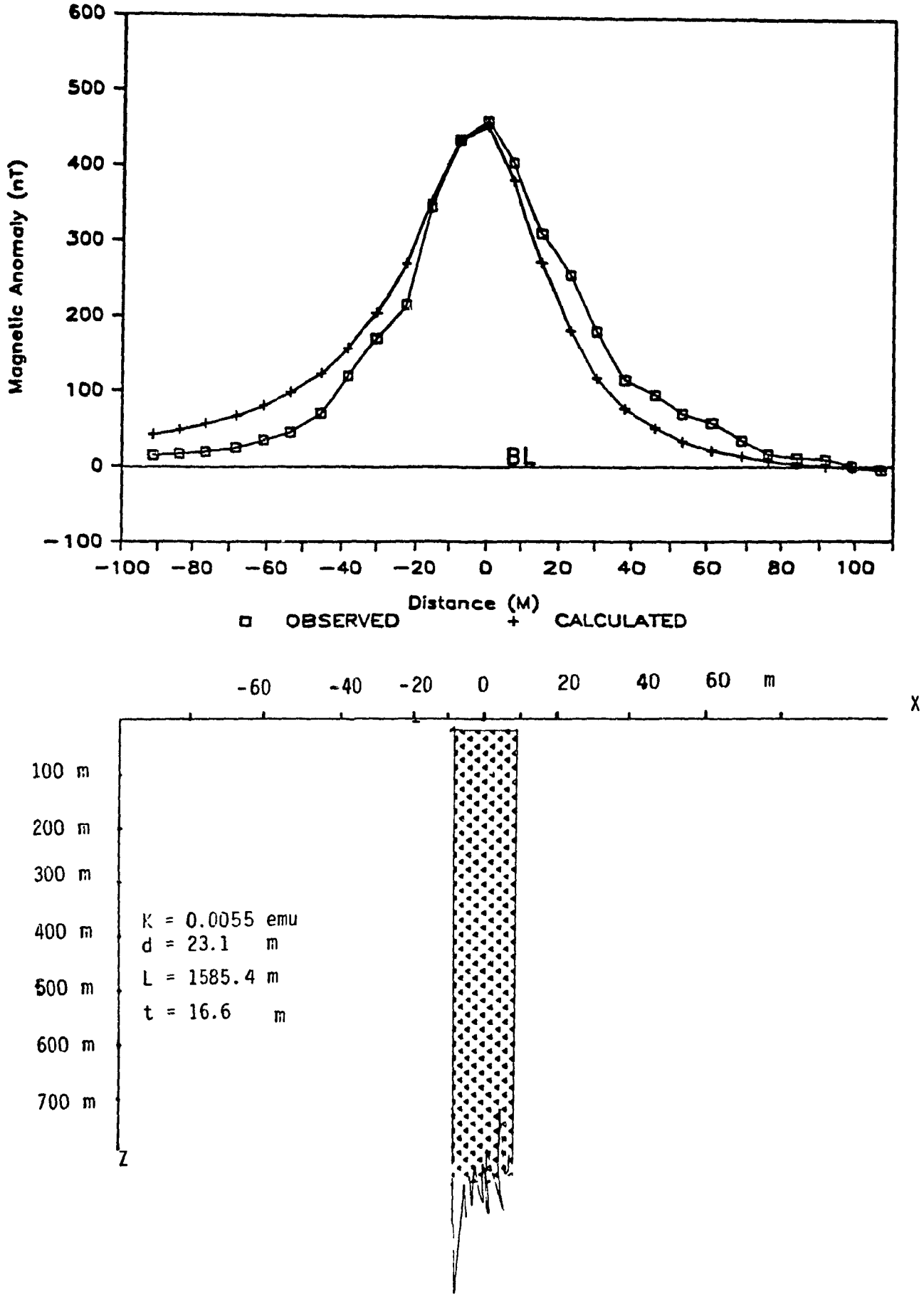

5.15b Observed and Model Curves on Line 0+00 (Anomaly (B) Area II).

Table 5.2c (fig.5.15c) :

1- Calculated parameters P(m):

(a): strike angle (β)= 46 degrees

(b): depth to the top (d)= 62.49 feet (19.1 m)

(c): depth to the bottom (D)= 446779.08 feet (136267.6 m).

(d): thickness * susceptibility (tk)= 0.286

(e): lenght of the magnetic body (L)= 446716.6 feet (136248.5 m)

2- Eigenvalues S(m):

(a): 3719.84

(b): 166.17

(c): 8.40

(d): 4.0×10^{-7}

3- Covariance matrix CM(m,m):

.0669	-.0001	-.0419	-.0205
-.0001	.0001	-.0028	.0001
-.0419	-.0028	11.7816	.0098
-.0205	.0001	.0098	.0112

4- Resolution matrix RM(m,m):

1.0000	0.0000	0.0000	0.0000
0.0000	1.0000	0.0000	0.0000
0.0000	0.0000	1.0000	0.0000
0.0000	0.0000	0.0000	1.0000

5- Standared deviation of the parameters SP(m):

(a): 0.26134

(b): 0.00827

(c): 3.43243

(d): 0.105728

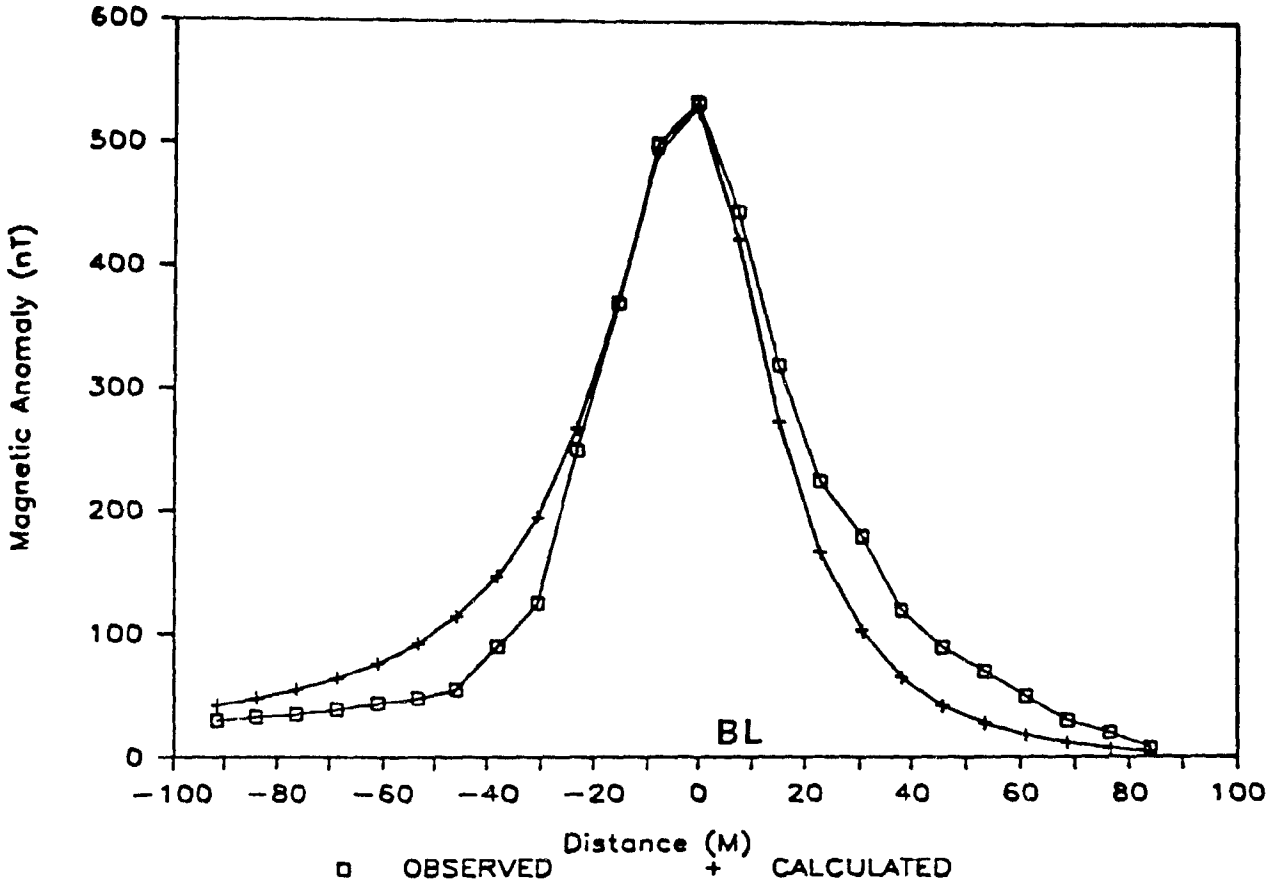

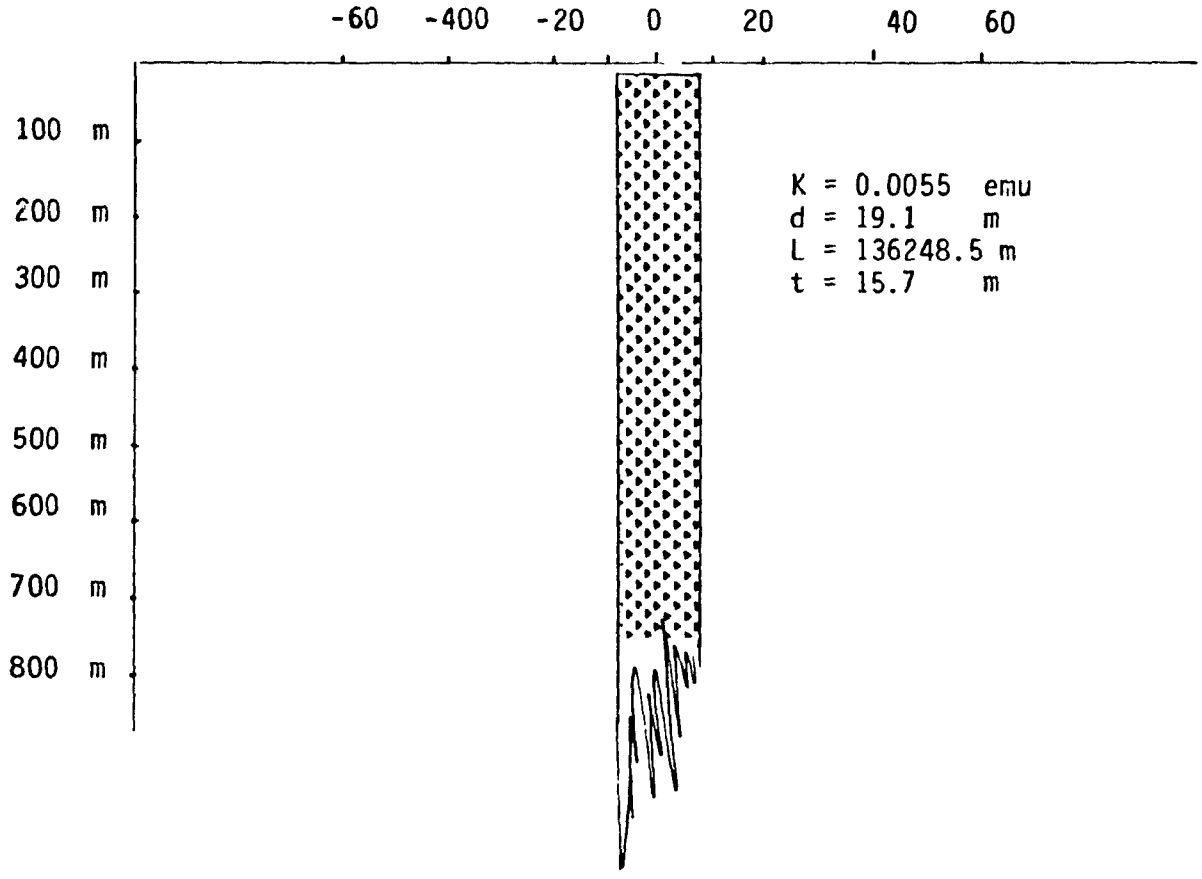

5.15C Observed and Model Curves on Line 8+00E Area I.

Table 5.15d - (fig. 5.15d) :

1- Calculated parameters P(m):

(a): strike angle (β)= 48 (degrees)

(b): depth to the top (d)= 85 feet (25.9 m)

(c): depth to the bottom (D)= 886.54 feet (270.4m)

(d): thickness * susceptibility (tk)= 0.250

(e): length of the magnetic body (L)= 801.54 feet (244.47 m)

2- Eigenvalues S(m):

(a): 2719.43

(b): 111.92

(c): 4.00

(d): 0.085

3-Covariance CM(m,m):

0.1216	0.0002	-0.1191	-0.0300
0.0002	0.0001	0.0031	0.0000
-0.1191	0.0031	44.8162	0.0311
-0.0300	0.0000	0.03110	0.0136

4-Standard deviation for the parameters SP(m):

(a): 0.349

(b): 0.0104

(c): 6.6944

(d): 0.1164

5-Resolution Matrix (m,m):

1.000	0.0000	0.0000	0.0000
0.000	1.0000	0.0000	0.0000
0.000	0.0000	1.0000	0.0000
0.000	0.0000	0.0000	1.0000

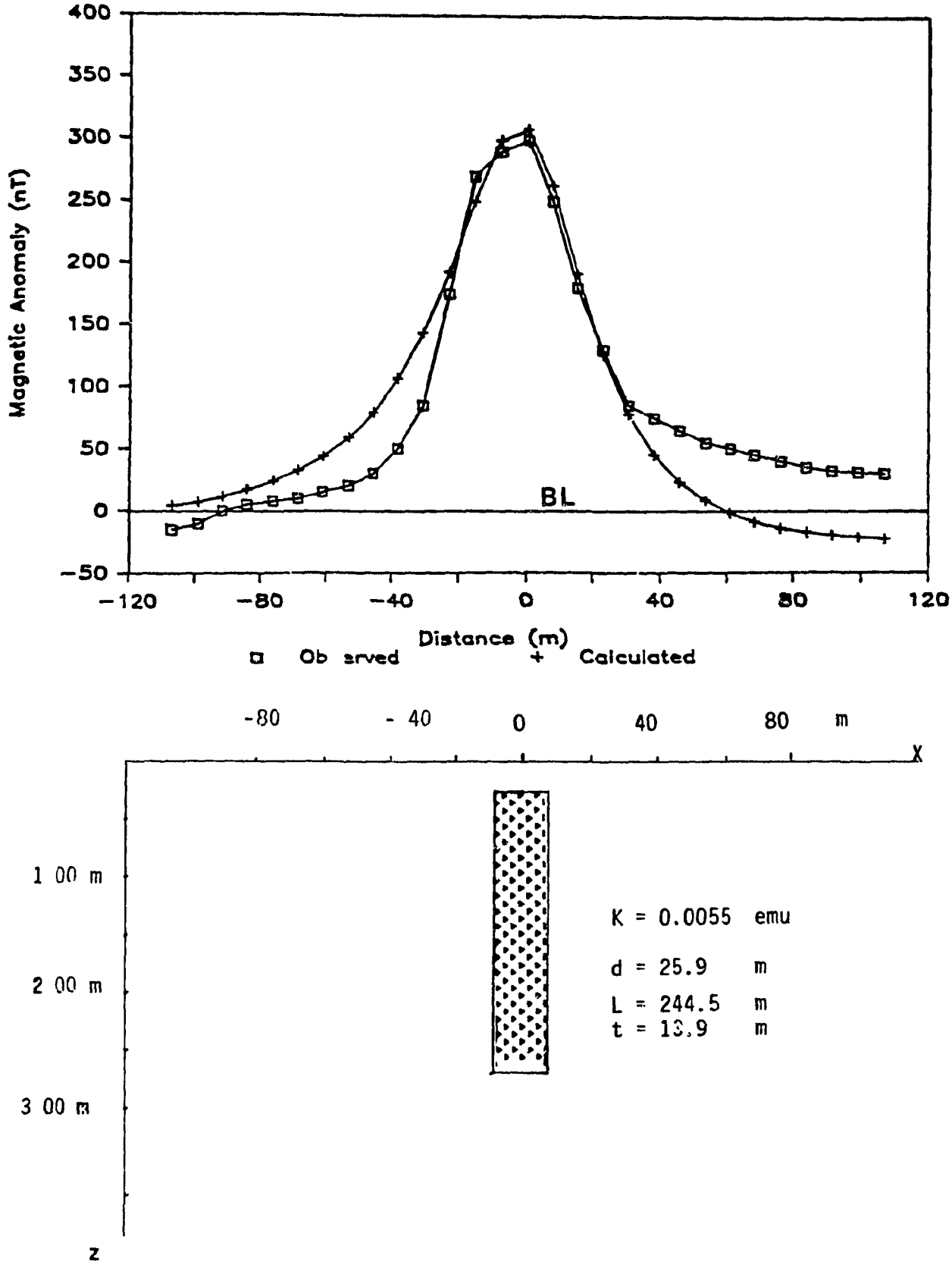

5.15d Observed and Model Curves on Line 1+00E Area I.

From Table (5.2 a,b,c,d) it can be notced that the condition number: (Smax / Smin), where S is eigenvalue, is very large. This very large condition number cause much problem in arriving at the inverse solution.

It is worth commenting here that parameters associated with the largest eigenvalues are most accurately found and most quickly resolved, whereas those parameters with the smallest eigenvalues are least accurately determined and converge more slowly.

The diagonal elements of the covariance matrix supplies the information about the variances, and the non diagonal elements have information regarding the correlation between the parameters.

The resolution matrix is important in the underdetermined inverse problem where it is normally not equal to an identity matrix, I. In overconstrained problemes, like the present one, it is an identity matrix as clearly seen in Table 5.2 (a,b,c,d). This simply means that the parameter values are uniquely resolved.

Chapter 6: Discussion of The Results

Chapter 6: Discussion of the Results

The results of the geophysical methods and geological information are discussed here.

1.1 Depth of Overburden:

The estimation of depth of overburden in area I and area II was done by DC resistivity (depth souding). Profiles were obtained at one station in line 4+00E in area I and line 0+00 (path) in area II respectively. An expanding Wenner array was used, and the interpretation was done by the resistivity inversion and by the cumulative $\Sigma\int_a$ plot, described by Telford et al (p. 670-671).

The overburden is estimated as approximately 3.5 m* thick in both areas, which is approximately similar to the results of the drilling by Canada Cement-Lafarage near area I, (Saull, V.A., 1987, Personal Communication). However, the thickness of the overburden could undergo a dramatic change even in the same profile.

The values estimated by the cumulative plot and resistivity inversion were confirmed by another plot of the data described in Appendix I.

* This value is obtained by DC resistivity inversion which is assumed more reliable than that obtained by EM16R. This may be due to the overburden being conductive (see EM16R results in appendix I).

6.2 Fault Location, Strike Extent and Direction

6.2.1 Area I:

EM-16 responses in area I were observed over the Delson Fault. These indicate that the contact is between two formations of different resistivity, and that there is no anomalous conductivity associated with the fault itself, as is the case of a water filled shear.

Two Radiohm (EM-16R) VLF traverses conducted on line 4+00E and line 4+00W verified the contact indicated by EM-16. Taking into account the errors usually inherent in the pace and compass technique, the location of the contact between the two methods generally agrees (fig. 3.17 a, b, in chapter 3).

The strike of the fault is well defined by VLF (Map 6.1) to be about E-W in direction.

Map 6.1 compares the location of the Delson fault, determined geologically, to the location determined by the VLF method.

The results indicate that between lines 2+00E and 8+00E the geologically mapped Delson fault is as much as 75 m south of where it was mapped by VLF. This is also true between lines 2+00W and 12+00W. In the vicinity of lines 0+00, 1+00E and 1+00W, the geologically mapped fault is as much as 30 m south of the VLF mapped one.

Minor responses occur on line 6+00E, 1+00W, 8+00E

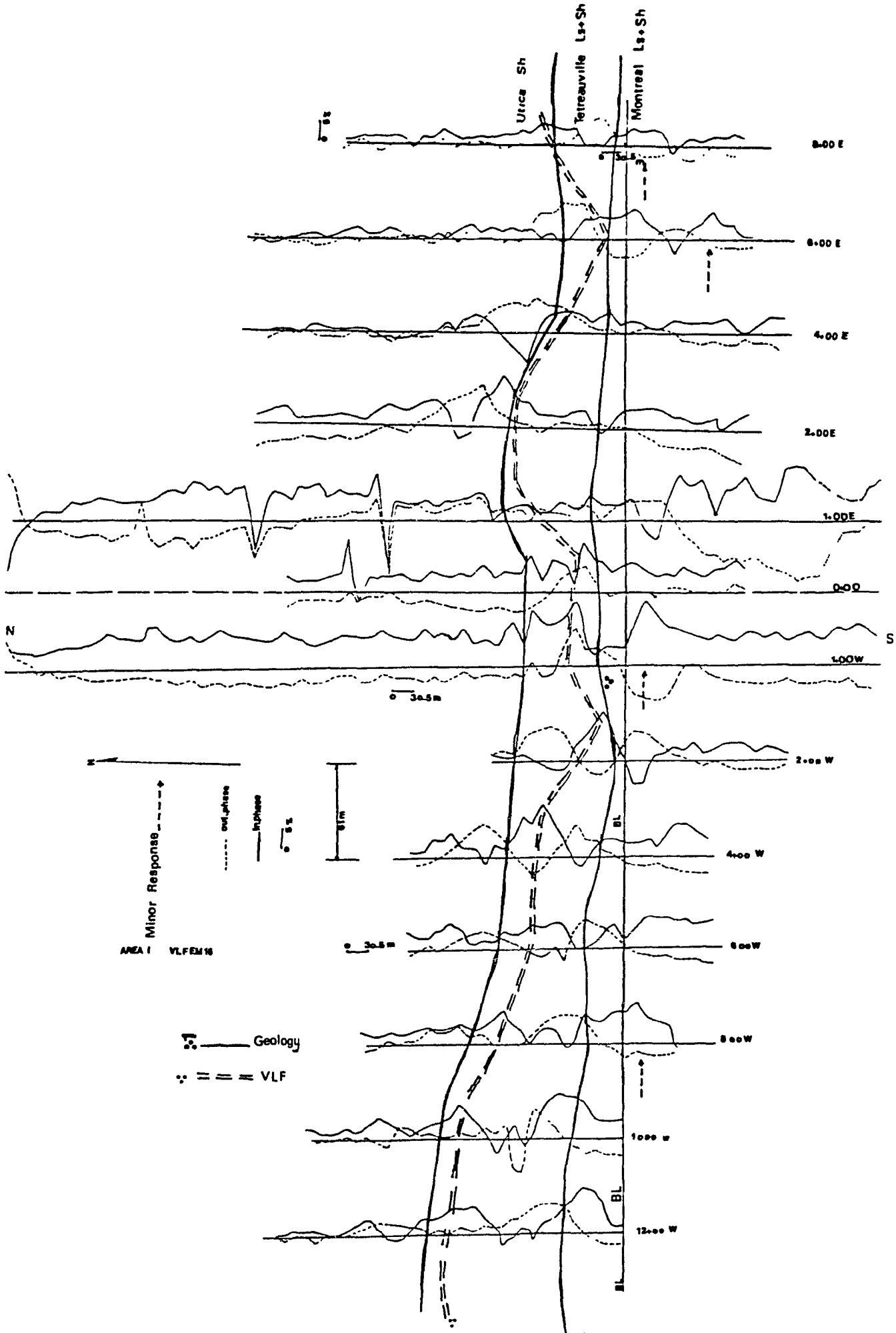

Map 6.1 (VLF-EM Survey in Area I).

and 8+00W see map (6.1). It can be inferred that the conductivity contrast, in these locations, is not large enough to give a good response since almost the same formation (Tetreauville: limestone and shale) and (Montreal: limestone and shale), (Globensky, Y., 1982), occurs on either side of the fault. There are no resistivity traverses on these profiles to substantiate the EM-16 results. It is difficult to say what causes these responses but it could be due to local changes in limestone-shale content.

6.2.2 Area II

Area I and area II are quite close together and so have common geological characteristics which appear on the geological map.

The Delson fault in area II, as also seen in area I, separates the same geological formations and even the depth of the overburden was also found to be the same as in area I. Nevertheless, there was no definite VLF response in area II. The EM-16R traverse was done to substantiate any EM 16 result. However, the EM-16R exhibited only a very weak variation in the apparent resistivity in the vicinity of station 6+00S (map 6.2). On the basis of this survey, it was impossible to infer the location of the the fault.

Based on this result, one can assume that the non-delineation of the fault is due to the high shale content in the formations across the fault, which may decrease the

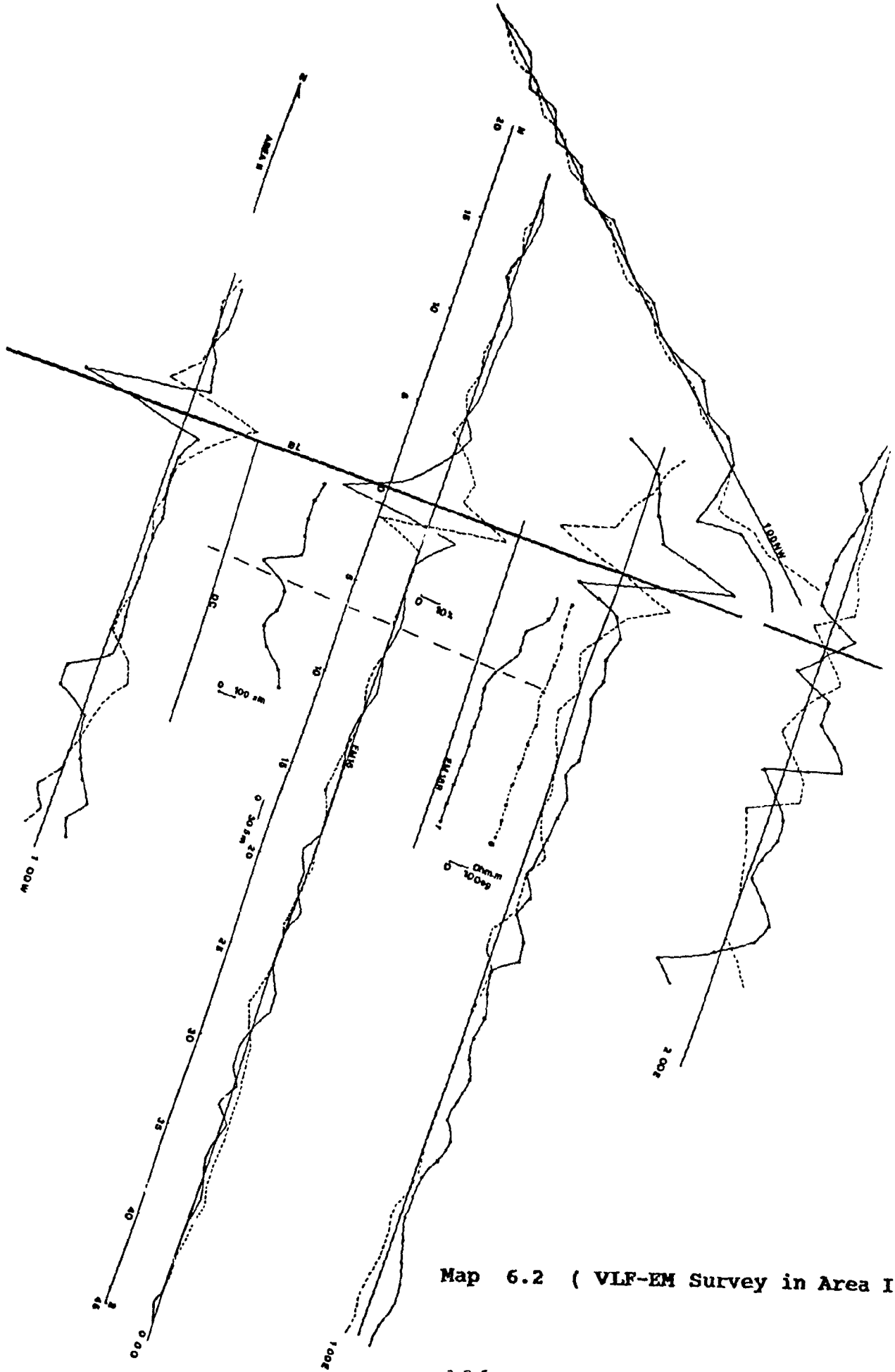

Map 6.2 (VLF-EM Survey in Area II).

resistivity contrast. There are no outcrop or drill hole data available to support this assumption, but the apparent resistivity contrast as shown on the EM-16R profile somewhat reinforces this assumption. The EM-16R results between stations 0+00 and 6+00S varies from 30 Ωm to 10 Ωm; while between stations 7+00S and 15+00S, it is almost constant 10 Ωm (map 6.2).

A DC resistivity profile conducted on the path by Wenner array resistivity profiling, showed about a 100 Ωm apparent resistivity contrast.

Nevertheless, there was an abrupt change in the DC apparent resistivity in the vicinity of station 6+00S , probably due to the overburden being thinner or to the presence of the fault itself.

6.3 Contact Location, Strike Extent, and Direction:

6.3.1 Area III

The stratigraphic contact is between Trenton limestone and shale and Utica shale (Globensky, Y., 1982). From the geological information, the physical properties especially the electrical conductivity between the two formations across the contact may be similar. It is thus not understandable that the amplitude of the EM-16 response over the contact was low. In fact it was difficult to delineate the contact from the EM-16 results alone. The EM-16R traverses and the DC Wenner resistivity profile were used to supplement the EM-16 results. The apparent resistivity contrast between the Trenton limestone and Utica

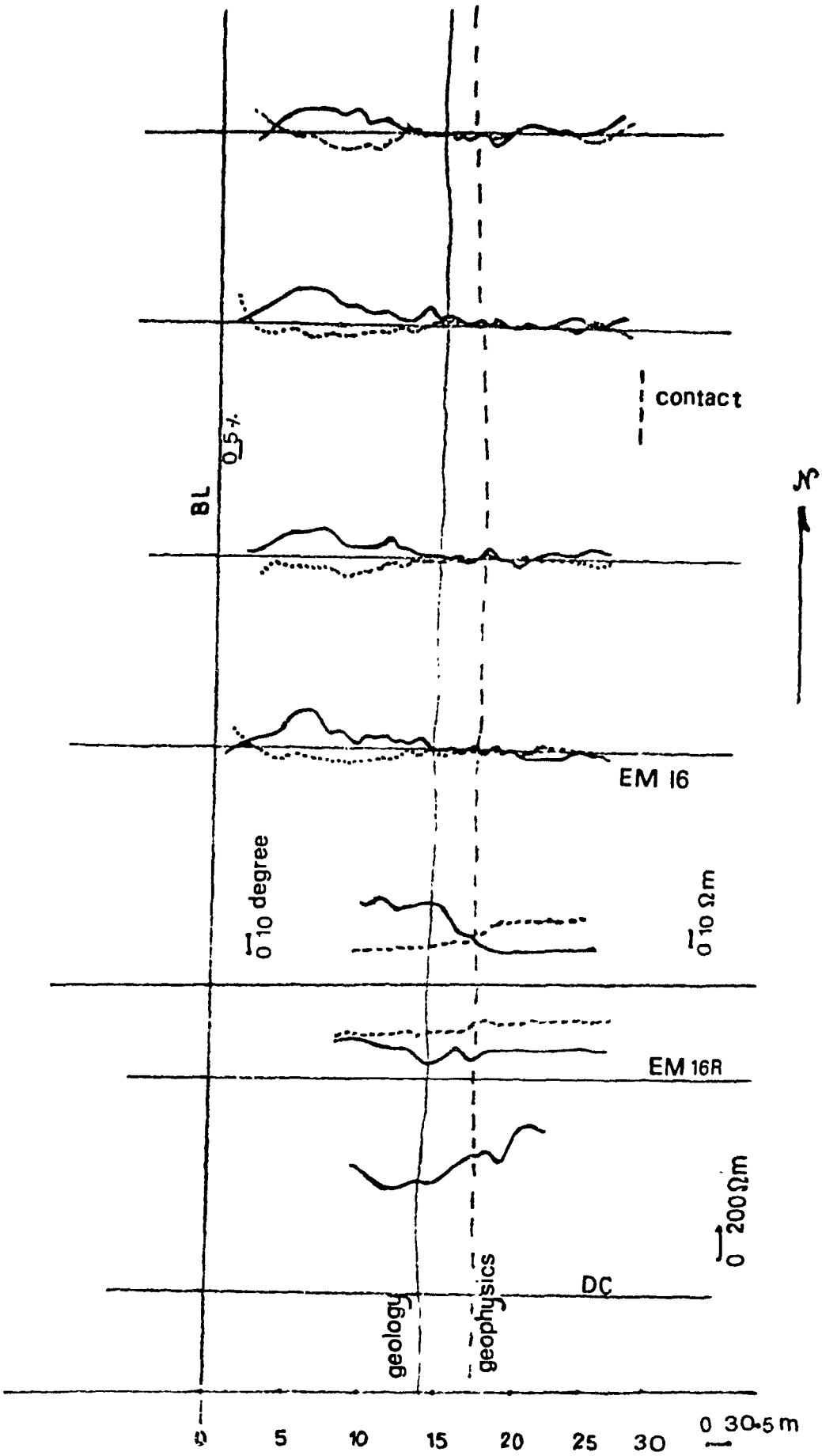

Map 6.3 (VLF-EM Survey in Area III).

shale is only of the order of less than 2 to 1 as indicated by the resistivity profiles.

The contact in area III inferred from the VLF and DC resistivity measurements is very close to its position shown on the geological map. The location of the contact was determined by Globensky (1982) to be about 400 m (1330 feet) east of the baseline, while the VLF measurements showed it to be at about ≈480 m (1570 feet) east of the BL (map 6.3). The contact seems to be within 260 feet of where Globensky mapped it and its strike is approximately north-south.

6.4 Intrusion Location, Strike Extent and Direction:

The magnetic measurements in areas I and II to supplement the VLF measurements over the Delson fault were actually of very little significant use in locating the fault (see lines 1+00E, 1+00W, 2+00E, 4+00E, and 6+00E in area I, and Line 0+00 in area II-map 6.4 a, b). This might be due to the small susceptibility contrast across the fault. On the other hand, the VLF measurements gave no indication of the magnetic body (see line 1+00E and line 1+00W in map 6.1). Again, it must be pointed out that the cultural background, character and complexity of the geology have significantly affected the response of each geophysical method.

However, the magnetic results are similar over the igneous intrusion in both areas. Obviously, the anomalies

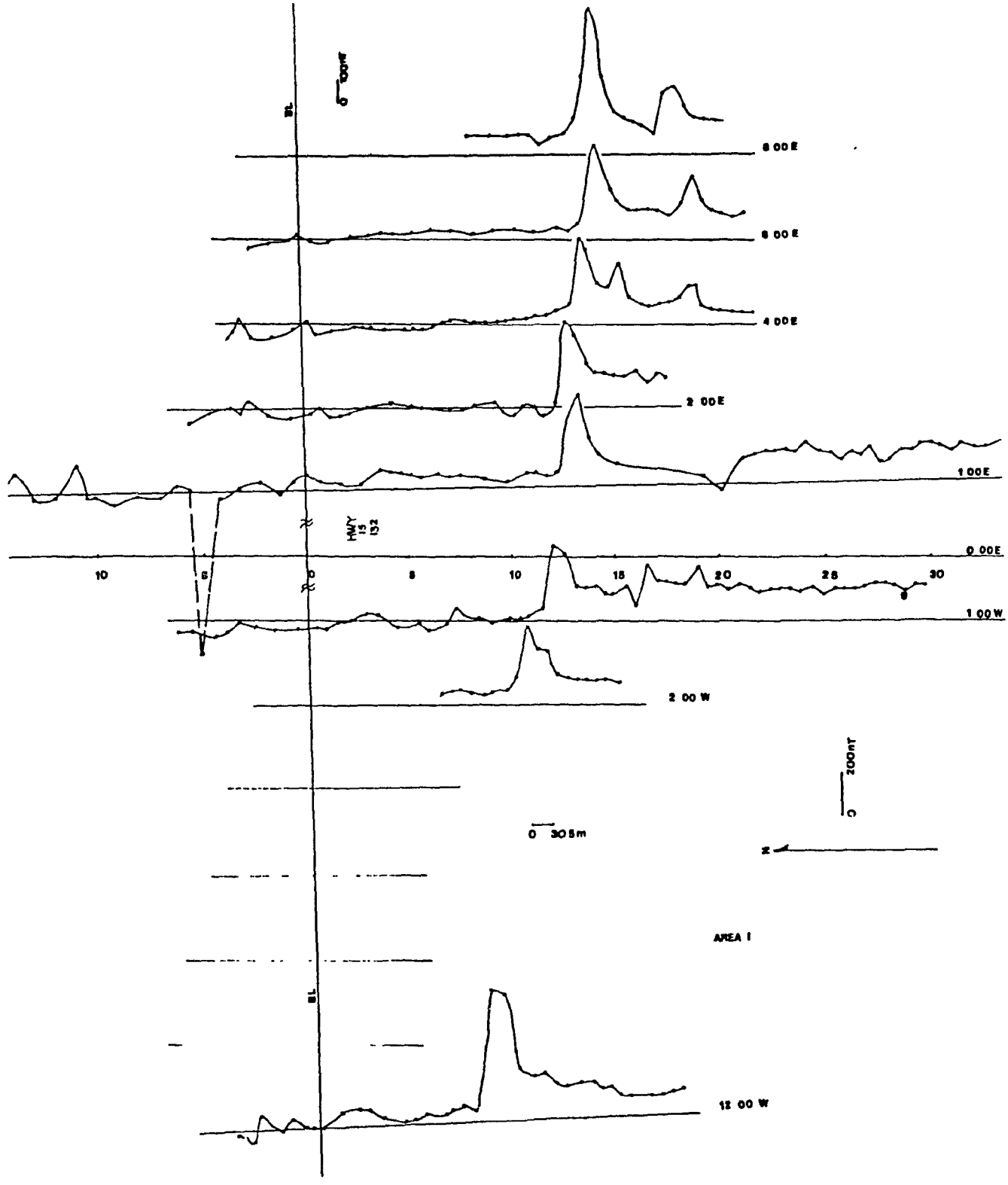

Map 6.4 a (Magnetic Survey in Area I).

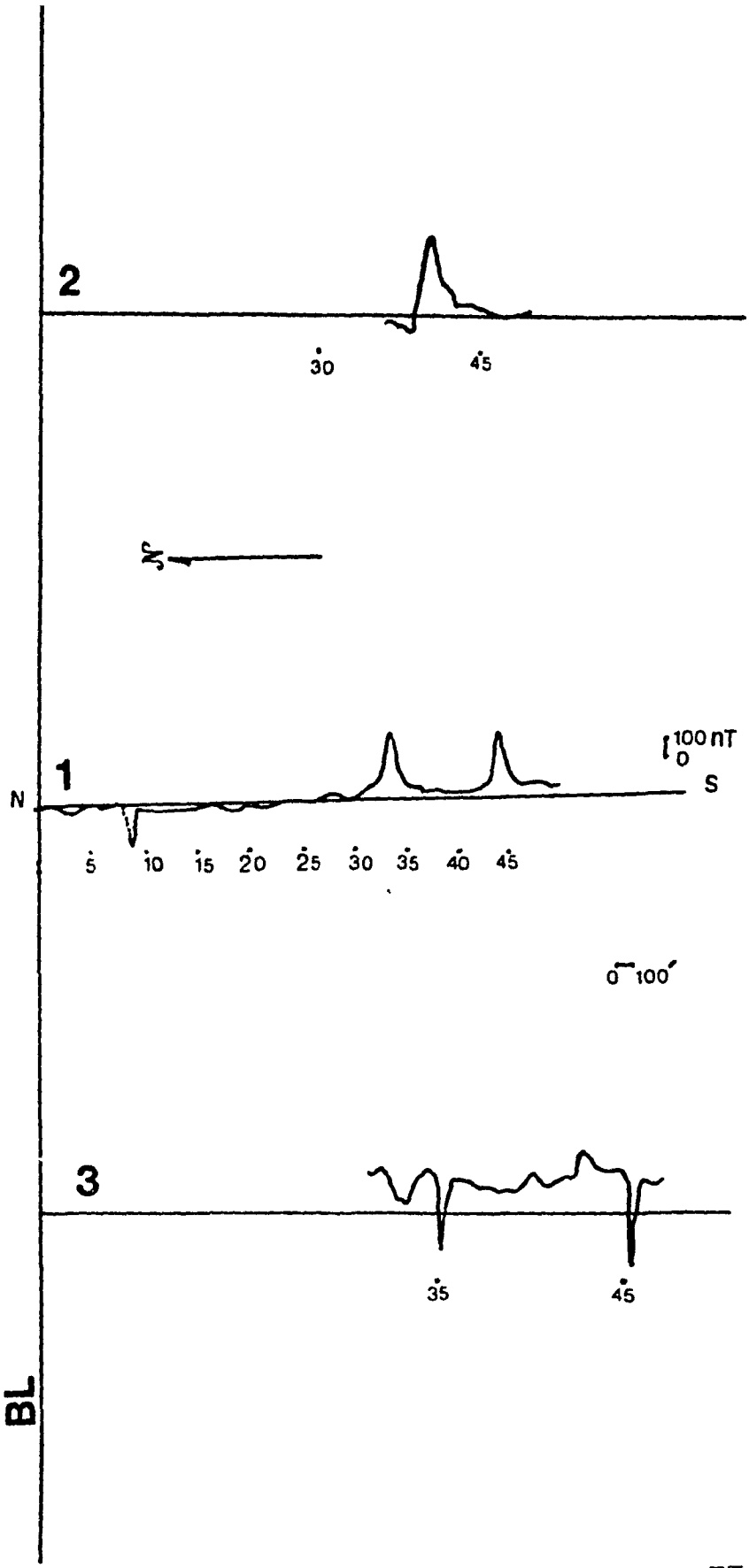

Map 6.4 b (Magnetic Survey in Area II).

are similar, having the same strike direction and the same dip angle. Their shapes (which are elongated in the form of a vertical thin-sheet) are similar (see map 6.4 a, b). An attempt was also made in area II to follow along the strike of the body to the west, but the farmland forced the measurements to be done along the roads, and a noisy and erratic response resulted (see for example profile (3) on Saint-Pierre road, map 6.4 b). Based on this survey and assuming the magnetic body is continuous from area I to area II, the body is roughly estimated at 5300 m in length and striking approximately E-W.

An attempt was also made to tie area I and area II together by using the VLF EM-16 to follow the strike of the fault. Again farm areas and small towns forced the following of roads so that unreliable results were obtained.

6.5 Discussion of Radon Emanation Survey:

The radioactivity surveys using the two methods: radon emanometer and gamma ray scintillometer did not give strong results. This might be due to the low radioactivity contrast in the surrounding rocks and in the overburden itself.

The geological data supports this assumption, as it indicates that shale is present in the two formations across the fault. The high shale content may also have helped to seal the fault and lessened the escape of radon

through fractures or faults. It also consequently would decrease the radon response over the fault.

The only two profiles that showed a radon response which would be expected over this fault are line 1+00W and line 2+00E. The indicated fault location agrees approximately with that obtained by the VLF. Since other lines showed no other definite response, it is impossible to indicate the location of the strike of the fault by this method. However, there is generally a trend of higher readings in the north (high shale content) as compared to the south (low shale content) (see map 6.5 a, b).

Owing to the lack of time,and to the problems in operating the emanometer, and also to the poor results of the preliminary scintillation survey, the radon method was not used in areas II and III.

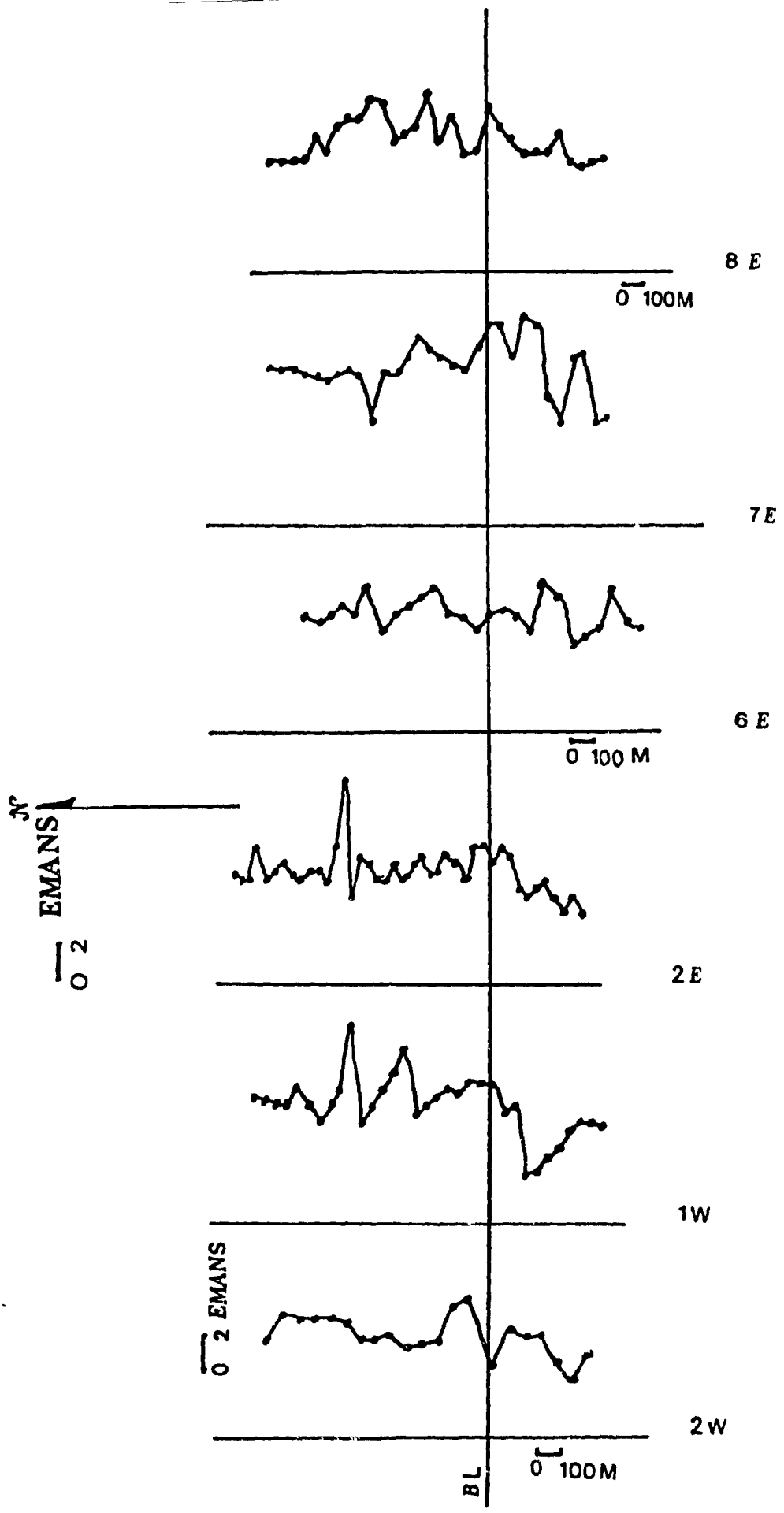

Map 6.5 a (Radon 222 Survey in Area I).

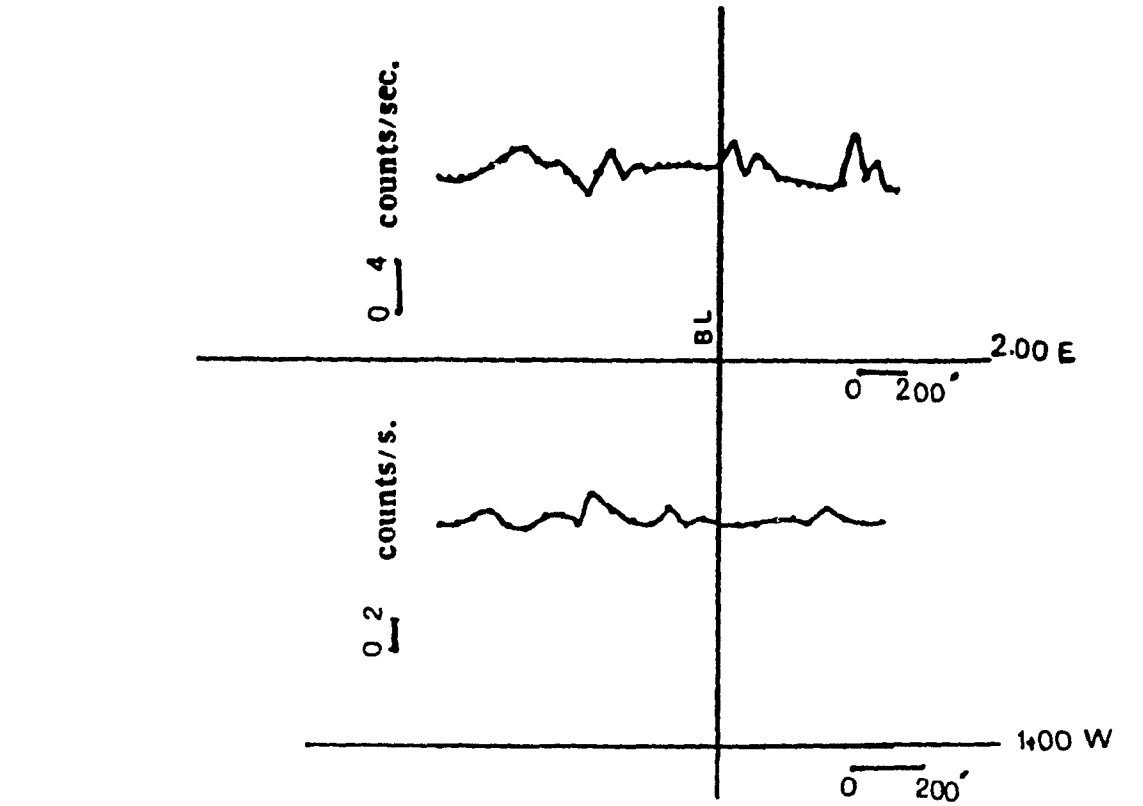

Area I

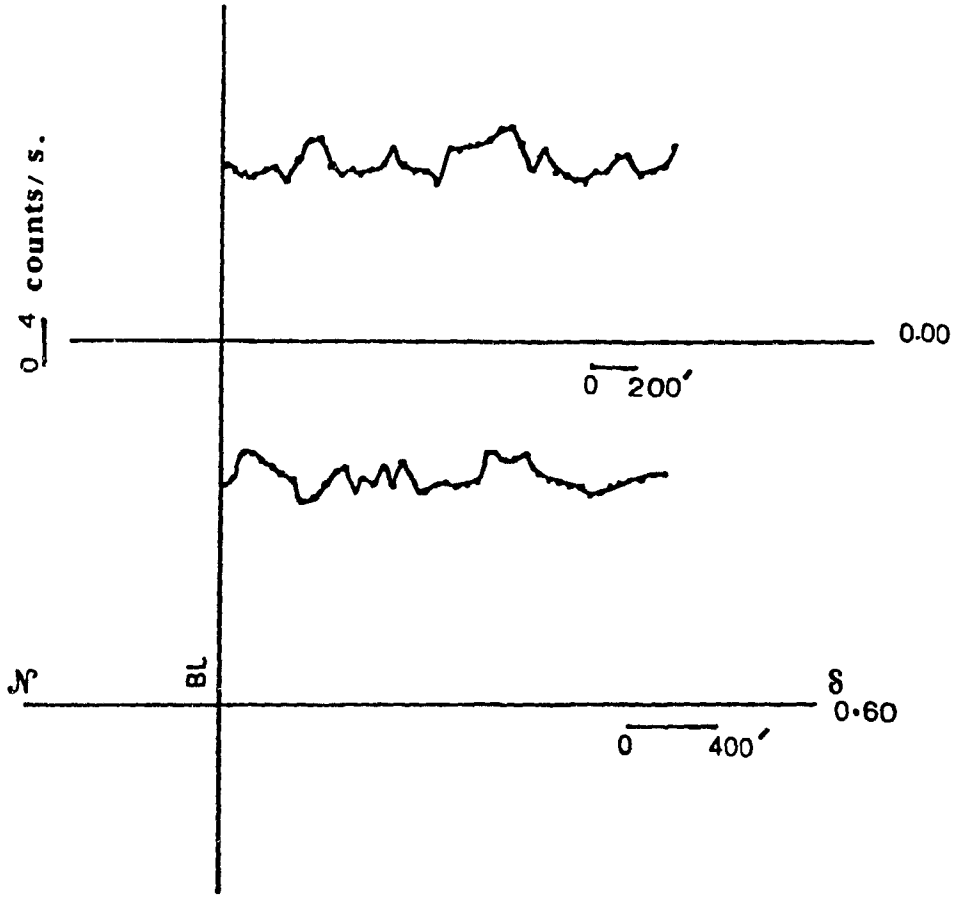

Area II

Map 6.5 b (Scintillation Survey in Areas I & II).

Chapter 7: Conclusions

Chapter :7 Conclusion

The present study shows the results of the application of different geophysical methods in the Delson region east of Montreal, where not only geological complexity but also the developed character (power lines, sewage lines, railways, farms, etc.)must be taken into account. The above factors significantly affected the response to each geophysical method and consequently complicated all the geophysical interpretations.

Owing to lack of time, the number of resistivity profiles (EM-16R, DC resistivity, and especially DC depth sounding) was kept as low as possible. However, the depth of overburden and bedrock topography have an adverse effect on the EM-16 results. Spots of thin and thick overburden can appear as zones of higher and lower apparent resistivity, respectively.

Only VLF EM-16 appears to be of significance when dilineating the Delson fault in area I and the contact in area III, and only when supplemented with the EM-16R results and DC resistivity.

The attempts to locate the Delson fault in area II by EM-16 and its supplements (EM-16R and DC resistivity profiling) must be regarded as unsuccessful.

Radon emanation surveys by emanometer and scintillometer methods were also of very little significance. This was probably due to the low permeability which is characteristic of high shale content zones.

The magnetic surveys appear significant here, in detecting intrusions with high magnetic susceptibility. The magnetic modelling of the anomalies was kept as close as possible to the existing geological information of the area.

Sharp magnetic anomalies suggest that the body is thin vertical and has a great depth extent. The modelling also confirms the body's great depth and that its average thickness-susceptibility is between 0.250 and 0.350 . When using modelling of any geophysical data, parameters should be constrained geologically in order to fit a correct model to a given set of data.

The strike of the discovered body is approximately E-W. Based on the assumption that the magnetic body is continuous from area I to area II, its strike length can be assigned 5300 meters.

However, the aeromagnetic map of the area which was taken in 1960 did not clearly indicate an anomaly over the magnetic body.

An attempt was made to tie area I and area II together in order to follow the strike of the magnetic intrusion by taking additional magnetometer readings, but erratic and noisy readings associated with the residential area made this impossible.

The obtaining of data from previous drill holes was attempted, (unsuccessfully) as it would have given more geological information on the subsurface structures as well as on some physical properties such as conductivity,

permeability, magnetic susceptibility, etc. If this data had been available, it would have been beneficial in the selection of more suitable geophysical methods as well as in the interpretation of the results gathered.

For future work more DC resistivity sounding should be conducted in order to determine the thickness of the overburden especially on the stations that exhibited an abrupt change in apparent resistivity, since bumps in the bedrock topography may appear as a contact in resistivity and VLF profiles.

Magnetic susceptibility measurements must be done on samples to determine the real suceptibility of the magnetic Intrusion.

BIBLIOGRAPHY

Abdoh, A., 1985, "Field Geophysical Studies in the pierrefonds - Ile Bizard Region, Western Montreal",MSc Thesis, McGill University, Montreal, Quebec

Clark, T.H., 1952, Montreal Area, Laval and Lachine Map Area, Department of Mines, Geological Report 46.

Clark, T.H., 1972, Montreal Area, Ministre des Richesses Naturelles, Quebec,Geological Report 152.

Cagniard, L., 1953, "Basic Theory of Magnetotelluric Method of Geophysical Prospecting", Geophysics, V.18, No.3, p. 608-635.

Cook, L.S., 1956, "Quantitative Interpretation of Vertical Magnetic Anomalies Over Veins", Geophysics, V.15, p. 667- 686.

Crossley, D.J., 1981, "Theory of EM Surface Wave Impedance Measurements, L.S. Collett and O.G. Jensen (eds.)", Geological Survey of Canada, Paper 81-15, report V.

Dobrin, M.B., 1976, "Introduction to Geophysical Prospecting", McGraw-Hill Book Company, p. 458-463.

Davis, Philip A., 1979, "Interpretation of Resistivity Sounding Data: Computer Programs for solutions to the Forward and Inverse Problems: Information Circular 17, Minnesota Geological Survey, 1633 Eustis St.,ST. Paul, MN 55108."

Fleischer, R.L., Hart, H.R., and Mogro-Campero, 1980, "Radon Emanation Over an Ore Body: Search for Long-Distance Transport of Radon, Instrument and Method", V.173, p.169-181.

Ghosh, D., 1971, "Inverse filter coefficients for the computation of apparent resistivity standard curves for horizontally layered earth." Geophysical Prospecting, Vol. 19 ,P. 769-775.

Globensky, Y., 1986, "Geologie de la Region de St-Chrysostome et de Lachine (sud)", Ministere de l'Energie des Resources", Geological Report 84-02.

Globensky, Y., 1987, Géologie des Basses-Terres du Saint-Laurent", Geological Report 85-02.

Jones, D., 1981, "Mapping Bedrock Terrain with EM-16R-VLF Unit", MSc. Thesis, McGill University, Montreal, Quebec.

Keller, G.V., and Frischknecht, F.C., 1966, "Electrical Methods in Geophysical Prospecting", International Series in Electromagnetic Waves, V.10, Pergamon, Toronto, p.523.

King, W.F., 1971 "Studies of Geological Structure

with the VLF Methods ". MSc Thesis, McGill University, Montreal, Quebec.

Kisak, E., 1976, "Finite Element Analysis and Magnetotelluric Response over Resistivity Anomalies and Topographic Effects", PhD. Thesis, McGill University, Montreal, Quebec.

Lourenildo, W. B. Leite and Jorge W.D. Leao, 1985," Ridge regression applied to the inversion of two-dimensional aeromagnetic anomalies", Geophysics. Vol. 50 No. 8. P. 1294-1306.

Marquardt,D. W., 1963 "An algorithm for least-squares estimation of nonlinear parameters." Journal Soc. Indust. Appl. Math. Vol. 2 P. 431-441.

Merrick, N.,P.,1977," A computer Program for the Inversion of Schlumberger Sounding Curves in the Apparent Resistivity Domain." Hydrogeological Report 1977/5, New South Wales Water Resources Commission, Sydney, Australia.

McDonald, D.G., 1965, "Gravity Field Studies in the St-Lawrence Lowlands", MSc Thesis, McGill University, Montreal, Quebec.

Parasnis,D.S., 1979,"Principles of Applied Geophysics, Chapman and Hall Ltd.,third edition, p.11".

Peterson, N.R., and Ronka, V., 1971, "Five Years of

Surveying With the VLF-EM Method", Geoexploration, V.9, p.7-26.

Roy, A., 1970, "Discussion: The Equivalent Source Technique", C.N.G., Dampney, Geophysics, V.35, p. 158-160.

Saull, V.A., 1978, "Personal Communications".

Skeels, D.G., 1947, "Ambiguity in Gravity Interpretation", Geophysics, V.12, p. 43-56.

Telford, W.M., King, W.F. and Becker, A., 1977, "VLF Mapping of Geological Structures", Geological Survey of Canada, paper 76-25.

Telford, W.M.,1987, "Personal Communications".

Telford, W.M., Geldart,L.P.,Sheriff, R.E., and Keys, D.A., 1976, "Applied Geophysics", Cambridge University Press, 1976, p.151-177.

Tanner, A.B., 1964, "Radon Migration in the Ground, a Review; in the Natural Radiation Environment", Eds: J.A.S. Adams and W.M. Louder, Chicago, University of Chicago Press, p. 161-190.

Whittles, A. B., 1969,"Prospecting with Radio frequency EM-16 in Mountainous regions." Western Miner, P.51-56.

Veinberg, A.K., 1967, "Technique of Magnetic Survey and Interpretation of the Results", Lectures read at the International Seminar of U.N.O. on " New Methods of Minera.. Exploration", Moscow.

Appendix I

* Depth sounding resistivity data in areas I, II.
* Z-A graph ;

$$Z = 1.38 \times (\lceil 1/\lceil a) \times a \quad \text{(Wenner)}$$

$\lceil 1$ = resistivity of overburden (Ωm)

$\lceil a$ = measured resistivity (Ωm)

a = electrode spacing (m).

* Cumulative graphes.
* Resistivity inversion results.
* VLF-EM16R interpretation results.

Depth sounding Wenner array data on Line 4+00 E area I

Electrode spacing (feet)	Apparent resistivity (ohm m.)	Z (meter) * (m)
2.0	6.3	4.2
3.0	4.5	8.8
4.0	4.8	11.0
5.0	49.6	1.3
6.0	54.7	1.5
7.0	62.0	1.5
8.0	52.3	2.0
9.0	66.7	1.8
10.0	66.0	2.0
12.0	77.3	2.1
14.0	90.6	2.1
16.0	92.5	2.4
18.0	101.8	2.4
20.0	105.6	2.6
22.0	114.7	2.6
24.0	128.2	2.5
26.0	138.9	2.5
28.0	154.8	2.5
30.0	162.1	2.5
32.0	162.9	2.6
34.0	170.9	2.7

36.0	181.0	2.6
38.0	183.8	2.8
42.0	200.6	2.8
52.0	248.3	2.9
58.0	287.9	2.7
70.0	325.5	3.0

* Telford, W.M., 1987 (Personal comunication)

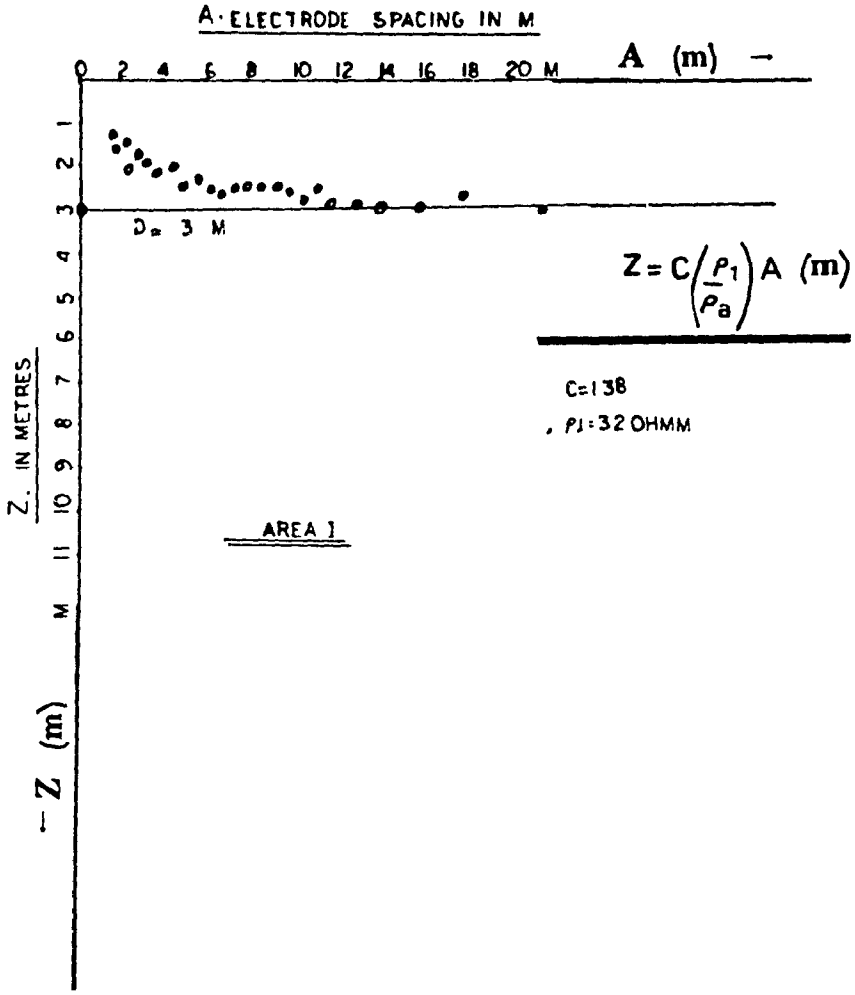
A-ELECTRODE SPACING IN M
0 2 4 6 8 10 12 14 16 18 20 M
A (m) →
D = 3 M
Z = C(ρ1/ρa) A (m)
C=138
ρ1=32 OHMM
Z. IN METRES
1 2 3 4 5 6 7 8 9 10 11 M
← Z (m)
AREA 1

Depth sounding Wenner array data on Line 0+00 (path)

arae II

Electrode spacing (feet)	Apparent resistivity (ohm m.)	Z (meter) (m)
5.0	23.4	2.2
10.0	22.0	4.6
15.0	23.0	6.6
20.0	24.1	8.4
25.0	27.8	9.1
30.0	31.59	9.6
35.0	33.52	10.7
40.0	39.72	10.1
45.0	40.52	11.3
50.0	43.10	11.7
55.0	47.39	11.7
60.0	49.42	12.3
65.0	52.28	12.5
70.0	55.64	12.8
75.0	58.89	12.8
80.0	61.27	13.2
85.0	61.05	14.0
90.0	68.94	13.2
95.0	67.28	14.2
100.0	70.86	14.3
105.0	70.37	15.0

110.0	73.74	15.1
115.0	77.08	15.1
120.0	74.70	16.1
140.0	88.47	15.8
150.0	86.18	17.4

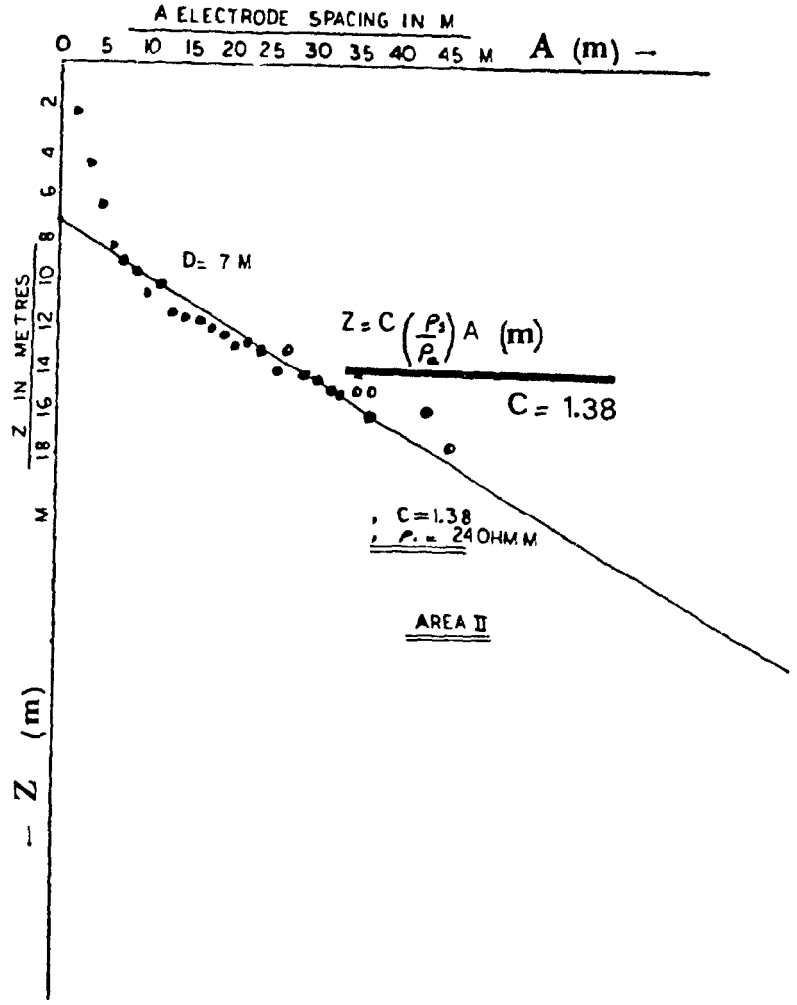
A ELECTRODE SPACING IN M
0 5 10 15 20 25 30 35 40 45 M
A (m) →
2
4
6
8
10
12
14
16
18
M
Z IN METRES
D= 7 M
Z = C (ρ3/ρa) A (m)
C = 1.38
, C=1.38
, ρa = 24 OHM M
AREA II
← Z (m)

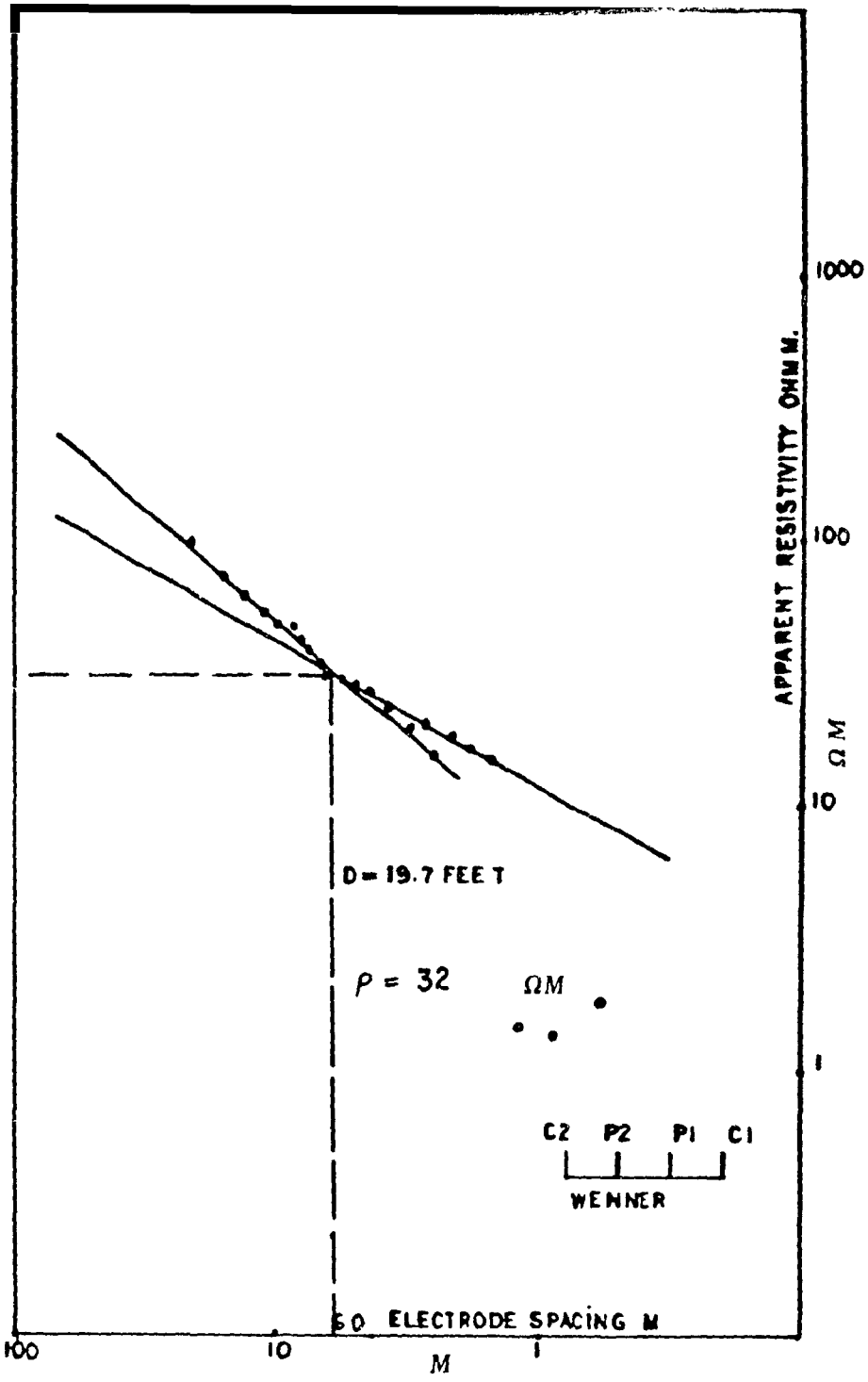

DC Resistivity Depth Sounding on Line 4+00E (Area I)

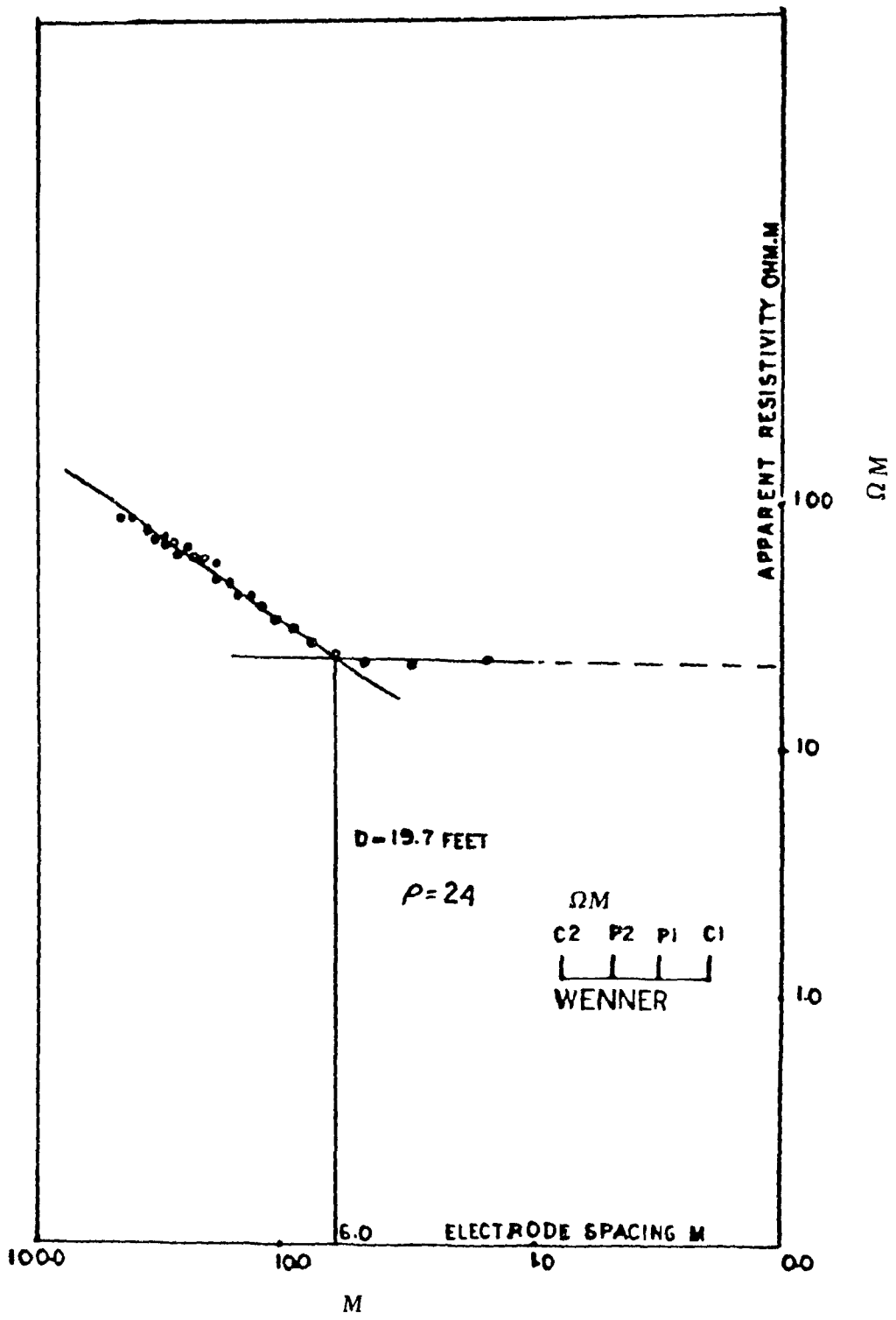

DC Resistivity Depth Sounding on Line 0+00 (Path), Area II . . . . . .

APPARENT RESISTIVITY VALUES : AREA NO. I

WENNER ARRAY

2 LAYER MODEL.

LAYER NO.	THICKNESS	RESISTIVITY
1	5.000	35.000
2		260.000

N	SPACING	MODEL RHO	FIELD RHO
1	1.00	33.104	48.000
2	1.14	32.417	49.600
3	1.29	31.572	54.700
4	1.47	30.579	62.000
5	1.67	29.471	52.300
6	1.90	28.304	66.700
7	2.15	27.153	66.000
8	2.45	26.103	77.300
9	2.78	25.244	90.600
10	3.16	24.659	92.500
11	3.59	24.425	101.800
12	4.08	24.607	105.600
13	4.64	25.260	114.700
14	5.27	26.434	128.200
15	5.99	28.169	138.900
16	6.81	30.505	154.800
17	7.74	33.472	162.100
18	8.80	37.100	162.900
19	10.00	41.407	170.900
20	11.36	46.406	181.000
21	12.92	52.095	183.800
22	14.68	58.461	200.600
23	16.68	65.474	208.100
24	18.96	73.091	248.300
25	21.54	81.248	287.900
26	24.48	89.872	325.500

RESISTIVITY INVERSION PROGRAM : AREA NO. I

WENNER ARRAY

LAYER NO.	THICKNESS	RESISTIVITY	THICK*RES	THICK/RES
1	3.89	25.878	100.542	.150
2		308.028		

NO	SPACING	MODEL RHO	FIELD RHO
1	1.000	33.160	33.104
2	1.136	32.309	32.436
3	1.292	31.341	31.563
4	1.468	30.289	30.591
5	1.668	29.198	29.481
6	1.896	28.120	28.325
7	2.154	27.110	27.135
8	2.448	26.223	26.108
9	2.783	25.511	25.239
10	3.162	25.027	24.657
11	3.594	24.825	24.425
12	4.084	24.962	24.610
13	4.642	25.500	25.262
14	5.275	26.502	26.445
15	5.995	28.035	28.182
16	6.813	30.165	30.514
17	7.743	32.959	33.481
18	8.799	36.480	37.097
19	10.000	40.790	41.407
20	11.365	45.940	46.423
21	12.915	51.978	52.079
22	14.678	58.937	58.454
23	16.681	66.839	65.477
24	18.957	75.687	73.083

RMS ERROR = 1.294

APPARENT RESISTIVITY VALUES : AREA NO. II

WENNER ARRAY

2 LAYER MODEL.

LAYER NO.	THICKNESS	RESISTIVITY
1	4.000	25.000
2		180.000

N	SPACING	MODEL RHO	FIELD RHO
1	1.00	22.480	22.100
2	1.17	21.676	23.400
3	1.36	20.777	22.000
4	1.58	19.854	23.000
5	1.85	19.005	24.100
6	2.15	18.341	27.800
7	2.51	17.971	31.590
8	2.93	17.992	33.520
9	3.41	18.484	39.720
10	3.98	19.508	40.520
11	4.64	21.113	43.100
12	5.41	23.339	47.390
13	6.31	26.218	49.420
14	7.36	29.773	52.280
15	8.58	34.013	55.640
16	10.00	38.935	58.890
17	11.66	44.516	61.270
18	13.59	50.712	61.050
19	15.85	57.457	68.940
20	18.48	64.663	67.280
21	21.54	72.223	70.860
22	25.12	80.016	70.370
23	29.29	87.914	73.740
24	34.15	95.789	77.080
25	39.81	103.517	74.700
26	46.42	110.988	88.470
27	54.12	118.111	86.180

RESISTIVITY INVERSION PROGRAM : AREA NO. II

INNER ARRAY

LAYER NO.	THICKNESS	RESISTIVITY	THICK*RES	THICK/RES
1	3.17	17.883	56.750	.177
2		177.324		

NO	SPACING	MODEL RHO	FIELD RHO
1	1.000	21.881	22.480
2	1.166	21.119	21.699
3	1.359	20.346	20.783
4	1.585	19.629	19.832
5	1.848	19.038	19.016
6	2.154	18.637	18.333
7	2.512	18.482	17.969
8	2.929	18.630	17.989
9	3.415	19.134	18.487
10	3.981	20.056	19.512
11	4.642	21.461	21.114
12	5.412	23.416	23.345
13	6.310	25.985	26.219
14	7.356	29.228	29.758
15	8.577	33.190	33.999
16	10.000	37.904	38.940
17	11.659	43.384	44.517
18	13.594	49.626	50.721
19	15.849	56.601	57.457
20	18.478	64.259	64.656
21	21.544	72.529	72.230
22	25.119	81.318	80.018
23	29.286	90.522	87.904
24	34.145	100.024	95.783

RMS ERROR = 2.308

EM16-R master curve interpretation results; two layer model known ($\rho 2 / \rho 1$). Area I, Line 4+00 E.

ρa (ohm m.)	Φ (degrees)	α	Q	$\rho 1$ (ohm m.)	$\rho 2$ (ohm m.)	H1 (m)
70	22	.675	1.63	26.3	313	7.9
60	24	.630	1.63	22.6	269	7.4
60	24	.630	1.63	22.6	267	7.4
80	26	.520	1.75	26.1	310.7	6.5
70	30	.300	2.6	10.4	123.8	2.4
70	31	.300	2.6	10.4	123.8	2.4
70	31	.240	2.6	10.4	123.8	2.4
80	30	.300	2.6	11.8	140.4	2.5
90	30	.300	2.6	13.3	158.3	2.7
100	32	.250	2.75	13.2	157.1	2.2
* 90	32	.250	2.75	12.0	142.8	2.1
100	30	.300	2.6	14.8	171.1	2.8
90	39	.026	3.0	10.0	119.0	0.2
50	44	.009	3.45	4.2	50.0	0.05

* Depth sounding (Wenner)

$\rho 1$= 25.9 ohm m.

$\rho 2$= 308 ohm m.

h1= 3.9 m.

EM16R resistivity

$\rho 1$= 12 ohm m.

$\rho 2$= 142 ohm m.

h1= 2.1 m.

EM16-R master curve interpretation results; two layer model known (ƒ2/ƒ1). Area II, Line 0+00 (path).

ƒa (ohm m.)	Φ (degrees)	α	Q	ƒ1 (ohm m.)	ƒ2 (ohm m.)	H1 (m)
30	40	.061	3	3.3	32.7	.26
30	38	.090	2.8	3.8	37.7	.42
20	40	.061	3	2.2	21.8	.22
20	40	.061	3	2.2	21.8	.22
?	?	?	?	?	?	?
8	38	.090	2.8	1	9.9	.22
10	41	.060	3	1.1	10.9	.15
10	40	.061	3	1.1	10.9	.15
10	40	.061	3	1.1	10.9	.15
*10	39	.070	2.95	1.15	11.4	.18
9	41	.06	3	1	9.9	.14
9	40	.061	3	1	9.9	.15
9	39	.070	2.95	1.03	10.2	.17

* Depth sounding (Wenner)

ƒ1= 17.9 ohm m.

ƒ2= 177.3 ohm m.

h1= 3.2 m.

EM16-R Resistivity

ƒ1= 1.15 ohm m.

ƒ2= 11.4 ohm m.

h1= 0.18 m.

Figure 6.

MASTER CHART FOR TWO-LAYER VLF RESISTIVITY INTERPRETATION

CONTOURS OF CONSTANT PHASE φ ARE SOLID LINES FOR CONSTANT |Q| ARE DASHED

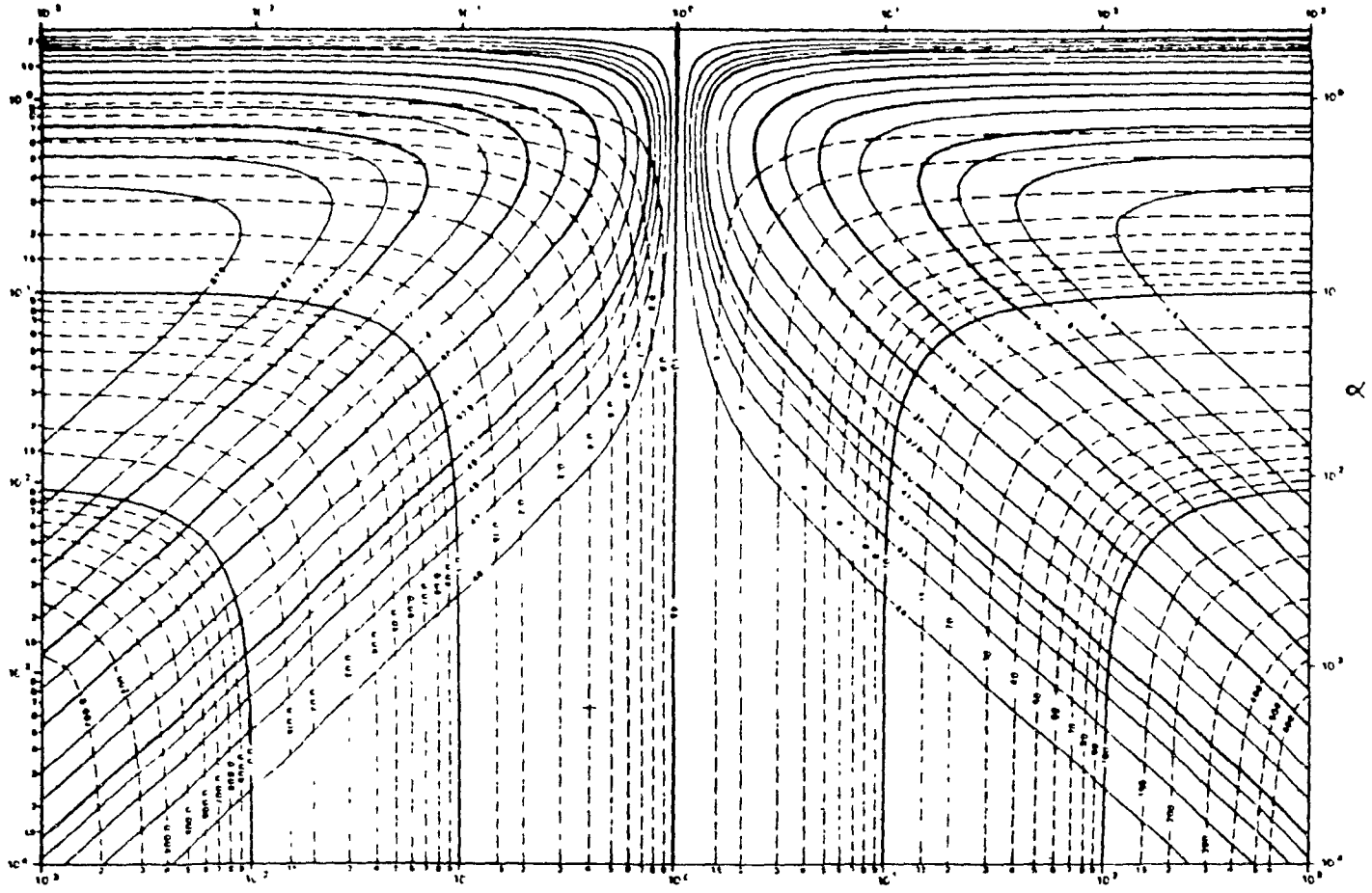

INTERPRETATION

KNOWN ρ compute $|Q| \cdot \sqrt{\bar{\rho}_{air}}$, locate (Q, φ) to give α, β ;

KNOWN ρ_{air} locate (β, φ) to give $|Q|, \alpha$ (2 values), compute $\rho = \rho_{air}/Q$;

compute h from $\alpha \sqrt{\frac{\omega\mu}{\rho}}$ h, compute ρ from $\beta \cdot \sqrt{\bar{\rho}_{air}}\,\rho$

Appendix II

* Sketch maps showing the profiles in areas I, II, III.

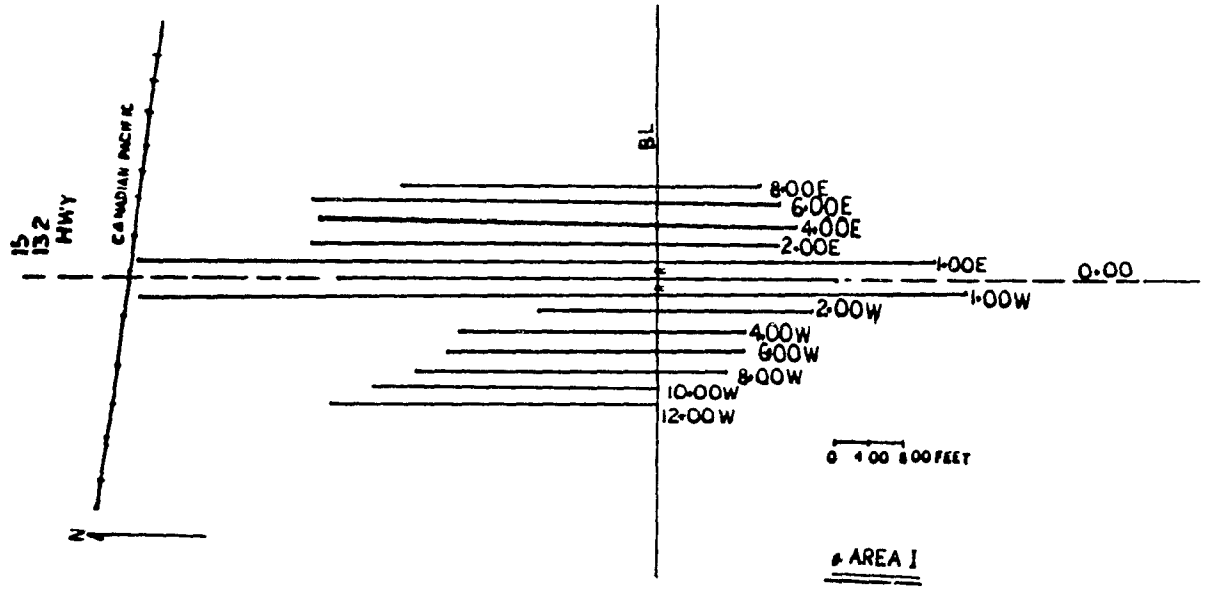

AREA I

1 FOOT = 0.305 METER

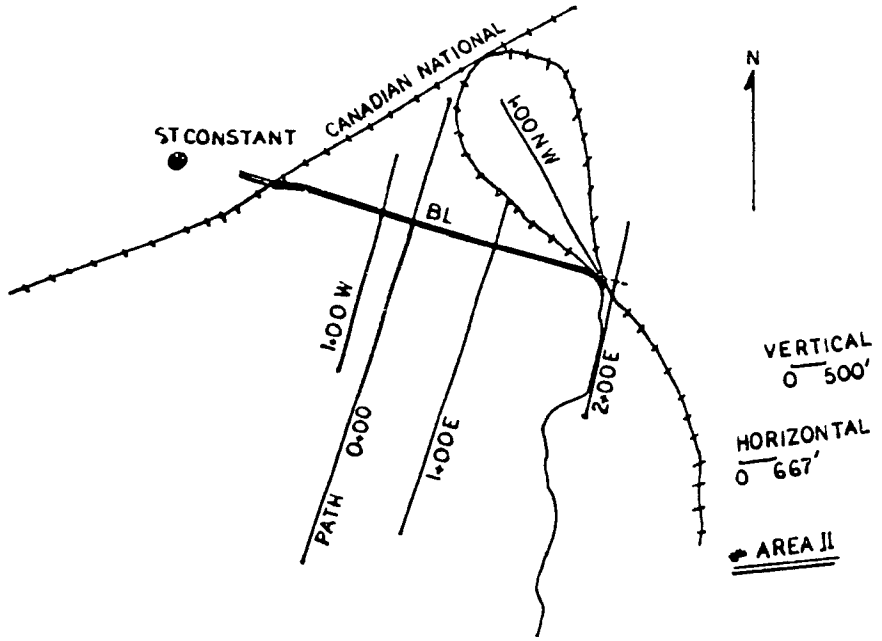

II

1 FOOT = 0·305 METER

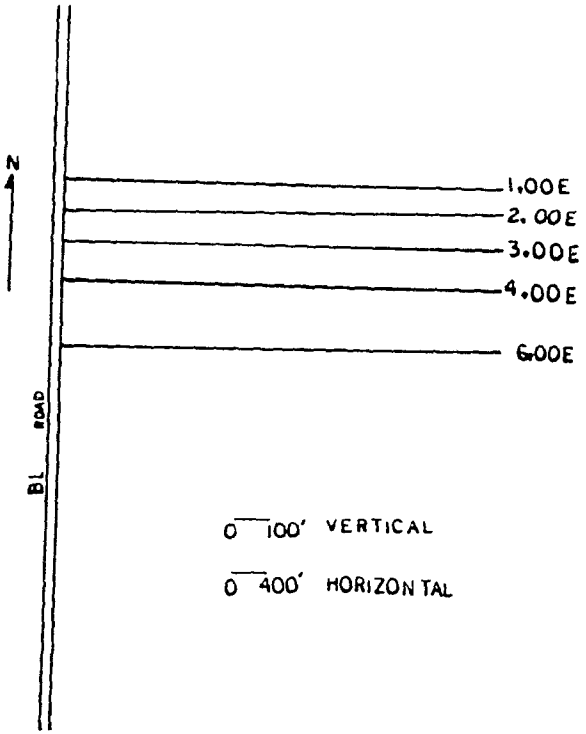
N
1.00E
2.00E
3.00E
4.00E
6.00E
BL ROAD
0 100' VERTICAL
0 400' HORIZONTAL

AREA III